NTNU

Norwegian University of
Science and Technology

Hydrothermal Synthesis of $LaFeO_3$

Anita Reksten

Chemical Engineering and Biotechnology
Submission date: June 2011
Supervisor: Tor Grande, IMTE
Co-supervisor: Kjell Wiik, IMT

Norwegian University of Science and Technology
Department of Materials Science and Engineering

Declaration (Erklæring)

I hereby declare that the work performed in this master thesis has been done independently, and in accordance with the rules and regulations which regulates the master programs at the Norwegian University of Science and Technology, NTNU.

(Jeg erklærer herved at jeg har utført arbeidet i forbindelse med denne masteroppgaven selvstendig og i henhold til Forskrift om krav til mastergrad ved NTNU.)

Trondheim, 22.06.2011

Anita Reksten

Abstract

This work explores the hydrothermal synthesis of $LaFeO_3$ (LFO) nanorods with a high aspect ratio. Synthesis of rod shaped LFO is a stepping stone to the synthesis of strontium doped LFO (LSF) nanorods with high aspect ratio. These LSF rods can be used to structure and increase the area of dense LSF oxygen permeable membranes, which can be applied in the partial oxidation of methane for the production of synthesis gas. Obtaining a larger surface area can increase the oxygen transport through the membrane when the transport is limited by surface exchange reactions. Increasing the oxygen transport is the objective of the work.

LFO was attempted synthesised by a direct and a two-step synthesis. Product morphology and phase composition have been explored by the use of SEM and XRD. In the direct synthesis the effect of potassium hydroxide concentration, molar ratio of iron to lanthanum and synthesis duration were varied to investigate the effect of these parameters. LFO was not produced in the direct synthesis; the products consisted of $La(OH)_3$ and Fe_2O_3. Since LFO was not obtained, a calculation exploring the temperature where LFO become more stable than $La(OH)_3$ and Fe_2O_3 was performed. The calculations show that the transition temperature where LFO is thermodynamically favoured is close to the operating synthesis temperature. The small driving force for formation of LFO at a temperature close to the transition temperature is the reason why LFO has not formed in the direct syntheses.

The two-step method consists of hydrothermal synthesis of $La(OH)_3$ nanorods, which were covered by iron nitrate solution and attempted converted into LFO by a topochemical reaction. In the study performed, the rod structure is lost when the product is calcined at 400 °C. LFO is not observed formed at this temperature, and LFO nanorods were therefore not obtained in the two-step synthesis.

Preface

This report is the master thesis work of the subject TMT4900 Material Chemistry and Energy Technology, and is a part of the Master of Science degree in Material and Energy Technology at the Department of Material Science and Engineering, IMTE, at the Norwegian University of Science and Technology, NTNU. A project work, 'Nanostructuring of oxygen permeable membranes', performed the autumn of 2010 is closely connected to the work of this master thesis. No parts of the project work have been recycled and used directly in this report. However, the content of some sections may be similar.

Acknowledgements

The work on this master thesis has been supervised by Professor Tor Grande. Gratitude is directed to Tor Grande for the valuable directions he has given concerning the experimental work and interpretations of the results and for being a source of inspiration. I would also like to thank Professor Kjell Wiik and Professor Mari-Ann Einarsrud for guidance and advices throughout the work.

Contents

List of Abbreviations

CVD	Chemical vapour deposition
DI-water	De-ionised water
LFO	$LaFeO_3$
LSF	$La_{0.2}Sr_{0.8}FeO_3$
MIEC	Mixed ionic-electronic conductivity
PTFE	Polytetrafluoroethylene
SEM	Scanning electron microscope
XRD	X-ray diffraction

1 Introduction

1.1 Motivation

Perovskite oxides with mixed conductivity, both oxygen-ionic and electronic conductivity, can be utilised in several applications. They can be employed in oxygen sensors, used as solid oxide fuel cell electrodes and membranes for separation of oxygen from the air. The latter application can also be applied in the process of supplying pure oxygen gas in the partial oxidation of methane to directly produce synthesis gas. Synthesis gas is a mixture of carbon monoxide and hydrogen gas, and is used for the production of important chemical products, such as ammonia and methanol. Partial oxidation of methane is the application intended for the membrane material in focus in this master thesis.

Production of high purity oxygen gas is today done by cryogenic distillation of air. The cryogenic method requires high energy consumption and is expensive. Separating oxygen from air by the use of oxygen-ion conducting membranes is a more cost-effective and a more environmental friendly alternative to cryogenic distillation. The development of this technology is therefore of interest to lower the energy consumption of the production of pure oxygen gas and reduce the cost of this product.

Material systems based on perovskites are commonly used for the applications mentioned above. In addition to conduct oxygen ions there are several other requirements these materials must meet in order to be of commercial interest, and be employed in the application of supplying pure oxygen gas in the partial oxidation of methane. They have to demonstrate dimensional and phase stability in the different environments they will be used in, and have chemical and thermal compatibility with other materials they will be in contact with. In addition to these requirements the material must be oxygen selective and show adequate transport of oxygen ions.

The transport of oxygen through a membrane consists of two steps, surface exchange reactions and bulk diffusion. Both of these two steps can be the rate determining step, limiting the overall transport of oxygen through the membrane. The surface exchange reactions are often the rate determining step, especially when working with thin membranes where the diffusion length through the bulk material is short. If the surface exchange reactions are limiting the transport, increasing the rate of these restrictive processes would increase the overall transport of oxygen. A promising strategy to enhance

the rate of surface exchange processes is to increase the specific surface area giving more sites for oxygen to be absorbed, or by increasing the catalytic activity of the surface. The project work performed autumn 2010 looked into the possibilities of increasing the membrane surface area by nanostructuring the surface to increase the oxygen transport.

1.2 Previous Work

The project work 'Nanostructuring of oxygen permeable membranes' [1] focused on the hydrothermal synthesis of the perovskite $La_{0.2}Sr_{0.8}FeO_3$ (LSF). This material is a mixed conductor, with oxygen-ionic conductivity. LSF was attempted synthesised hydrothermally with a high aspect ratio as an experiment to increasing the specific surface area of an LSF membrane in this project. Synthesis of high aspect ratio LSF was the first step in the work of increasing the specific surface area of the membrane. Unfortunately, LSF was not successfully synthesised, and the product obtained in the syntheses did not consist of LSF but four other phases: lanthanum hydroxide, iron oxide, strontium hexaferrite and strontium carbonate. This master thesis work will continue the research performed in the project work, with some alterations.

1.3 Aim of the Work

It is believed that a simplification of the LSF system by the removal of strontium will be easier to work with. Strontium will therefore be removed from the system. The objective of this work is to investigate the possibility of making $LaFeO_3$ (LFO) hydrothermally with a high aspect ratio, and gain a more fundamental understanding of hydrothermal synthesis of lanthanum iron oxide. More knowledge will hopefully lead to progress in hydrothermal synthesis of similar advanced ceramic materials. Perhaps strontium can be reintroduced and LSF synthesised later on, based on experience gained in this work. The focus will for now be on LFO, and two synthesis methods for producing this perovskite will be attempted: a direct hydrothermal synthesis and a two-step hydrothermal synthesis. Several parameters will be varied in the direct hydrothermal synthesis, and the effect these parameters have on product morphology and phase composition will be explored. The two-step synthesis consists of hydrothermal synthesis of lanthanum hydroxide nanorods which will be converted into lanthanum ferrite by a topochemical reaction in a second step.

2 Background

This chapter will first give an overview of the application intended for the membrane material, which is supplying pure oxygen in the partial oxidation of methane to produce synthesis gas, in Section 2.1. Then, a general introduction to the hydrothermal synthesis will be given in Section 2.2 , before literature on hydrothermal synthesis of lanthanum ferrite will be looked into in Section 2.3. Finally in Section 2.4, a well known synthesis mechanism for the formation of a perovskite will be presented.

2.1 Ceramic Membranes for Methane Conversion

The topic of this section is oxygen permeable membranes used in the partial oxidation of methane. The first section will give an overview to the subject and explain the operating principle of the membrane, which is followed by a section treating the material system used for this application.

2.1.1 Introduction and Operation Principle

Dense ceramic membranes made of perovskite oxides with mixed oxygen-ionic and electronic conductivity can be used to separate oxygen from air at elevated temperatures [2]. This oxygen separation property can be utilised in the partial oxidation of methane to produce synthesis gas from natural gas, according to the reaction in Equation 2.1.

$$CH_4(g) + \frac{1}{2}O_2(g) \rightarrow CO(g) + 2H_2(g) \tag{2.1}$$

The development of mixed ionic-electronic conductivity (MIEC) membrane reactor technology for oxygen separation eliminates the need for expensive oxygen produced by the energy consuming cryogenic method. External energy supply is not required because of the exothermicity of the partial oxidation of methane [2]. The operation principle for these membranes is illustrated in Figure 2.1.

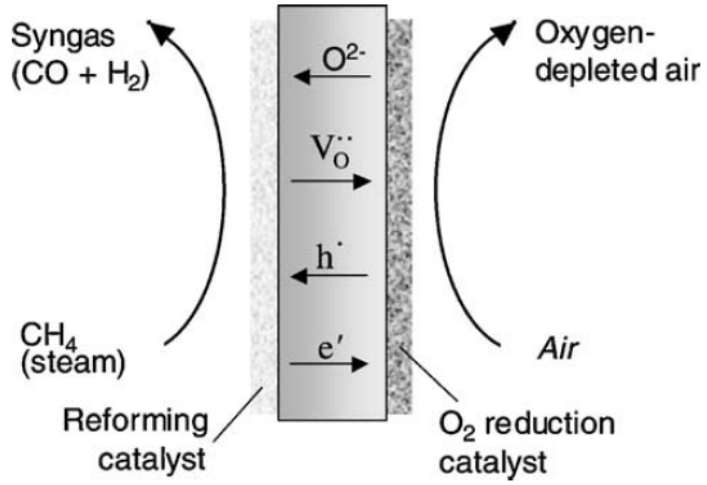

Figure 2.1: Illustration of the operating principle of a ceramic membrane reactor for the partial oxidation of methane to produce synthesis gas [2].

The driving force of the oxygen to pass through the membrane is a differential partial pressure of oxygen on the two sides of the membrane. The pressure differential is provided by using air on one side of the membrane and a reducing gas on the other side so that the oxygen is depleted. In the application of methane conversion methane is the reducing gas, reacting with the oxygen to form hydrogen and carbon monoxide on the other side of the membrane as showed in Figure 2.1. As oxygen is transported in the ionic form there must exist a simultaneous flux of electrons in the opposite direction of the oxygen ion transport to charge compensate and fulfil the electric neutrality criteria [3]. The transport of oxygen vacancies ($V_O^{\bullet\bullet}$) and electron holes ($h^{\bullet}$) are also indicated in the illustration in Figure 2.1. The transport of oxygen vacancies in one direction is another way of describing transport of oxygen ions in the opposite direction, as the oxygen ions diffuse through the membrane by jumping from one oxygen vacancy to another. The same principle applies for electrons moving in one direction and electron holes in the opposite.

In order for MIEC membranes to be employed in the production of synthesis gas from natural gas the membranes have to meet a number of requirements. Most important is the ability to supply a certain oxygen flux through the membrane. Secondly, the membrane material must be sufficiently stable dimensionally and chemically to allow long term operation at relevant operation conditions [4]. The operating temperature is typically temperatures between 600 °C and 1000 °C. The membrane material will be exposed to both a highly reducing environment on one side of the membrane and a highly oxidising environment on the other, and the membrane material must endure

both. It is also important that the membrane is dense without cracks or pores going through the material to ensure that oxygen ions are the only specie transported through the membrane. If this requirement is fulfilled the membrane can separate oxygen from air with infinite selectivity [2].

2.1.2 Material System

Several structures can be utilised as ceramic membranes, however the best structures in terms of oxygen permeation properties are either fluorite or perovskite crystal structure [3]. LSF is an acceptor doped perovskite, and acceptor doped perovskites is a promising class of materials which can be used in the field of dense oxygen permeable membranes. The general form for this type of structure is given in Equation 2.2 [4].

$$Ln_{1-x}Ae_xTm1_yTm2_{1-y}O_{3-\delta} \tag{2.2}$$

The A site ion in the structure described in Equation 2.2 is a lanthanide (Ln=La, Pr, Nd, Sm, Gd) or an alkaline earth (Ae= Ca, Sr, Ba) and the B site is occupied by one or two different transient metal (Tm1=Cr, Mn, Fe, Co Tm2=Co, Ni, Cu.) [4]. The partial substitution of metals cations in the ABO_3 perovskite structure by cations of lower valences, aliovalent doping, causes the formation of oxygen vacancies. Disordering of these oxygen vacancies at elevated temperatures is the reason the acceptor doped perovskites exhibit oxygen-ionic conductivity [2]. The transition metals occupying the B site can exist in different valence states in the structure, and is the reason for the electronic conductivity demonstrated by acceptor doped perovskites [4].

LSF is an acceptor doped perovskite with lanthanum being the lanthanide (Ln), strontium the alkaline earth element (Ae) and iron the transition metal (Tm) in the structure in Equation 2.2. In this case only one transient metal is present in the structure. The introduction of oxygen vacancies and the presence of two different valence states of iron in LSF are explained by the three defect reactions demonstrated in the equations 2.3, 2.4 and 2.5 [4]. These reactions are written in Kröger–Vink notation. In this example LSF is thought produced by aliovalent doping of $SrFeO_3$ into $LaFeO_3$. This process is shown by the reaction in Equation 2.3.

$$SrFeO_3 \xrightarrow{LaFeO_3} Sr'_{La} + Fe^{\bullet}_{Fe} + 3O^x_O \tag{2.3}$$

Strontium is introduced into the structure and occupies a lanthanum lattice site, indicated by Sr'_{La}. Strontium is positively charged and is divalent, lanthanum is positively charged and trivalent. When strontium occupies a lanthanum lattice site a negative charge is located at this site compared to if no dopant was introduced into the lattice. This is notified by $'$. Fe^{+IV} from strontium ferrite is doped into the structure and occupies a lattice site which originally was occupied by Fe^{+III}, described by $Fe^{\bullet}_{Fe}$. This gives this site a positive charge compared to if Fe^{+III} was located at this lattice position, marked by $^{\bullet}$. The oxygen ions introduced occupies oxygen lattice sites, O^x_O, which do not change the relative charge located at the lattice sites, and is notified by an x in the upper, right corner to the oxygen symbol.

The second equation, Equation 2.4, describes the redox process that introduces the oxygen vacancies which are the origin of the oxygen-ion conductivity. The ionic conductivity is proportional to the concentration of oxygen vacancies [4].

$$2Fe^{\bullet}_{Fe} + O^x_O \leftrightarrow 2Fe^x_{Fe} + V^{\bullet\bullet}_O + \frac{1}{2}O_2 \tag{2.4}$$

In the reaction in Equation 2.4 two electrons are transferred from one oxygen ion to two Fe^{+IV} ions, oxidising the oxygen to gaseous oxygen and resulting in the formation of an oxygen vacancy, $V^{\bullet\bullet}_O$.

The reaction in Equation 2.5 describes the defect chemistry giving rice to the electric conductivity.

$$2Fe^x_{Fe} \leftrightarrow Fe'_{Fe} + Fe^{\bullet}_{Fe} \tag{2.5}$$

In Equation 2.5 it is demonstrated that one electron is transferred from one Fe^{+III} ion to another. This results in the formation of iron ions with different valency, one divalent, Fe'_{Fe} , and one tetravalent, $Fe^{\bullet}_{Fe}$.

As explained on basis of the three defect reactions LSF exhibits oxygen-ionic and electronic conductivity, and is therefore a candidate material for oxygen permeable membranes. Lanthanum ferrite is not a mixed conductor, this material is not an acceptor doped perovskite, and can not be used for the application of separating oxygen from air. However the objective of this work is to make lanthanum ferrite nanorods hydrothermally to gain more knowledge about this type of synthesis, which hopefully can be used to successfully synthesise LSF nanorods and related one dimensional materials hydrothermally in the future.

2.2 Hydrothermal Synthesis

Hydrothermal synthesis is the method chosen for the synthesis of lanthanum ferrite nanorods. There exist several other techniques to produce rods in nanoscale, like chemical vapour deposition (CVD), electro spinning and lithography. These methods are expensive and may be incompatible with synthesis of lanthanum ferrite. CVD does for instance requires the ability of the target material to form an eutectic mixture with a catalyst material. Finding a catalytic material which forms an eutectic solution with multiple components with a specific ratio between the components would be challenging. CVD is therefore not an option of making nanorods of advanced ceramic materials, and is not an option for the synthesis of lanthanum ferrite, and certainly not LSF. Electro spinning and lithography are both complicated and expensive alternatives. Hydrothermal synthesis however, is a cost-effective and a relative easy method, and has the advantage that it can be carried out at relatively low temperatures [5]. Two synthesis methods which also offer the possibility of producing oxide nanostructures at reduced temperatures are sol-gel and co-precipitation. However, the product obtained from these two methods often requires a calcination and a milling step [6]. Calcination and milling are usually not needed after hydrothermal synthesis, which shortens the synthesis route of hydrothermally produced products.

The term hydrothermal is of geological origin, and the hydrothermal technique was developed in the search of understanding of the formation of minerals in nature in the presence of water [6]. The geologist Sir Roderick Murchison was the first to use the term in the 19th century. In spite the fact the term has existed for more than 150 years, a straightforward, unambiguous definition does not exist. Byrappa and Yoshiumura [6] has proposed the definition; "Any heterogeneous chemical reaction in the presence of a solvent (whether aqueous or nonaqueous) above room temperature and at pressure greater than 1 atm in a closed system". If water is the solvent used, the process is said to be hydrothermal. In cases where nonaqueous solvents are used the term solvothermal process should be applied.

Hydrothermal synthesis is performed in a sealed container called an autoclave. Figure 2.2a shows an example of how this container may look, and a schematic drawing of the structure and its components is shown in Figure 2.2b. The apparatus will be described in more detail in Section 3.1.1 Autoclave.

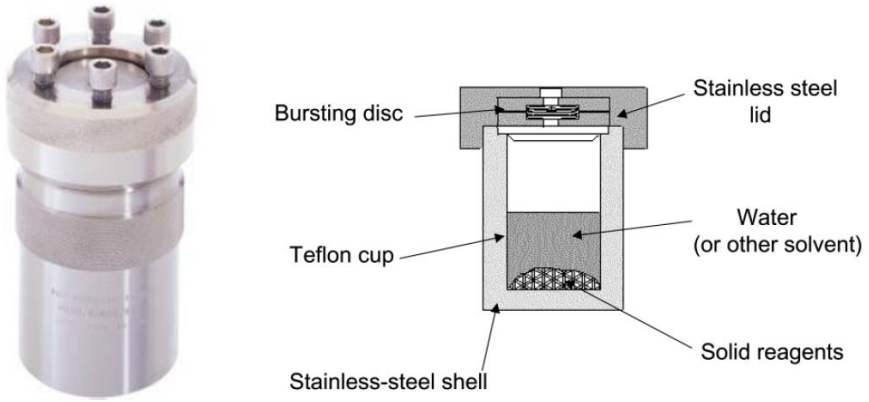

(a) Autoclave (b) Schematic drawing

Figure 2.2: (a) Image of an autoclave [7]. (b) A schematic drawing of an autoclave [8].

An autogenous pressure is generated inside the autoclave when it is heated. By increasing the temperature and pressure simultaneously, the water can be brought to temperatures above the boiling point. The phase diagram of water is shown in Figure 2.3a. The critical point of water is at 374 °C and 218 atm [5]. The critical point is the position in the phase diagram where water becomes supercritical. This point in the phase diagram is demonstrated in Figure 2.3a. In the supercritical state water is neither in a gaseous state nor in a liquid state, but something between the two, with properties of both the liquid and the gas.

The autogenous pressure is highly dependent on the temperature, but this is not the only parameter affecting the pressure in the autoclave. Other influences are compounds present in the solution and the fill factor. The fill factor is the ratio between the volume of the solution in the autoclave and the total volume available for the solution. This parameter has a major impact on the pressure generated inside the autoclave. The effect temperature and the fill factor have on the pressure is shown by the plot diagram in Figure 2.3b. The fill factors in the figure are indicated by percentage of filling ratio.

Some syntheses performed hydrothermally involve water in a supercritical state. However, in most hydrothermal syntheses the temperature and the pressure are kept below the critical point. These syntheses are performed under mild hydrothermal conditions, and take advantage of higher reactivity and increased solubility of metal salts and complexes without bringing the water to a supercritical state. Because of the increased reactivity and solubility many inorganic materials can be prepared at temperatures substantially lower

than those required in traditional solid-state reactions [5]. Lanthanum ferrite will in this work be prepared under mild hydrothermal conditions.

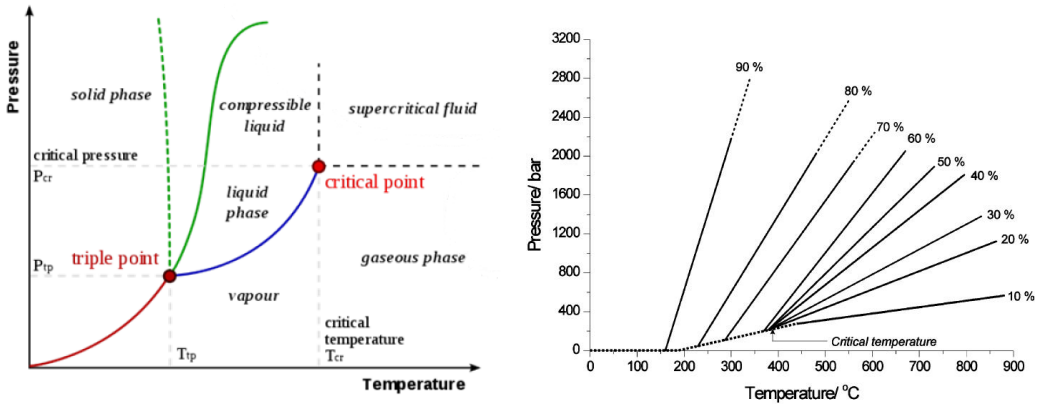

(a) (b)

Figure 2.3: (a) Phase diagram of water [9]. (b) Temperature and pressure dependence of fill factor [8].

Bringing water to mild hydrothermal conditions causes the density and viscosity of water, and the diffusivity of the reactants to change. A consequence of this change in behaviour is that the solubility is increased and the diffusion process is speeded up, which increases the chemical reactivity of the reactants in the solution. The increased chemical reactivity enables a reduction of the synthesis temperature for some materials which normally demands a higher synthesis temperature [10]. The reduced temperature also makes it possible to synthesise compounds that would be unstable at higher temperatures.

To summarise, hydrothermal synthesis is a fairly simple method, which is cost-effective and can produce crystalline material in nanoscale, at relative low temperatures because of increased chemical reactivity. These advantages are the reason for choosing hydrothermal synthesis as the synthesis method for producing LSF and LFO.

2.3 Hydrothermal Synthesis of Lanthanum Ferrite

During the past century the interest for low dimensional nanostructured materials has increased. The unique electronic, optical and mechanical properties provided by such structures, and the potential applications in nanodevices and in functional materials can account for this growing interest [11]. Such structures also exhibit large surface areas, which is the property desired for the lanthanum ferrite structure in this work. Reports on lanthanum ferrite synthesised in nanodimensions with high aspect ratio by hydrothermal synthesis have not been found in the literature. Hydrothermal synthesis of lanthanum ferrite in cubic shape has therefore been studied to obtain an understanding of the synthesis method and will be the starting point for this work.

Hu et al. have made cubic shaped lanthanum ferrite powder crystals with sizes varying from 1 μm to 13 μm [12]. LFO cubes obtained by Hu et al. are displayed in Figure 2.4. In this work the synthesis of $LaFe_{1-x}Cr_xO_3$ ($0 \leq x \leq 1$) was investigated. The synthesis was carried out at 240 °C for five days. Alkalinity of the initial reactant mixture was found to have a strong impact on the final composition. Dependent on the Fe/Cr ratio the value of x approached zero with increasing concentration of potassium hydroxide. At fixed ratio of Fe/Cr at 0.5 a potassium hydroxide concentration of 15.6 M gave a product consisting of $LaFeO_3$. A reaction mixture with high initial potassium hydroxide concentration will therefore be used in the attempt to produce LFO in this work. However, smaller crystallites than the obtained product in the work of Hu et al. are desirable. The synthesis duration will therefore be explored. Shorter synthesis duration will be investigated to examine if smaller crystallites are obtained, since the crystallite growth period is reduced.

The fill factor which is used in the work of Hu et al. has not been stated clearly in the experimental section in the article. However, it is described that 5 g of potassium hydroxide has been used when $LaFe_{0.5}Cr_{0.5}O_3$ is synthesised. Later in the article it is stated that the optimum potassium hydroxide concentration when synthesising $LaFe_{0.5}Cr_{0.5}O_3$ is 9 M [12]. If 5 g of potassium hydroxide is used to form a 9 M solution and the molar weight of potassium hydroxide is 56.1 g/mol, the solution volume has to be 9.9 mL. An autoclave which rooms 18 mL was used for the synthesis in the work by Hu et al., which gives a fill factor of 55 %. The fill factor used in the work of Hu et al. is therefore believed to be 55 %. The work of Hu et al. will be used as the basis for the direct synthesis performed in the work of this master thesis.

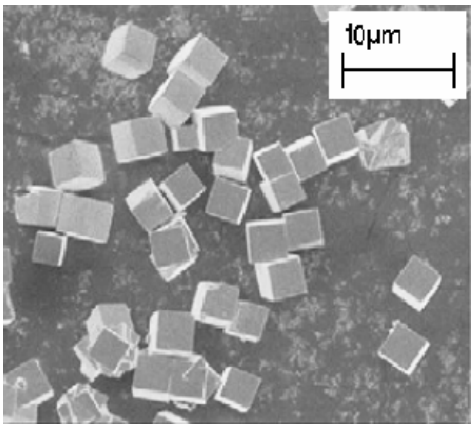

Figure 2.4: SEM image of the lanthanum ferrite crystallites obtained in the work of Hu et al. [12].

Lanthanum ferrite has also been synthesised hydrothermally by Zheng et al. [13], however this was done under carbonate-containing medium. Iron nitrate, lanthanum nitrate, sodium hydroxide and sodium carbonate were mixed and transferred to an autoclave which was heated for 5 - 7 days at 240 - 260 °C. The fill factor was 80 - 85 %. The product obtained by this synthesis consisted of cubic crystals of lanthanum ferrite with particle size of 10 - 20 μm. Synthesising LFO by the use of carbonate containing medium will not be attempted in work of this master thesis. The reason is that it is not desirable to introduce another synthesis condition parameter into the synthesis. Another reason is that strontium carbonate is a very stable compound; it was formed in the syntheses of LSF when trace amount of carbonate was present in the project work [1]. In order for LSF to be synthesised by this method in the future, carbonate medium can not be introduced into the system. If a carbonate containing medium was used for the synthesis of LSF strontium carbonate would probably form, and would be destructive for the formation of LSF.

2.4 Synthesis Mechanism

A better understanding of the chemical processes taking place within the autoclave during synthesis would be extremely valuable. Control over the product could be achieved by tuning the reaction parameters known to impact the product, and would eliminate lengthy experiments based on trial and error when investigating the effect of reaction conditions on the product [8]. Unfortunately, the formation of perovskite materials like lanthanum ferrite under hydrothermal conditions is not well understood. Since sealed steel

containers are used for performing hydrothermal syntheses it is challenging to obtain experimental data under real reactions conditions and thereby obtaining information about the processes taking place. The only well explained mechanism described on perovskite formation is the mechanism of barium titanate. Because of the commercial value of tetragonal barium titanate and the advantageous control over particle morphology offered by hydrothermal synthesis, the mechanism of forming barium titanate has been more widely studied than other perovskites. A patent for the hydrothermal synthesis route of this material was described almost 70 years ago [8]. The morphology, crystal structure and particle size of barium titanate are very dependent on the reaction conditions, small variations can have a big impact on the outcome. As the formation mechanism of a structure with material system closer to LFO has not been found in the literature, the mechanism for formation of barium titanate will be described.

Two mechanisms for the formation of barium titanate have been proposed, 'in situ reaction mechanism' and 'dissolution precipitation mechanism', both are illustrated in Figure 2.5.

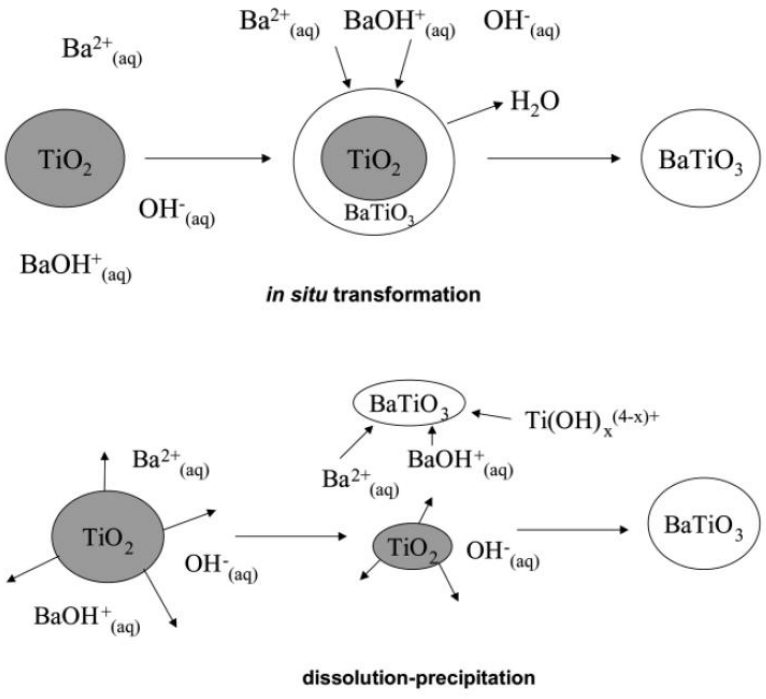

Figure 2.5: Illustrations of the two proposed mechanisms for the formation of $BaTiO_3$, 'in situ reaction mechanism' and 'dissolution precipitation mechanism' [8].

The first alternative, 'in situ reaction mechanism', envisages a complete dissolution of the barium salt before a heterogeneous reaction of the barium ions and solid titanium oxide particle takes place. A continuous layer of barium titanate forms on the titanium oxide particle, when the particle is completely covered, divalent barium ions diffuse through the barium titanate layer and reacts with the remaining titanium oxide in the core of the particle.

The 'dissolution precipitation mechanism' involves dissolution of both barium salt and titanium containing reagent, which is followed by crystallisation of barium titanate from the solution. These two reactions mechanisms are considered to be two extreme types of mechanisms. In reality these two processes might occur simultaneously, or at different stages in the reaction. For instance, reactants may dissolve and form barium titanate from the solution on particles of titanium oxide. However, these simplified processes give a starting point of how mixed-metal oxides might form under hydrothermal conditions [8].

3 Experimental

Details concerning the experimental work performed will be presented in this chapter. A presentation of the synthesis procedures carried out and the characterisation method and instruments used in this work will be given.

3.1 Apparatus and Chemicals

The syntheses of the lanthanum ferrite by direct hydrothermal synthesis and lanthanum hydroxide in the first step of two-step synthesis have been performed in an autoclave, this apparatus will therefore be presented in this section. The chemicals used in order to conduct the syntheses will also be listed.

3.1.1 Autoclave

The hydrothermal syntheses were performed in a Parr 4748 Large Capacity Bomb. It consists of a stainless steel body with six cap screws in the screw cap, which is used to seal the flanged cup inside the steel body. This cup has a volume of 125 mL, is removable and made out of polytetrafluoroethylene (PTFE). An expandable wave spring maintains continuous pressure on the seal during the cooling cycle when PTFE parts might otherwise relax and leak. If the pressure of the autoclave accidentally should reach the 240 bar range, a safety rupture disc above the PTFE cup will blow out through an opening in the bomb head to release the pressure. To avoid blow out, and to ensure safe operation, the pressure should not exceed 130 bar. A schematic drawing the autoclave construction is shown in Figure 3.1. An image of the real autoclave components of the autoclave used in this work, the Parr 4748 Large Capacity Bomb, is shown in Figure 3.2.

The PTFE cups can stand temperatures up to 250 °C, temperatures exceeding 250 °C can not be applied in the syntheses [7]. The PTFE cup is used to prevent contact of the steel body and corrosive reagents, like strong acids and bases. Under high pressures the PTFE has a tendency to creep or flow, which causes the cups to deform during operation. This is especially pronounced when high operation temperatures are used, in the range 200 °C - 250 °C. The deformation is negligible below 150 °C. As the creep effect becomes more pronounced it will be difficult for the cups to maintain a tight seal. It is therefore important that the cups are replaced after a given number of

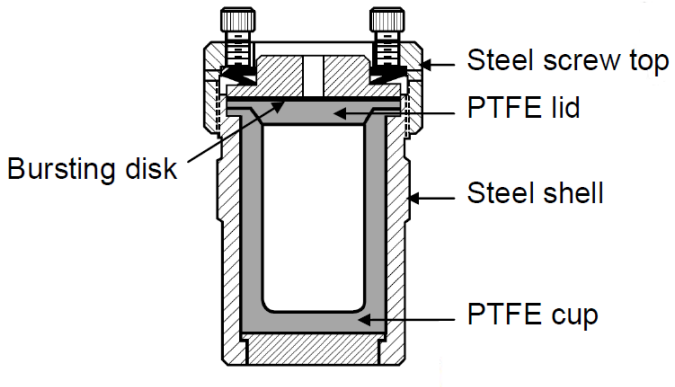

Figure 3.1: A schematic drawing of an autoclave [7].

Figure 3.2: Image of the autoclave Parr 4748 Large Capacity Bomb and its components.

synthesis cycles. The lifetime of the cups will be dependent on the pressure and the temperature to which they are exposed. Lifetimes have been reported as short as 10-30 runs, or as many as 100 runs [7].

After a synthesis has been performed it can be difficult to remove the cup from the steel body and to get the lid off the cup because of the creeping effect and deformation of PTFE. This is especially prominent when a synthesis has been carried out at a high temperature. After the vessel has been cooled down to room temperature, additional cooling in a refrigerator or freezer may be necessary to shrink the material enough to allow removal of the cup from the steel body, and to get the lid off the cup [7].

When the Parr 4748 Large Capacity Bomb is used for processes including inorganic material, the fill factor limit is 66 % [7]. It is important that the vessel is not completely filled, as there must be space available in the autoclave for the vapour forming during heating. When a water-based solution is heated to 250 °C it will expand approximately 25 %, compared to the solution volume at room tempearture. To ensure enough vapour space the total volume of precursor solution must never exceed the limiting fill factor [7].

3.1.2 Chemicals

The chemicals used in the synthesis of lanthanum ferrite are listed in Table 3.1, with the supplier and purity of the chemicals.

Table 3.1: Chemicals used in the synthesis of lanthanum ferrite, their supplier and purity level.

Chemical	**Formula**	**Supplier**	**Purity** [%]
Lanthanum nitrate	$La(NO_3)_3{\cdot}6H_2O$	Sigma-Aldrich	99
Iron nitrate	$Fe(NO_3)_3{\cdot}9H_2O$	Sigma-Aldrich	98
Potassium hydroxide	KOH	Sigma-Aldrich	90
Ammonia	25 % NH_3	Sigma-Aldrich	(not listed)

3.2 Synthesis Procedure

The experimental procedure for the hydrothermal syntheses, both the direct synthesis and the two-step synthesis, will be presented in the following sections.

3.2.1 Direct Hydrothermal Synthesis

The direct hydrothermal synthesis procedure started with the mixing of $Fe(NO_3)_3{\cdot}9H_2O$ and $La(NO_3)_3{\cdot}6H_2O$ in amounts resulting in the molar ratio and concentrations planned for each synthesis. Lanthanum and iron nitrate were dissolved in de-ionised water (DI-water) while the solution was stirred. KOH was added to the solution until the desired concentration was obtained. DI-water was added until the total volume of the solution was 75 mL. The reaction mixture was then transferred into a 125 mL PTFE-lined autoclave from Parr, giving a fill factor of 60 %. Crystallisation was carried out under autogenous pressure at 240 °C for 48 or 100 hours, the heating and cooling rates were 180 °C/h. The pressure inside the autoclave at this temperature is calculated to 21 bar. This calculation is shown in Appendix A.1. After the autoclave was cooled and depressurised the product was retrieved and washed. In order to get the lids off the cups, the cups were immersed in a beaker with ice and water for a short period of time, enough for the PTFE to shrink so that the lids could be removed. The washing procedure consisted of centrifugation with DI-water at 14 000 rpm for 10 minutes, and was performed repeatedly until the pH of the water poured off was 7. After the product was washed it was dried at 100 °C for one hour.

The synthesis parameters used in the direct hydrothermal syntheses are listed in Table 3.2. All the syntheses were carried out at a temperature of 240 °C, with heating and cooling rates of 180 °C/h, and a reactant solution volume of 75 mL which gives a fill factor of 60 %. Synthesis number 1, 2 and 3 are syntheses exploring the effect of potassium hydroxide concentration. Syntheses number 4 and 5 were performed to investigate the impact of changing the molar ratio of iron to lanthanum to 2 and 0.5. The effect of increasing the synthesis duration to 100 hours was explored in synthesis number 6.

A calcination study was performed on the product of synthesis number 3. Calcination was carried out for 2 hours at 600, 700 and 800 °C, with heating and cooling rates of 180 °C/h.

Table 3.2: Overview of the conditions used in each synthesis in the direct hydrothermal syntheses.

Synthesis	C_{La} [M]	C_{Fe} [M]	$R_{Fe/La}$	C_{KOH} [M]	Duration [h]
1	0.2	0.2	1	9	48
2	0.2	0.2	1	13	48
3	0.2	0.2	1	16	48
4	0.2	0.4	2	13	48
5	0.4	0.2	0.5	13	48
6	0.2	0.2	1	16	100

3.2.2 Two-Step Hydrothermal Synthesis

First step: Synthesis of lanthanum hydroxide nanorods
The first step of the two-step synthesis is hydrothermal synthesis of lanthanum hydroxide nanorods. This was performed in a 125 mL PTFE-lined autoclave from Parr. The synthesis conditions used are listed in Table 3.3.

Table 3.3: Overview of the conditions used in the synthesis of lanthanum hydroxide nanorods.

Temperature [°C]	C_{La} [M]	C_{KOH} [M]	Fill factor [%]	Duration [h]
180	0.031	5	60	12

This method was based on the synthesis of lanthanum hydroxide nanorods reported in the work by Wang et al. [14]. However, Wang et al. used La_2O_3 as the lanthanum reactant in their work, while in this work $La(NO_3)_3{\cdot}6H_2O$ has been used as the lanthanum precursor.

The same synthesis and washing procedure as described for the direct hydrothermal synthesis in Section 3.2.1 were used in the synthesis of lanthanum hydroxide nanorods, but with the conditions listed in Table 3.3. To investigate the behaviour of the nanorods at elevated temperature, pure lanthanum hydroxide was calcined at 350, 400, 500, 550 and 600 °C for 1 hour with heating and cooling rates of 180 °C/h.

Second step: Iron nitrate coverage and calcination
Coating of lanthanum hydroxide nanorods with iron nitrate solution and heat treatment of the obtained mixture was the second step of the two-step synthesis. This step was performed by two different methods: one with and one without the use of ultrasonic stirring.

The first method, without sonication, started with preparation of iron nitrate solution, by dissolving $Fe(NO_3)_3{\cdot}9H_2O$ in DI-water. NH_3 was added to the solution to adjust the pH to 10. A magnetic stir bar was used to stir the solution, and 0.25 g of $La(OH)_3$ obtained in the first step was added. This gave an iron to lanthanum molar ratio of 1:1. The beaker was placed on a hot plate and heated at 120 °C while being stirred. When all the water had evaporated, a dry layer of the product was left in the beaker. The powder was collected and characterised. A calcination study of the product was performed. Calcination was carried out for 1 hour at 200, 400, 500, 550, 600 and 650 °C with heating and cooling rates of 180 °C/h. This method will be referred to as the two-step hydrothermal synthesis without sonication.

The second method used ultrasonic stirring to disperse the lanthanum hydroxide nanorods. This synthesis route started with the preparation of a 0.25 M iron nitrate solution where $Fe(NO_3)_3{\cdot}9H_2O$ was dissolved in DI-water. From this solution 5.27 mL was measured out by the use of a graded cylinder, and transferred to a beaker. NH_3 was added to the solution to adjust the pH to 10. Lanthanum hydroxide synthesised in the first step was weighed out, 0.25 g, and transferred to the solution. This gave a molar ratio of iron to lanthanum of 1:1. An ultrasonic finger, a Branson Digital Sonifier Model 102C, was used to stir the solution. This was done with a 15 % pulse for 4 minutes. Then, the beaker was placed on a hot plate and heated at 80 °C while being stirred with a magnetic stir bar. The solution was sonicated again after 30 minutes by the ultrasonic finger, this was carried out with 15 % pulse for 4 minuts. After the second sonication, the beaker was placed on the hot plate at 80 °C and stirred by a magnetic stir bar. When all the water had evaporated, a dry powder was obtained. The powder was collected and characterised. A calcination study of the product was performed, like the one decribed for the method without soication. This method will be referred to as the two-step hydrothermal synthesis with sonication.

3.3 Characterisation

The morphology of the obtained product has been investigated by the use of a scanning electron microscope (SEM), while the phases present in the product have been explored by the use of X-ray diffraction (XRD). Details concerning the instruments, sample preparation and execution of the two methods will be presented in the following sections.

3.3.1 X-Ray Diffraction

X-ray diffraction has been performed with the instrument AXS D8Focus which has a Cu Kα X-ray tube, to explore the phase composition of the obtained products. The XRD spectra were obtained by scanning in the $2\,\theta$ range from $15\,^\circ$ to $85\,^\circ$ with a step size of $0.017\,^\circ$ and a 0.8 s counting time at each step. A substrate of single crystalline silicon was used as the sample holder in the scanning of the powder samples. The samples were prepared by first dissolving the powder in 96 % ethanol by the use of an ultrasonic bath. A small amount of this solution was transferred to the silicon substrate with a pipette. Evaporation of the ethanol follwed, and a thin layer of powder was left on the substrate. The substrate with the powder layer was placed in the D8Focus sample position and scanned while being rotated.

3.3.2 Scanning Electron Microscope

The morphology of the product has been investigated by the use of the scanning electron microscopy FE-SEM Zeiss Ultra 55 LE. The samples were prepared by dissolving the powder in 96 % ethanol by the use of an ultrasonic bath. A drop of this solution was transferred to a suitable substrate. After the ethanol had evaporated, a small amount of powder was left on the substrate. The sample was then covered by carbon to ensure conductivity of the sample and to minimise charge building up during scanning. This was done by the use of the carbon coater Agar Turbo Carbon Coater.

4 Results

The results of the syntheses performed will be presented in this chapter. First, results of the direct hydrothermal synthesis of lanthanum ferrite will be given in Section 4.1. Then, results of the two-step synthesis will be presented in section 4.2, where topochemical conversion of lanthanum hydroxide nanorods to lanthanum ferrite was attempted.

4.1 Direct Hydrothermal Synthesis of LFO

The results of the direct hydrothermal synthesis will be presented in this section. This includes the results of the study where potassium hydroxide concentration was varied, the molar ratio of iron to lanthanum was changed and the synthesis with increased synthesis duration. An overview of all synthesis parameters for all six syntheses can be found in Table 3.2 on page 19. A calcination study was performed on one of the synthesis products, and will also be presented in this section. The phase composition and morphology of the products have been investigated by the use of XRD and SEM respectively. Complete XRD spectra of all XRD scans presented in this section are given in Appendix B.1.

4.1.1 Variation of Potassium Hydroxide Concentration

The study of the effect of varying the potassium hydroxide concentration was performed. Three syntheses with potassium hydroxide concentrations of 9, 13 and 16 M were carried out, corresponding to synthesis number 1, 2 and 3. A comparison of the XRD scans obtained of the powders prepared is given in Figure 4.1. The concentration of potassium hydroxide increases upwards in the figure.

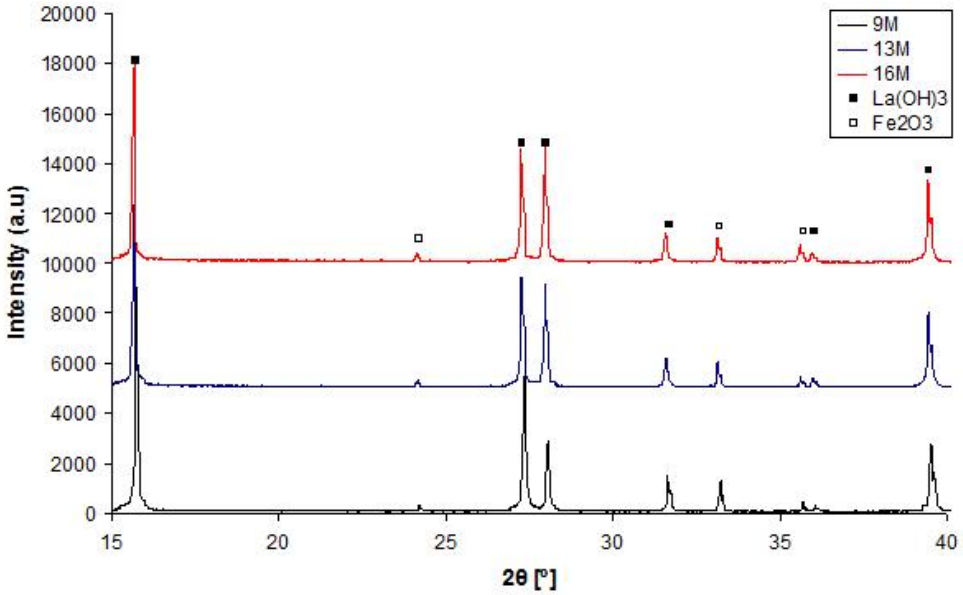

Figure 4.1: XRD spectra of synthesis number 1, 2 and 3 carried out with potassium hydroxide concentration of 9 M, 13 M and 16 M in the direct hydrothermal synthesis.

Analysis of the XRD spectra shows that there are two phases present in the products obtained when potassium hydroxide concentration was varied. These phases are $La(OH)_3$ and Fe_2O_3, with diffraction peaks located respectively below black squares and below open squares in the XRD scans. There are no differences in phase composition between the three syntheses. Lanthanum ferrite is not observed in the product of the syntheses performed.

SEM images showing the morphology of these synthesis products are presented in Figure 4.2. The images demonstrate that the products consist of platelets and rods. From the project work [1], it is known that lanthanum hydroxide forms rod structures, and iron oxide form platelet structures. The phase of the rods and platelets are therefore assigned to lanthanum hydroxide and iron oxide respectively. From the images in Figure 4.2 it is observed that the lanthanum hydroxide rods increase in diameter and decrease in length with increasing potassium hydroxide concentration, causing the aspect ratio to decrease with increasing potassium hydroxide concentration. A trend of increasing thickness of the iron oxide platelets is also seen with increasing concentration of potassium hydroxide.

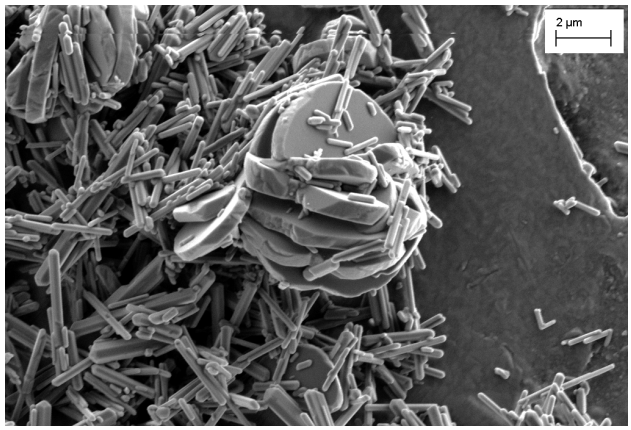

(a) 9 M KOH

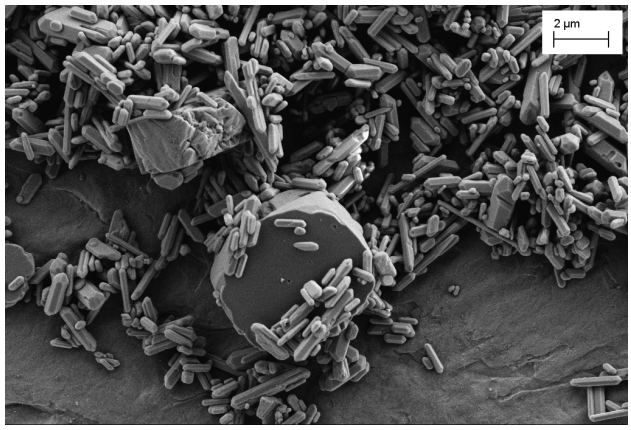

(b) 13 M KOH

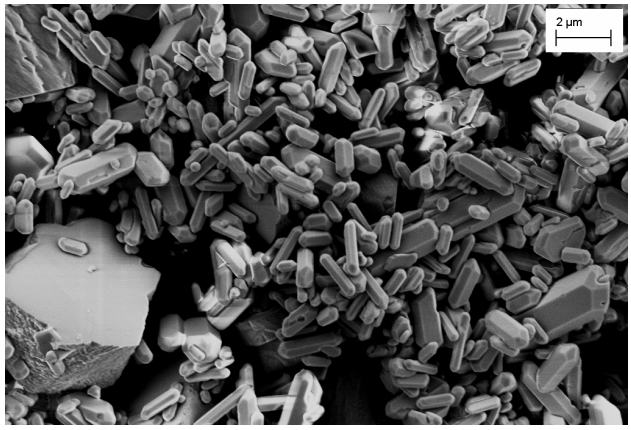

(c) 16 M KOH

Figure 4.2: SEM images of the products obtained from synthesis number 1, 2 and 3, where the potassium hydroxide concentration was varied, (a) 9 M, (b) 13 M and (c) 16 M.

4.1.2 Changing the Iron to Lanthanum Ratio

The effect of changing the molar ratio of iron to lanthanum, $R_{Fe/La}$, was explored. Two syntheses were performed, one with iron to lanthanum ratio of 2 and one with ratio of 0.5, these correspond to synthesis number 4 and 5. The XRD spectra of the products obtained are given in Figure 4.3, scan of the product with $R_{Fe/La}$ equal to 2 is the bottom spectrum, and scan of the product with $R_{Fe/La}$ equal to 0.5 is the top spectrum.

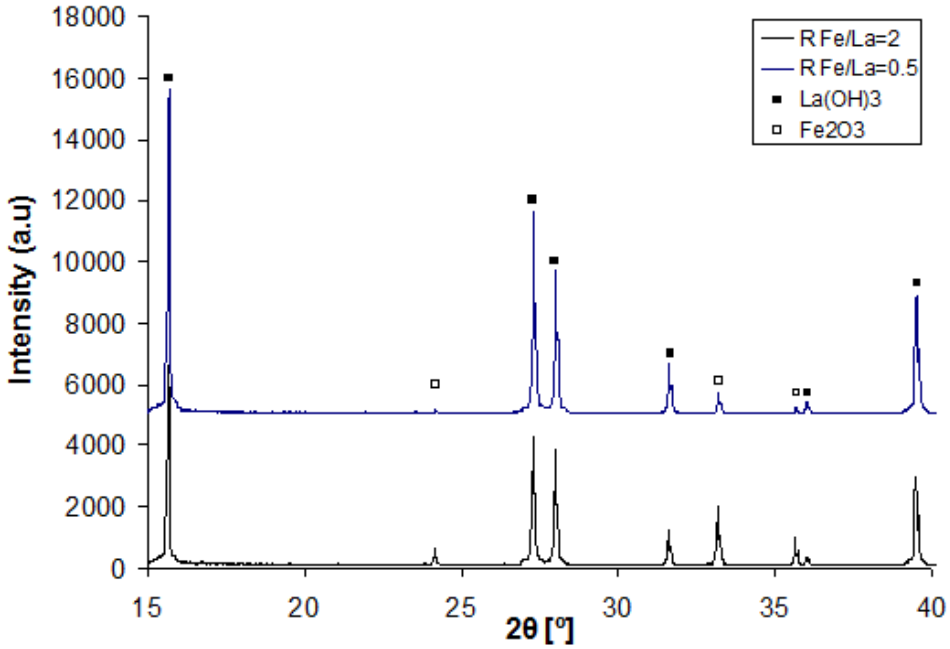

Figure 4.3: XRD spectra of the products obtained in synthesis number 4 and 5, where $R_{Fe/La}$ was changed from stoichiometric ratio to 2 and 0.5.

Analysis of the XRD spectra show that both synthesis products contain lanthanum hydroxide, with peaks below the black squares, and iron oxide, with peaks beneath the open squares in Figure 4.3. Lanthanum ferrite was not found in the products. The product morphology of these two products are displayed in Figure 4.4.

From Figure 4.4 it is seen that the products of the syntheses where $R_{Fe/La}$ has been varied consist of rods and platelets. Comparing the morphology of the products observed in Figure 4.4a where $R_{Fe/La}$ was 2 and Figure 4.4b where $R_{Fe/La}$ was 0.5, it can be seen that the length of the lanthanum hydroxide in average is shorter for the product where $R_{Fe/La}$ was 0.5.

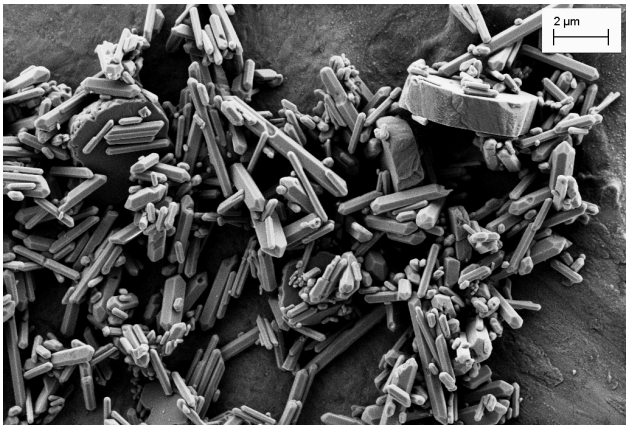

(a) $R_{Fe/La}$ equal 2

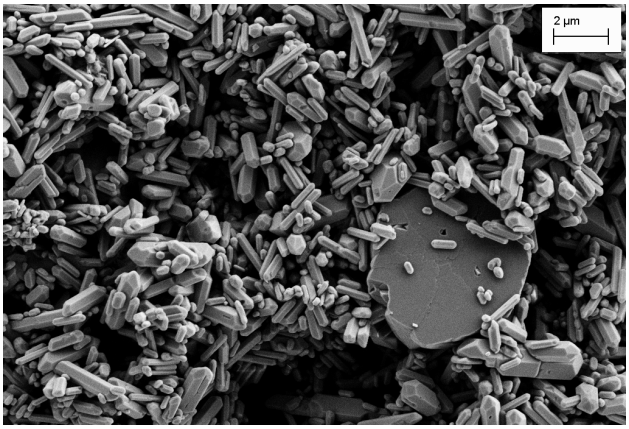

(b) $R_{Fe/La}$ equal 0.5

Figure 4.4: SEM images of the products obtained from synthesis number 4 and 5, with molar ratio of iron to lanthanum of (a) 2 and (b) 0.5.

4.1.3 Increasing Synthesis Duration

The effect of increasing the synthesis duration was explored in synthesis number 6, where the synthesis duration was 100 hours. The XRD scan of the obtained product is presented in Figure 4.5.

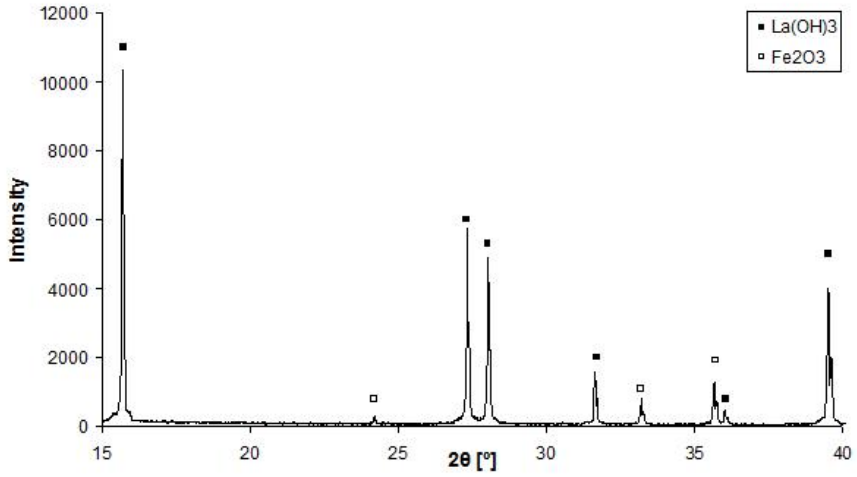

Figure 4.5: XRD spectrum of the product obtained in synthesis number 6, where the synthesis duration was increased to 100 hours.

The XRD scan show that the product consists of lanthanum hydroxide, with peaks located below the black squares, and iron oxide, with peaks below the open squares. Lanthanum ferrite is not present in the product. The morphology of this synthesis product is dispalyed in Figure 4.6.

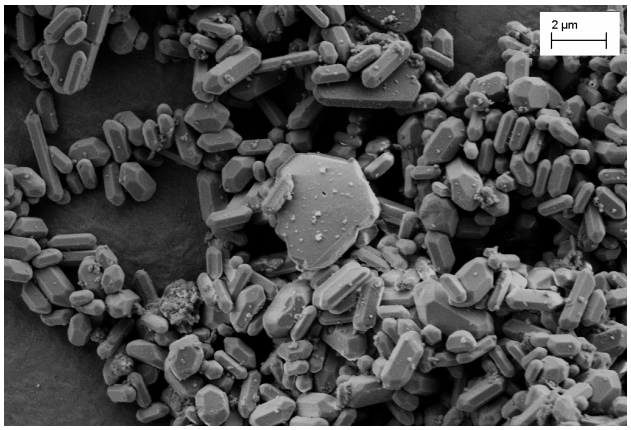

Figure 4.6: SEM image of the product obtained in synthesis number 6, where the synthesis duration was increased to 100 hours.

Platelets and rods are the structures observed in the product when the synthesis duration has been increased to 100 hours, shown in Figure 4.6. With the exception of the synthesis duration, the synthesis parameters used in this synthesis and in synthesis number 3 are identical. The duration of synthesis number 3 was 48 hours. The product morphology of synthesis number 3 is presented in Figure 4.2c. Comparing the lanthanum hydroxide rods obtained in these two syntheses it can be seen that the thickness of the rods in average is larger for the synthesis with increased duration.

4.1.4 Calcination Study

The product of synthesis number 3 was calcined for 2 hours at 600, 700 and 800 °C. The XRD scans of the calcined products are shown in Figure 4.7. The calcination temperature for the products which scans are presented in the figure increases upwards in the diagram. The bottom scan is of the raw product.

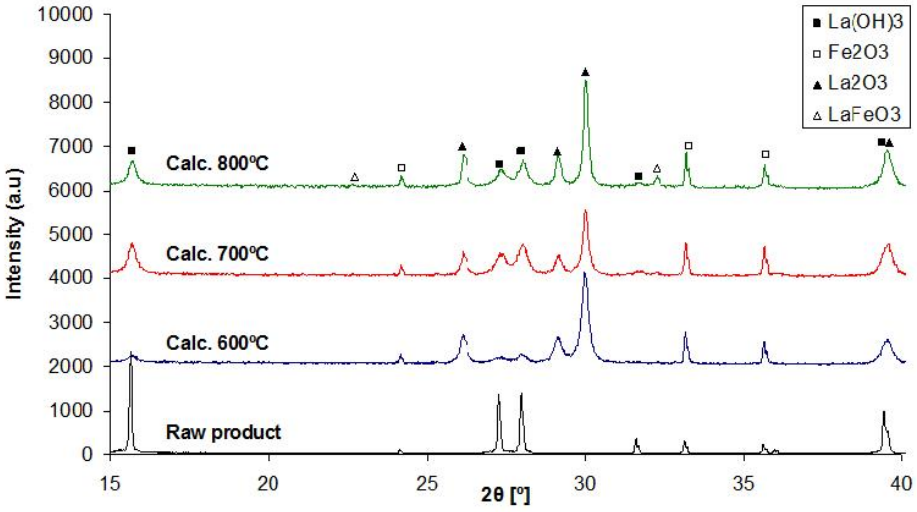

Figure 4.7: XRD spectra of raw product and calcined synthesis product of synthesis number 3. Calcination was performed for 1 hour at 600, 700 and 800 °C.

From Figure 4.7 it can be observed that lanthanum hydroxide and iron oxide are present in the raw product after calcination at all three temperatures, with diffraction peaks located below the black squares and the open squares respectively. After calcination at 600 °C lanthanum oxide has formed, and is also present in the product calcined at 700 and 800 °C. The peaks of lanthanum oxide are located below the black triangles. In the XRD scan of the sample calcined at 800°C small diffraction peaks of lanthanum ferrite have appeared. These peaks are located beneath the open triangles in Figure 4.7. The product morphology after calcination at 800 °C is presented in Figure 4.8.

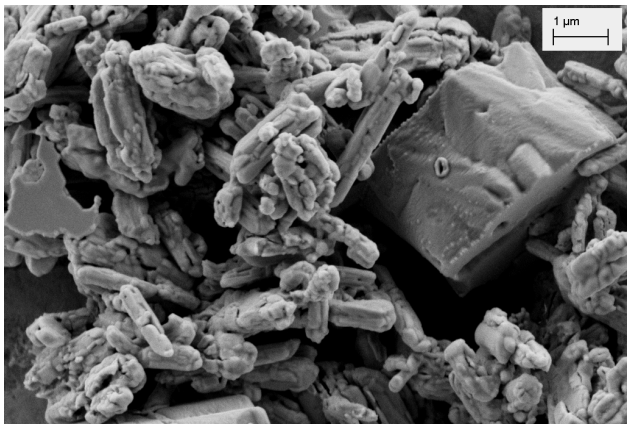

Figure 4.8: SEM image of calcined product of synthesis number 3. Calcination was performed for 1 hour at 800 °C.

The SEM image in Figure 4.8 shows that the rods in the product have lost the smooth surface planes and have started to rupture, compared to the rod structure seen in the uncalcined product in the SEM image in Figure 4.2c. The structure of the thick iron platelets has not altered much compared to the structure observed in the uncalcined product.

4.2 Two-Step Hydrothermal Synthesis of LFO

The results of the two-step synthesis will be presented in this section. Hydrothermal synthesis of lanthanum hydroxide nanorods is the first step in the two-step method, and the result of this synthesis will be presented first. A calcination study of the hydrothermally obtained lanthanum hydroxide was performed, and the result of this study will be presented in Section 4.2.2. Then, the results of the experiments of covering and reacting lanthanum hydroxide nanorods with iron nitrate will be given. Results of both methods

attempted, with and without the use of ultrasonic stirring, will be presented in Section 4.2.3 and Section 4.2.4 respectively. The phase composition of all products has been investigated by use of XRD, and SEM has been used to explore the morphology of the products. Complete XRD spectra of the XRD scans presented in this section are given in Appendix B.2.

4.2.1 Synthesis of Lanthanum Hydroxide Nanorods

The morphology and phase composition of the lanthanum hydroxide synthesised hydrothermally as the first step of the two-step synthesis will be presented in this section. The XRD spectrum of the obtained product is showed in Figure 4.9.

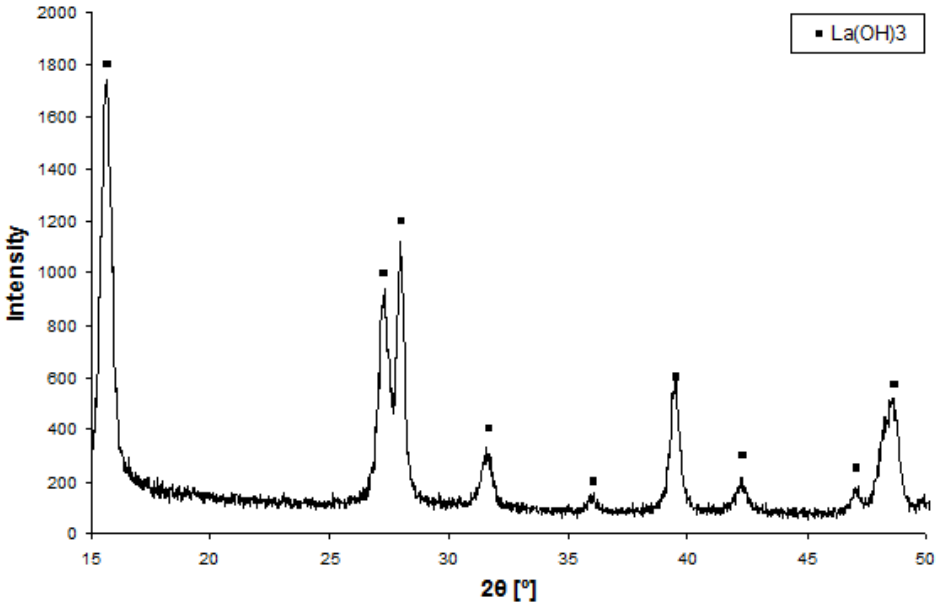

Figure 4.9: XRD spectrum of the as-synthesised product of the hydrothermal synthesis of lanthanum hydroxide nanorods.

From Figure 4.9 it can be observed that the product consists of lanthanum hydroxide, and is phase pure. Diffraction peaks of lanthanum hydroxide are located beneath the black squares in the figure. Several diffraction peaks are observed in the XRD scan, indicating that the lanthanum hydroxide nanorods do not have a strong preferential orientation. The rods are therefore not single crystalline, but consist of randomly oriented crystals and are polycrystalline. An SEM image displaying the morphology of the product is shown in Figure 4.10.

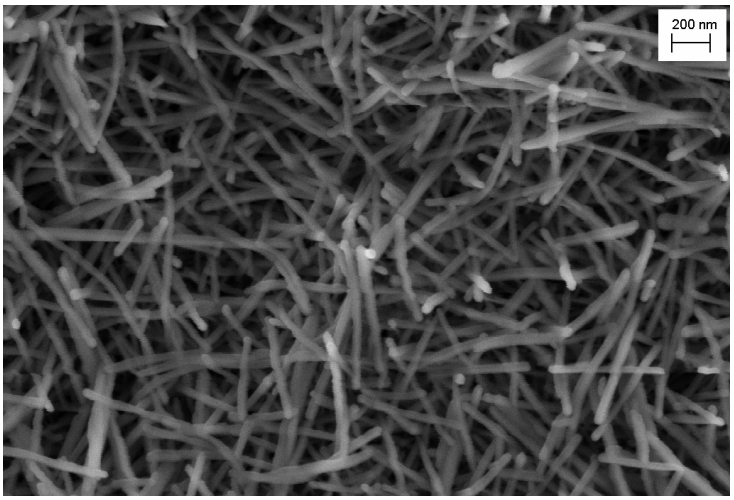

Figure 4.10: SEM picture of the hydrothermally synthesised lanthanum hydroxide nanorods morphology.

Figure 4.10 shows that the product consists of nanorods, the shortest rods observed in the product are approximately 0.5 μm, and the longest are 2 μm. The diameter of the rods is 80 nm. The aspect ratio is therefore in the range from 6.25 to 25.

4.2.2 Calcination Study of Lanthanum Hydroxide Nanorods

Pure lanthanum hydroxide nanorods were calcined for 1 hour at 300, 350, 400, 500, 550 and 600 °C. XRD spectra of the calcined products are shown in Figure 4.11. The calcination temperature for the products which scans are presented in the figure increases upwards in the plot diagram. The bottom spectrum is of the raw product.

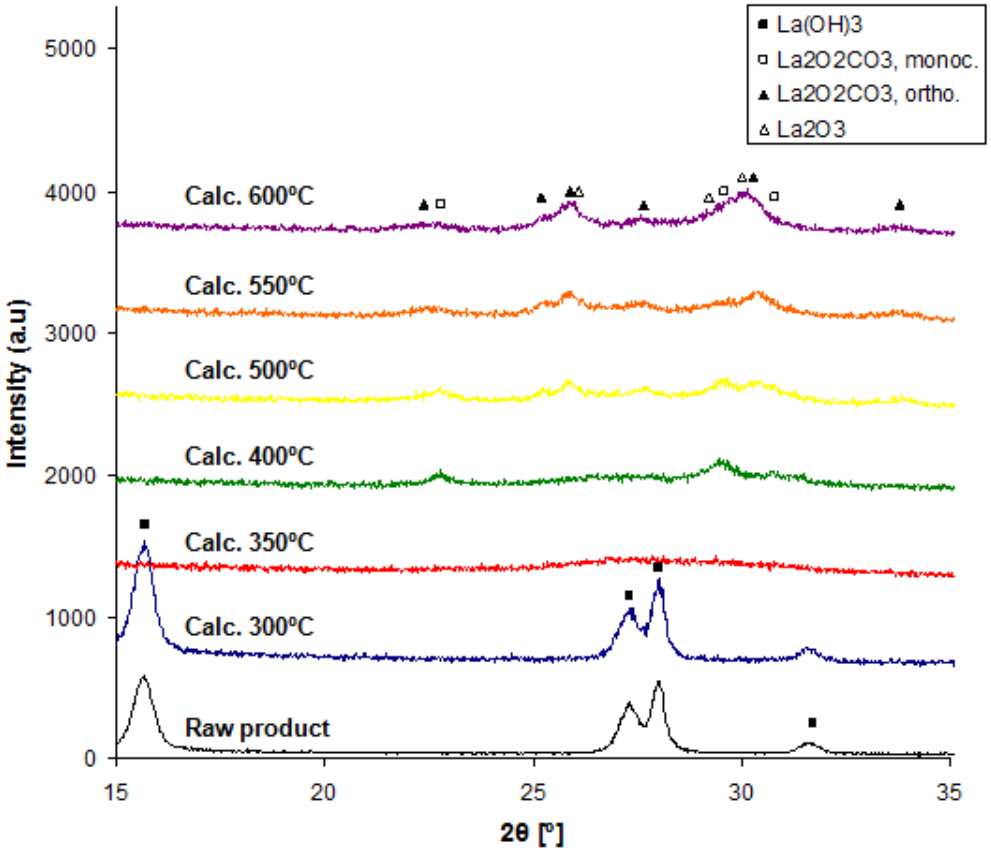

Figure 4.11: XRD spectra of the raw product and the calcined lanthanum hydroxide. Lanthanum hydroxide was held at 300, 350, 400, 500, 550 and 600 °C for 1 hour.

An enlargement in the intensity direction in the spectra of the calcined products at 350 °C and at higher temperatures have been performed to clearly show the small diffraction peaks in these spectra. These magnified scans are displayed in Figure 4.12. The same colour of the spectra have been used to indicate products calcined at the same temperature in Figure 4.11 and Figure 4.12.

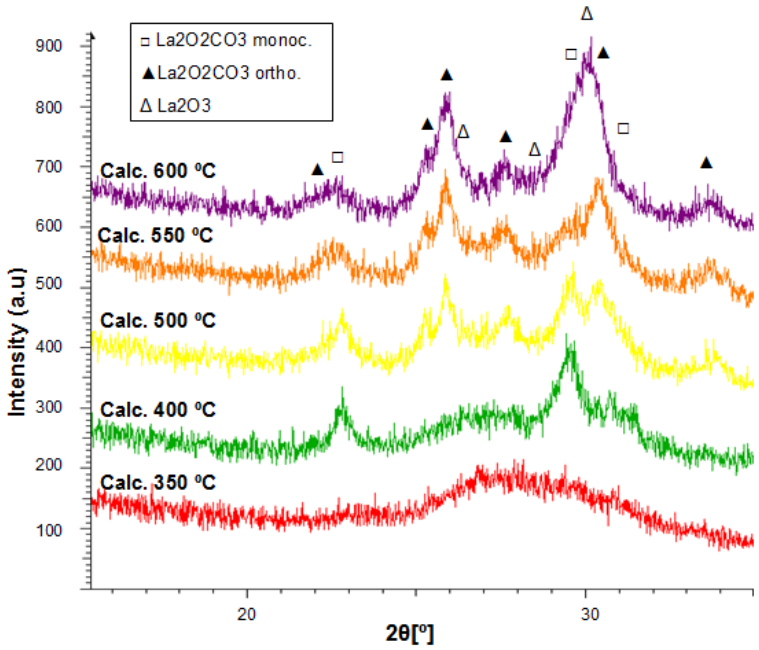

Figure 4.12: XRD spectra of the calcined lanthanum hydroxide at 350, 400, 500, 550 and 600 °C for 1 hour.

Figure 4.11 shows that the phase composition of the product calcined at 300 °C, is the same as the phase composition of the raw product, which consists of lanthanum hydroxide. The diffraction peaks of this phase are located below the black squares. At 350 °C this phase is lost, which is seen in Figure 4.12. There are no diffraction peaks present in this XRD scan, indicating that the product consists of an amorphous phase after being heating to 350 °C. After calcination at 400 °C diffraction peaks of monoclinic $La_2O_2CO_3$ appears, which are located below the open squares. At 500 °C diffraction peaks belonging to orthorhombic $La_2O_2CO_3$ start to appear, which are located beneath the black triangles. These two lanthanum oxide carbonate phases are present after calcination at 550 °C, and at this temperature La_2O_3 has formed, which peaks are shown below the open triangles. The lanthanum oxide carbonate phases and the lanthanum oxide phase make up the phase composition for the product calcined at 600 °C.

The morphologies of the product after calcination at 300, 350 and 400 °C are displayed in the SEM images in Figure 4.13, and SEM images of calcined products at 500, 550 and 600 °C are shown in Figure 4.14.

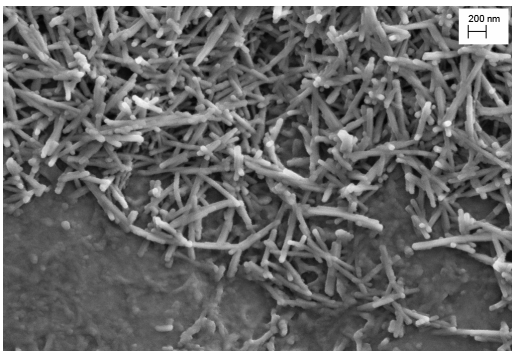

(a) 300 °C

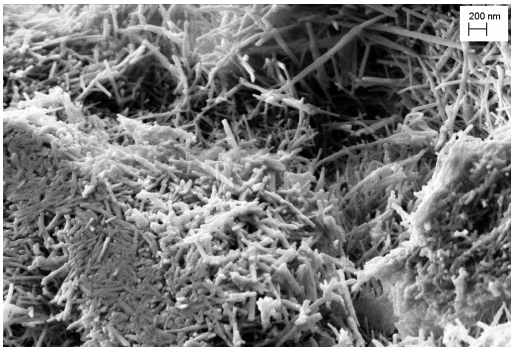

(b) 350 °C

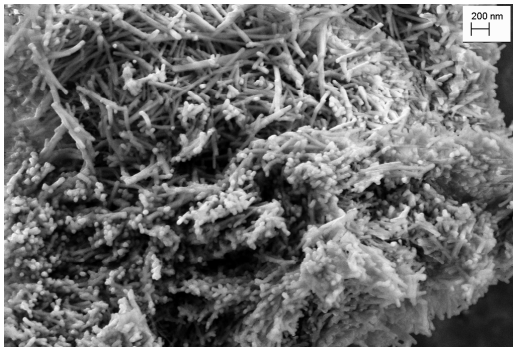

(c) 350 °C

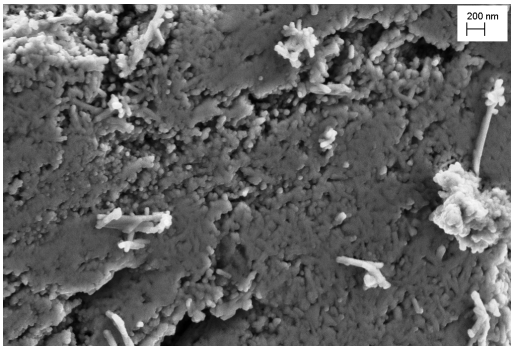

(d) 400 °C

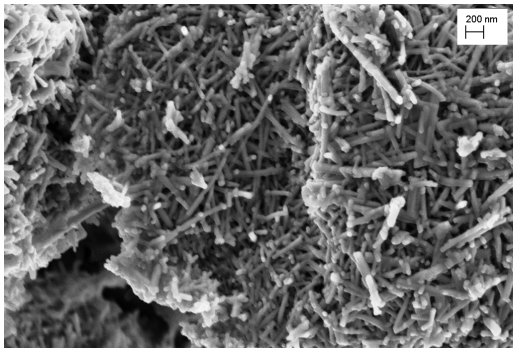

(e) 400 °C

Figure 4.13: SEM pictures of pure lanthanum hydroxide nanorods after 1 hour calcination at (a) 300 °C, (b) and (c) 350 °C and (d) and (e) 400 °C.

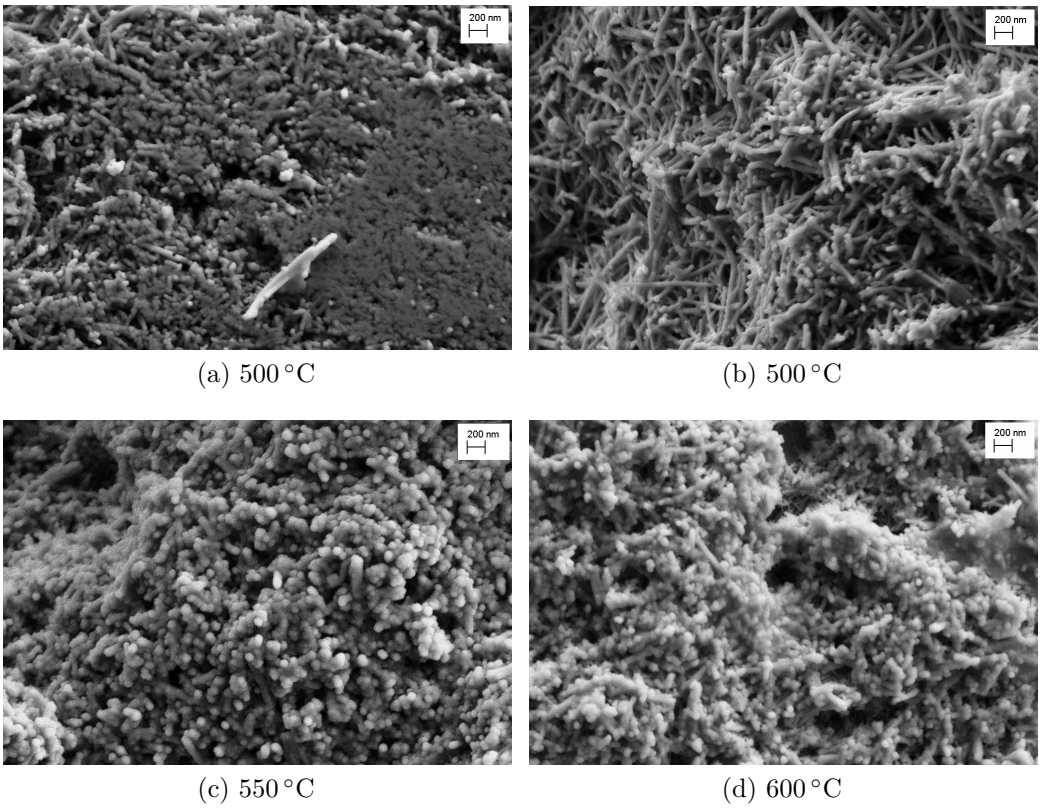

(a) 500 °C (b) 500 °C

(c) 550 °C (d) 600 °C

Figure 4.14: SEM pictures of pure lanthanum hydroxide nanorods after 1 hour calcination at (a) and (b) 500 °C, (c) 550 °C and (d) 600 °C.

Investigating the morphology of the product calcined in Figure 4.13, the rod structure of the product calcined at 300 °C in Figure 4.13a is similar to the rod structure observed in the raw product in Figure 4.10. Partly agglomeration can be observed in the sample calcined at 350 °C. This is seen to the bottom left in Figure 4.13b. The morphology of the product calcined at 400 °C is similar to the morphology observed at 350 °C, however this product is even more agglomerated as can be observed in Figure 4.13d, but some areas still contains rod structure as in the area imaged in Figure 4.13e.

The calcined products at 500, 550 and 600 °C are displayed in Figure 4.14. In the product calcined at 500 °C it is seen that the rods have agglomerated even more than the product calcined at 400 °C, this is observed in Figure 4.14a. However, in some parts of the product the rods have not agglomerated to a large extent, and intact nanorods are still present, which can be seen in Figure 4.14b. In the products calcined at 550 and 600 °C it can be seen that the rods have ruptured and formed small particle spheres, which can be observed in Figure 4.14c and in Figure 4.14d.

The phase composition and morphology observed in the products after calcination at the different calcination temperatures are summarised in Table 4.1.

Table 4.1: Summary of the phases and the morphologies present after calcination of pure lanthanum hydroxide nanorods at 300, 350, 400, 500, 550 and 600 °C.

Calcination temperature [°C]	**Phases**	**Morphology**
Raw powder	$La(OH)_3$	Nanorods
300	$La(OH)_3$	Nanorods
350	Amorphous	Nanorods, agglomeration
400	$La_2O_2CO_3$ monoc.	Nanorods, agglomeration
500	$La_2O_2CO_3$ monoc., $La_2O_2CO_3$ ortho.	Nanorods, agglomeration
550	$La_2O_2CO_3$ monoc., La_2O_3, $La_2O_2CO_3$ ortho.	Spherical particles
600	$La_2O_2CO_3$ monoc., La_2O_3 $La_2O_2CO_3$ ortho.	Spherical particles

4.2.3 Two-Step Synthesis, Method without Sonication

The phase composition and morphology of the product of the two-step hydrothermal synthesis, method without the use of sonication, will be presented in this section. The product was calcined for 1 hour at 200, 400, 500, 550, 600 and 650 °C. XRD scans of the raw product and calcined products are shown in Figure 4.15. The XRD spectrum of the raw product is given in the bottom of the figure. The scans presented above this spectrum are shown in order of increasing calcination temperature upwards in the figure.

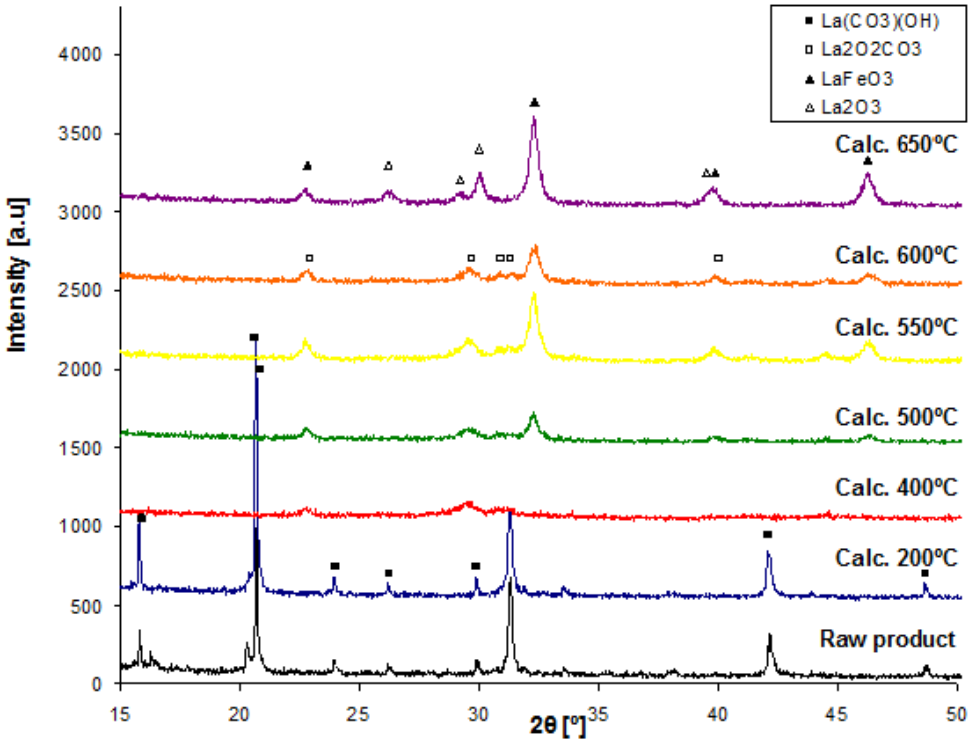

Figure 4.15: XRD spectra of the raw product and the calcined products of the two-step synthesis, method without use of sonication. Calcination temperatures were 200, 400, 500, 550, 600 and 650 °C, and the samples were held at this temperature for 1 hour.

In the raw product and in the calcined product at 200 °C the XRD spectra show presence of $La(CO_3)(OH)$ in Figure 4.15, with peaks below the black squares. These two XRD spectra have one unidentified peak located at 32 °. All phases with combinations including lanthanum, iron, oxygen, hydrogen, nitrogen and carbon have been explored if they could fit with this peak.

Lanthanum in the elemental state has a diffraction peak located at 32 °. However, lanthanum in this state is not believed to be present in this product. Another match was not found with the use of the EVA software used for identifying the phases belonging to the diffraction peaks of the XRD spectra. It is therefore an uncertainty about the determined lanthanum hydroxide carbonate phase, other phases may be present in the product.

From further investigation of Figure 4.15, it is observed that a new phase with small diffraction peaks appears in the product calcined at 400 °C. This phase is $La_2O_2CO_3$, which is present in the product calcined at 500, 550 and 600 °C as well. Diffraction peaks of this phase, lanthanum oxide carbonate, are located below the open squares in the XRD spectra. Lanthanum oxide carbonate has disappeared after calcination at 650 °C, and peaks of La_2O_3 are observed at this temperature. These peaks are located beneath the open triangles. It is therefore believed that the carbonate of lanthanum oxide carbonate decomposes in the temperature interval 600 °C to 650 °C, which results in formation of lanthanum oxide. At 500 °C $LaFeO_3$ has formed. Diffraction peaks of this phase are located below black triangles, and are also present after calcination at 550, 600 and 650 °C.

An iron containing phase is not seen until lanthanum ferrite has formed after calcination at 500 °C. Iron is present in the product, as the product after covering lanthanum hydroxide with iron nitrate has a reddish - brown colour, as opposed to the white lanthanum hydroxide powder. Any diffraction peaks of an iron phase may not be seen in the XRD spectrum at lower temperature because the iron phase or phases are not crystalline. Another explanation is that the iron phase is correlated with the unidentified peak at 32 °, however, research of possible phases including iron have been performed and resulted in no matching phase with this peak.

The morphology of the raw product of the two-step synthesis products, where sonication was not applied, is presented in Figure 4.16.

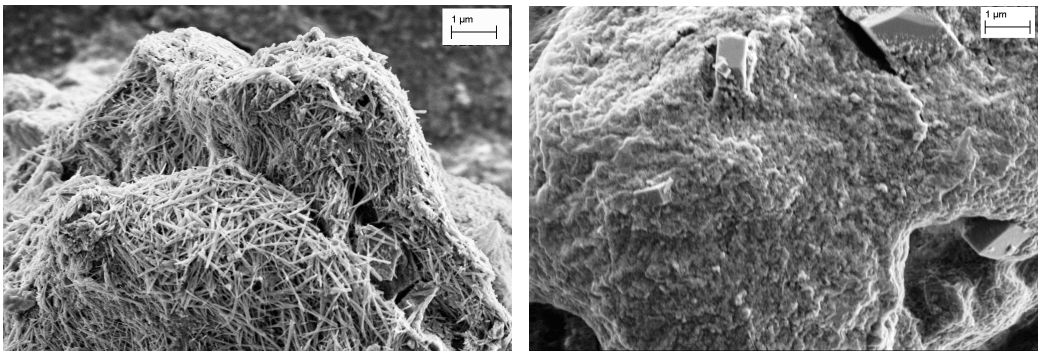

(a) Raw product (b) Raw product

Figure 4.16: SEM images of two particles found in the raw product of the two-step synthesis, method without the use of ultrasonic stirring. The product is not homogeneous, and rods are found in some parts of the product (a), but are not present in other parts (b).

Nanorods are found in the product as shown in Figure 4.16a. However the product is not homogeneous, and particles without rods are found, which can be observed in Figure 4.16b. Images of the morphologies observed after the product was calcined at 200, 400, 500, 550, 600 and 650 °C are displayed in Figure 4.17

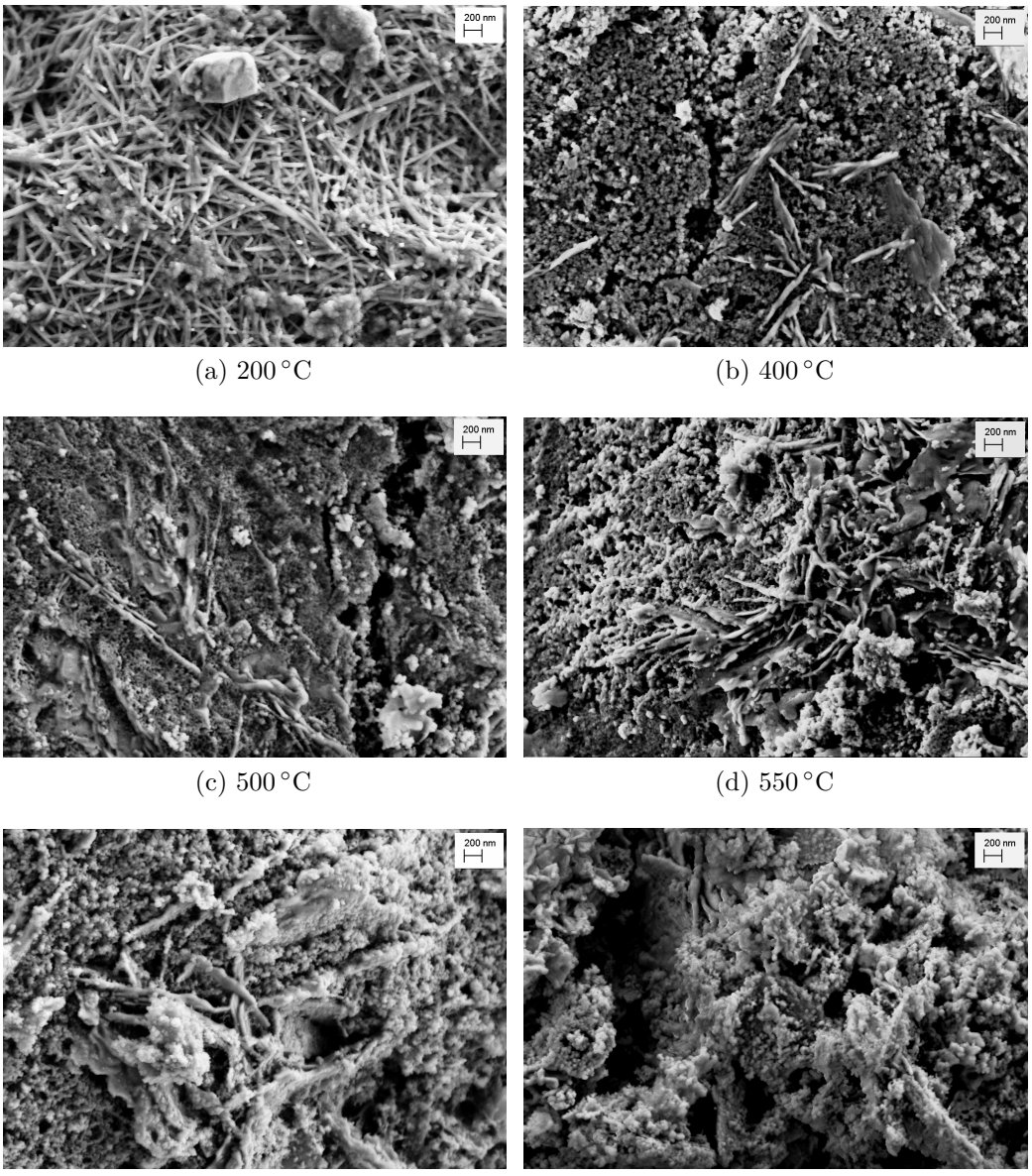

(a) 200 °C (b) 400 °C

(c) 500 °C (d) 550 °C

(e) 600 °C (f) 650 °C

Figure 4.17: SEM images of calcined products of the two-step synthesis, method without the use of sonication, after 1 hour at (a) 200 °C, (b) 400 °C, (c) 500 °C, (d) 550 °C, (e) 600 °C and (f) 650 °C.

The morphology of the calcined product at 200 °C is shown in Figure 4.17a. This SEM image show that the rod structure is preserved after 1 hour calcination at 200 °C, however the product does not consists solely of nanorods. A cubic shaped crystallite is observed in this image. Product calcined at 400 °C or at higher temperature does not contain nanorods. Agglomeration of the rods has started before 400 °C, which can be seen in Figure 4.17b. In this sample a long, thin structure in the surface of the agglomerated layer can also be observed. The morphology of the calcined product at 500 °C is displayed in Figure 4.17c. The morphology of this product resembles the morphology observed in the 400 °C sample. Increasing the calcination temperature 50 °C, to 550 °C, a structure growing out of the surface is observed, which can be seen in Figure 4.17d. After calcination at 600 °C and 650 °C small spherical particles have started to form, and are present in the images displayed in Figure 4.17e, and Figure 4.17f.

The phase compositions and the morphologies of the raw product and the products calcined at the different temperatures are summarised in Table 4.2.

Table 4.2: Summary of the phase compositions and morphologies of the products after calcination at 200, 400, 500, 550, 600 and 650 °C.

Calcination temperature[°C]	**Phases**	**Morphology**
Raw powder	$La(CO_3)(OH)$	Nanorods, cubes, particles without rods
200	$La(CO_3)(OH)$	Nanorods, cubes, particles without rods
400	$La_2O_2CO_3$	Agglomerated layer with a long, thin structure in the surface
500	$LaFeO_3$, $La_2O_2CO_3$	Agglomerated layer, long, thin structure in surface, spherical particles
550	$LaFeO_3$, $La_2O_2CO_3$	Agglomerated layer, outgrowing planes of the surface, spherical particles
600	$LaFeO_3$, $La_2O_2CO_3$	Spherical particles, outgrowing structure
650	$LaFeO_3$, La_2O_3	Spherical particles, outgrowing structure

From Table 4.2 it is seen that the nanorod structure is lost between 200 and 400 °C, and that formation of lanthanum ferrite is not observed before the calcination temperature is raised to 500 °C. The rod structure and the lanthanum ferrite phase are therefore not obtained simultaneously. The

two-step synthesis method without ultrasonic stirring did not result in the formation of lanthanum ferrite nanorods.

4.2.4 Two-Step Synthesis, Method with Sonication

Ultrasonic stirring was applied in the two-step synthesis in order to obtain a more homogeneous distribution of the rods than obtained in the two-step synthesis where ultrasonic stirring was not used. The XRD spectrum of the raw product is shown in Figure 4.18.

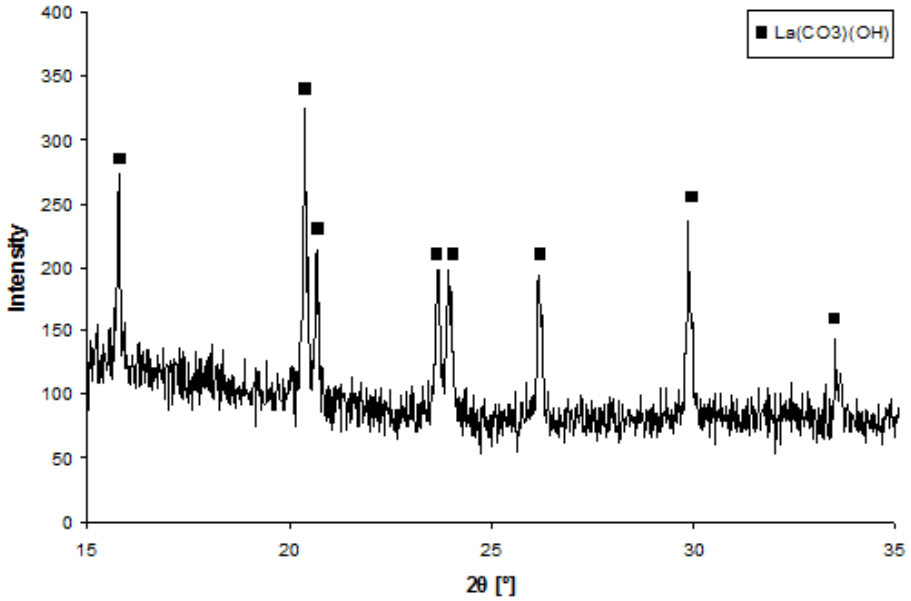

Figure 4.18: XRD spectrum of the raw product obtained in the two-step synthesis where ultrasonic stirring was applied.

From the XRD spectrum of the raw product obtained in the two-step synthesis where ultrasonic stirring was used, it can be observed that the product consists of $La(CO_3)(OH)$. The morphology of this product is displayed in Figure 4.19.

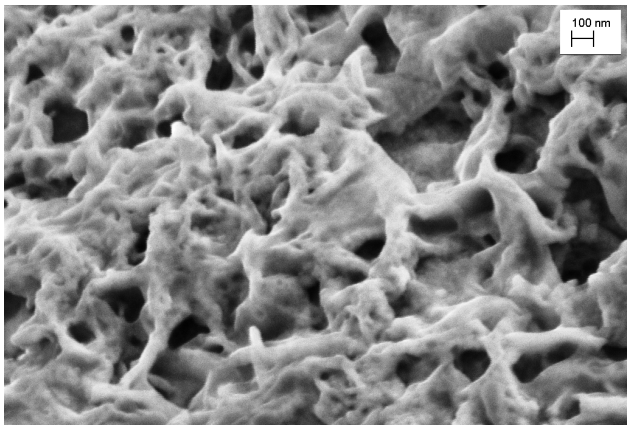

(a) Raw product

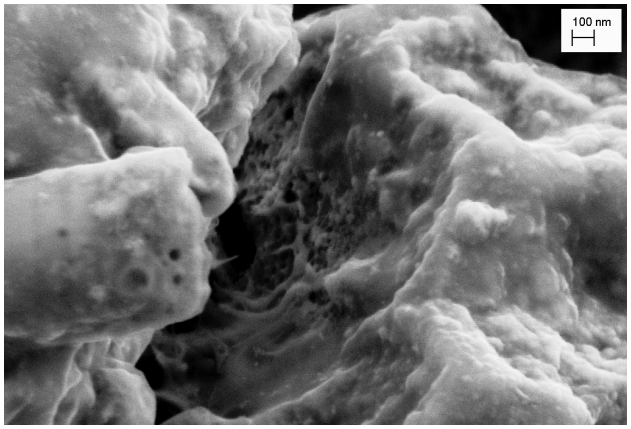

(b) Raw product

Figure 4.19: SEM images of the raw product of the two-step synthesis where sonication was applied.

The morphology of the synthesis product obtained in the two-step synthesis where ultrasonic stirring was applied did not contain any nanorods as can be seen in Figure 4.19. Rods were not observed after calcination either. SEM images and XRD spectra of the calcined products are therefore not presented.

5 Discussion

The results presented in the preceding chapter will now be reviewed and discussed. First, the aspects of the direct synthesis method will be looked into in Section 5.1, before the two-step syntheses are explored in Section 5.2. The last section, Section 5.3, will discuss possibilities for research which can be performed to further investigate hydrothermal synthesis of lanthanum ferrite.

5.1 Direct Hydrothermal Synthesis of LFO

Discussion related to the direct synthesis will be presented in this section. The focus will be on the thermodynamic stability of lanthanum ferrite under the reaction conditions applied in the direct synthesis. The calcination study of the direct synthesis product will also be explored, and will be presented in Section 5.1.2.

5.1.1 Stability of Lanthanum Ferrite

The product obtained in the syntheses performed by direct synthesis contained two phases, lanthanum hydroxide and iron oxide. The objective of synthesising LFO in a rod shaped nanostructure with a high aspect ratio was not achieved. Several attempts were performed, where synthesis parameters were varied to find a set of reaction conditions resulting in lanthanum ferrite. This included variation of the potassium hydroxide concentration, changing the iron to lanthanum ratio and an increase of the synthesis duration. This was done in order to reproduce the work by Hu et al. [12], where LFO was synthesised hydrothermally. The work performed by Hu et al. is described in Section 2.3.

The phases present in the synthesis products obtained in the project work, where $La_{0.2}Sr_{0.8}FeO_3$ was attempted synthesised, did also contain lanthanum ferrite and iron oxide, as well as strontium hexaferrite and strontium carbonate [1]. Strontium was removed from the system in this work, so no strontium containing phases are present in the synthesis products obtained in the master thesis work. As the synthesis products of both the project work, and the master thesis work contains iron oxide and lanthanum hydroxide, these two phases seem to be the most stable phases under the reaction conditions used.

To explore if iron oxide and lanthanum hydroxide are the most stable phases under the conditions employed in the direct syntheses, research on the stability of lanthanum ferrite has been performed. Thermodynamic calculations of the

temperature where LFO becomes more stable than iron oxide and lanthanum hydroxide have been executed. This temperature will be referred to as the transition temperature. The reaction describing the transition from iron oxide and lanthanum hydroxide to lanthanum ferrite is shown in Equation 5.1.

$$2\,La(OH)_3 + Fe_2O_3 \rightarrow 2\,LaFeO_3 + 3\,H_2O\,(liq) \tag{5.1}$$

The Gibbs energy for this reaction, $\Delta G_r(T, a_w)$, has been calculated as a function of temperature and water activity, according to Equation 5.2.

$$\Delta G_r(T, a_w) = \Delta G_r^\circ(T) + RTlna_w^3 = \Delta G_r^\circ(T) + 3RTlna_w \tag{5.2}$$

The water activity is dependent on the potassium hydroxide concentration of the solution. A model describing this relation has been included in the calculations [15]. Since potassium hydroxide concentrations of 9, 13 and 16 M have been used in the direct syntheses, the calculations were based on these three concentrations of potassium hydroxide. The detailed calculations are presented in Appendix A.2. A diagram of the obtained results where the Gibbs energy in Equation 5.2 has been plotted as a function of temperature is displayed in Figure 5.1.

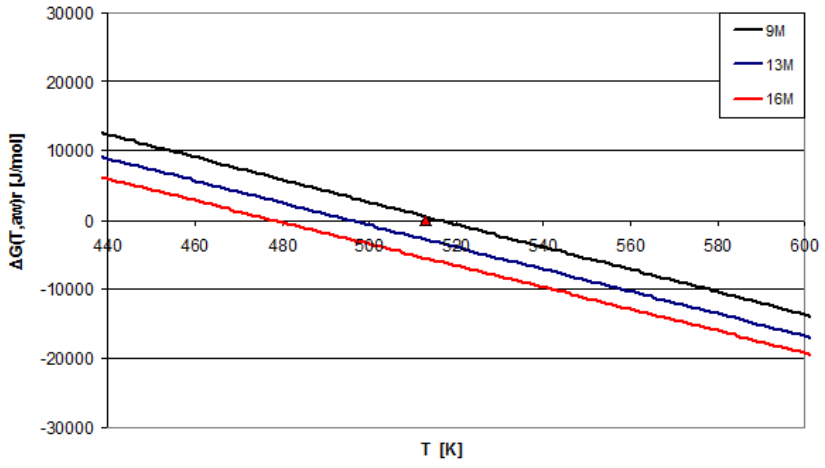

Figure 5.1: Gibbs energy as a function of temperature for the reaction where iron oxide and lanthanum hydroxide reacts and form LFO and water from a solution with 9, 13 and 16 M potassium hydroxide concentration.

From Figure 5.1 it can be observed that the transition temperatures where Gibbs energy is zero are 244 °C (517 K), 224 °C (497 K) and 206 °C (479 K), when concentrations of potassium hydroxide of respectively 9, 13 and 16 M are used. The synthesis temperature in the direct synthesis was 240 °C (513 K), this temperature is indicated by the red triangle in the figure. The transition temperature is at a higher temperature than the synthesis temperature in the case where 9 M potassium hydroxide is employed in the synthesis. This indicates that lanthanum ferrite should not be stable under these synthesis conditions. When potassium hydroxide concentrations of 13 and 16 M are used, the transition temperatures are lowered to a temperature below the synthesis temperature. This indicates that lanthanum ferrite is stable under these reaction conditions, and should have been observed in the synthesis product of the syntheses where 13 and 16 M potassium hydroxide concentrations were applied. At least, according to the thermodynamic calculations performed. However, lanthanum ferrite is not observed after syntheses using these reaction conditions.

Some approximations are performed in the calculation of the transition temperatures, which could cause the calculated temperatures to deviate from the actual transition temperatures. The water activity has been included in these calculations by the use of a model which describes the water activity as a function of potassium hydroxide concentration and temperature [15]. This model is developed from regression of experimental data, and may not be completely accurate at the specific conditions used in this work. The difference in heat capacity between products and reactants, ΔC_p, is used in the calculation of the standard enthalpy and entropy, which are included in order to calculate the Gibbs energy as a function of temperature. The heat capacities of the reactants and products used to calculate ΔC_p are dependent on temperature. However, this temperature dependence has not been included in the calculations, because heat capacities as a function of temperature for all the reactants and products were not found in literature. The difference in heat capacity of products and reactants is calculated at 298 K and is assumed to be independent of temperature, which can give an error in the calculated transition temperatures. However, making this assumption is not believed to contribute in a large degree to the error quantity.

Even though the calculation may not give the precise transition temperatures, the transition temperatures calculated are believed to be close to the actual temperatures where lanthanum ferrite becomes more stable than iron oxide and lanthanum hydroxide. The calculations show that for a given concentration of potassium hydroxide there exists a border temperature to the stability region of lanthanum ferrite, which decreases with increasing potassium

hydroxide concentration. For the potassium hydroxide concentrations applied in this work this transition temperature is close to the synthesis operation temperature used in the direct hydrothermal syntheses.

The difference of the free energy between iron oxide and lanthanum hydroxide compared to lanthanum ferrite is small close to the temperature transition. A small driving force for nucleation of lanthanum ferrite in the temperature region just above the transition temperature is believed to be the reason why it has not been possible to produce lanthanum ferrite in the direct hydrothermal syntheses, even though the calculation indicates that the potassium hydroxide concentration was high enough to stabilise lanthanum ferrite. Considering homogeneous nucleation theory, the critical size of a stable nucleus forming in a solution varies inversely with the driving force for nucleus formation [16]. Since the driving force for nucleation is small, the critical size of a stable nucleus would be large. In order to obtain stable lanthanum ferrite nucleus which do not dissolve, the nucleus must be of a certain size. Unattainable nucleus exceeding the critical nucleus size could explain why lanthanum ferrite has not been able to form, even though the thermodynamic calculation indicates that it should form.

The formation of lanthanum ferrite under the conditions used can be hindered kinetically as the thermodynamics of the system indicate that lanthanum ferrite is stable. The kinetics governing the system is time dependent. Without the appropriate synthesis duration, the reaction might not be complete even when the correct synthesis conditions are applied [17]. The request to form smaller crystallites than observed in the work by Hu et al. [12], by reducing the synthesis duration to 48 hours, may not have been beneficial for the synthesis of LFO. However, a synthesis performed with synthesis duration of 100 hours was conducted, and lanthanum ferrite was not observed in this synthesis product either. The presence of other species in the reaction mixture, even pollutants, can affect the kinetics of this type of system. This could be the explanation to why Hu et al. [12] obtained lanthanum ferrite in the synthesis products. In their syntheses chromium species were present in the reaction solution, which could have altered the kinetics of the system, to the extent that LFO was attainable. However, this is a speculation.

5.1.2 Calcination of the Direct Synthesis Product

A calcination study of the product obtained in the direct synthesis, synthesis number 3, was performed to explore if it was possible to form lanthanum ferrite rods, by calcining the synthesis product. The product of this synthesis

was heated at 600, 700 and 800 °C for 2 hours. The XRD spectra of the calcined products show that small LFO diffraction peaks are present after calcination at 800 °C. This is demonstrated in Figure 4.7. Lanthanum ferrite is not present in the product calcined at 600 and 700 °C. In addition to LFO in the product calcined at 800 °C, the presence of lanthanum oxide, iron oxide and lanthanum hydroxide is observed. Lanthanum hydroxide is not believed to be present at the actual calcination temperatures, as this phase should have decomposed at a lower temperature according to the calcination study of pure lanthanum hydroxide, and the decomposition temperature of lanthanum hydroxide reported by Ozawa et al. [18]. The first decomposition step reducing lanthanum hydroxide to lanthanum oxide hydroxide is stated to be at a temperature of 340 °C. The second step, dehydration of lanthanum oxide hydroxide to lanthanum oxide, is reported at 500 °C. After calcination at 600 °C and higher temperatures, lanthanum hydroxide should have decomposed, and not be present in the calcined product.

A possible explanation why lanthanum hydroxide is seen in the products after calcination is that lanthanum oxide may have taken up water from the atmosphere during cooling which have caused the formation of lanthanum hydroxide. When pure lanthanum hydroxide was calcined this was not seen, however in this study lanthanum oxide carbonate had formed, which alters the system. The different behaviour during heating seen between the lanthanum hydroxide rods obtained in the direct synthesis number 3 and in the first step in the two-step synthesis is probably caused by the different synthesis conditions they were synthesised under. Products of the two syntheses have rods with different morphologies and sizes. The rods obtained in the first step of the two-step synthesis have a smaller diameter and are longer than the rods in synthesis product 3.

Lanthanum ferrite rods were not obtained by calcination of the product obtained in synthesis 3. The rods have started to rupture at 800 °C, and only a small amount of LFO has formed at this temperature. In retrospect, a calcination of the product obtained in synthesis number 1 would have been a better alternative for this calcination study. The lanthanum hydroxide rods and the iron oxide platelets are thinner in this product compared to the product of synthesis 3. SEM images of the morphology of the two synthesis products are shown in Figure 5.2.

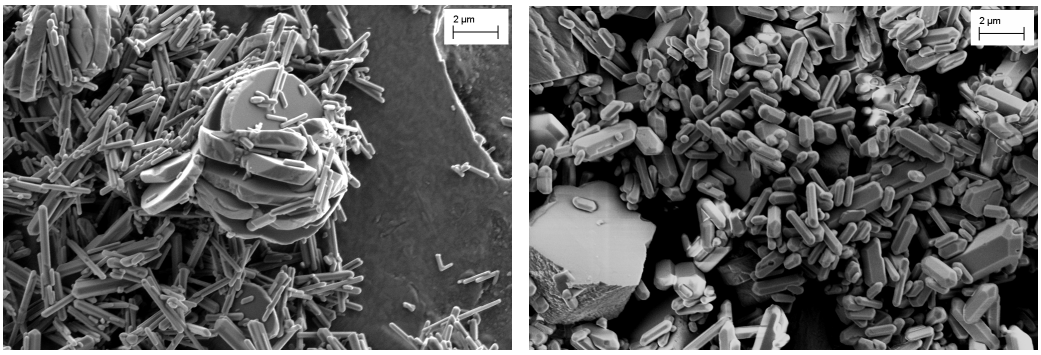

(a) Synthesis number 1, 9M KOH (b) Synthesis number 3, 16M KOH

Figure 5.2: SEM images of the products obtained in (a) synthesis number 1, and (b) synthesis number 3.

A calcination study performed on the product obtained in synthesis number 1 could possibly result in the formation of LFO at a lower temperature than 800 °C. The larger surface area, caused by smaller rod diameter, of the lanthanum hydroxide rods in synthesis product number 1 would make them more reactive compared to the rods in the product of synthesis number 3. The smaller rod diameter would also give a reduced diffusion length required to introduce iron into the centre of rod of structure. Another reason why the product of synthesis number 1 should have been chosen as the sample for the calcination study is the fact that the larger surface area of the rods and platelets in the product of synthesis 1 gives an increased area of contact between iron oxide and lanthanum hydroxide.

5.2 Two-Step Synthesis of LFO

Discussion related to some of the phenomena seen in the two-step synthesis will be treated in this section. Emphasis will be placed on the agglomeration observed in the calcination study pure lanthanum hydroxide rods. A section discussing the crystallinity of the obtained rods, and possible consequences of having polycrystalline rods in the two-step synthesis will also be presented.

5.2.1 Agglomeration of Lanthanum Hydroxide Rods

The calcination study of the pure lanthanum hydroxide nanorods showed rod agglomeration after the product is heated to 350 °C (Figure 4.13). The agglomeration becomes more severe when the product is calcined at higher temperatures, and eventually results in complete loss of the rod structure. Studying the XRD spectra of the raw and the calcined lanthanum hydroxide products, shown in Figure 4.11, it can be seen that pure, crystalline lanthanum hydroxide is present in the raw product and in the product calcined at 300 °C. When the temperature is raised to 350 °C diffraction peaks are no longer observed in the XRD scan, indicating that the crystallinity is lost. An amorphous phase has formed at this temperature.

The onset of agglomeration observed at 350 °C is believed to be correlated with the amorphous phase which has formed at the same temperature. When the product becomes non-crystalline the structure is randomly oriented. Further growth of the structure at this point can proceed in all directions. If the rods lie close enough, they can start to grow into one another. The result is agglomeration of the product. This is believed to be the mechanism for the agglomeration seen in the calcination study of the pure lanthanum hydroxide nanorods. The formation of the amorphous phase observed at 350 °C may be correlated to the first dehydration step of lanthanum hydroxide, which is reported located at 340 °C by Ozawa et al. [18]. In this dehydration step lanthanum hydroxide decomposes to lanthanum oxide hydroxide. Because of the formation of an amorphous phase these lanthanum hydroxide nanorods are not suitable as a template for lanthanum ferrite nanorods. In order to achieve directed growth of the lanthanum ferrite, the template should have a regular arrangement that results in a directed growth of the target structure, and should certainly not agglomerate and cause loss of the template structure.

Looking at the morphology evolution of the two-step synthesis product from the method where ultrasonic stirring was not applied, agglomeration has begun in the temperature interval 200 - 400 °C (Figure 4.17). This is expected

from the calcination study performed on pure lanthanum hydroxide where the onset of agglomeration was at 350 °C. The agglomeration and loss of rod structure in the two-step synthesis product are believed to be caused by the same mechanism as explained for the pure lanthanum hydroxide. Rods are not observed in the product calcined at 400 °C, and diffraction peaks of the lanthanum ferrite is not seen before the product is calcined at 500 °C (Figure 4.15). Lanthanum ferrite nanorods were not obtained in the two-step synthesis.

The use of lanthanum hydroxide nanorods has been explored as a template for lanthanum oxide and holmium and ytterbium doped lanthanum oxide nanorods by Li et al. [19]. This work reports to successfully convert lanthanum hydroxide nanorods into doped and undoped lanthanum oxide nanorods. Because of this, their work will be compared to the work performed during this master thesis to investigate the reason for the loss of rod structure. Differences between the two experimental methods will be addressed to explore the reasons why the outcome is so different in the two studies. The lanthanum hydroxide nanorods synthesised by Li et al. have been prepared by another synthesis method than hydrothermal synthesis. In their work synthesis was carried out by homogeneous precipitation where lanthanum hydroxide was formed, which was followed by a heat treatment. The as-synthesised hydroxide precursors were calcined at 800 °C for 2 to 3 hours in air to obtain La_2O_3:Ho^{+3} and La_2O_3:Yb^{+3}, Ho^{+3} [19]. The amount of holmium and ytterbium doped into the structure was a few molar percent. The hydroxide nanorods obtained in this work are reported to have an average diameter of 28 nm and a length of 380nm [19]. Compared to the rods obtained in this master thesis work, which had a diameter of 80 nm and length of 0.5 μm - 2 μm, the nanorods synthesised by Li et al. are thinner and shorter.

The calcined rods in the work of Li et al., heated for 3 hours at 800 °C, do not show any agglomeration as can be observed in Figure 5.3. However, the size of the lanthanum oxide rods obtained has shrunk compared to the lanthanum hydroxide rod template [19]. The fact that non-agglomerated rods are obtained after calcination at 800 °C is in contrast to the observation made in the calcination of the pure lanthanum hydroxide nanorods in this master thesis work.

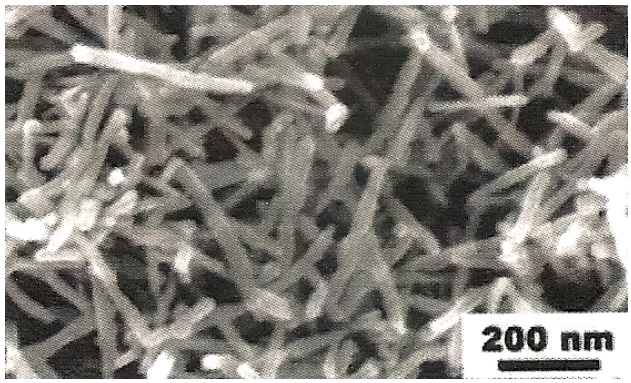

Figure 5.3: SEM image of La_2O_3:Ln^{+3} (Ln=Ho/Yb) nanorods obtained after calcination of $La(OH)_3$:Ln^{+3} nanorods at 800 °C for 3 hours in the work of Li et al. [19].

The main differences of the attempts of converting lanthanum hydroxide to lanthanum oxide in the two approaches are the size of the rods and the calcination procedure. These differences may be the cause to the completely different outcome. Calcination in the work by Li et al. is stated to have been performed in air. The calcinations carried out in the master thesis work have also been performed in air.

Even though the calcination performed by Li et al. has been carried out in air, it is not stated that lanthanum oxide carbonates have formed during the calcination like observed in the calcination study performed in this master thesis work. The XRD spectrum of the as-prepared $La(OH)_3$:Ln^{+3} (Ln=Ho/Yb) calcined at 500 °C obtained in the work of Li et al. is shown indicated by the letter (b) in Figure 5.4 This spectrum has been compared to the XRD spectrum attained after calcination at 500 °C for 1 hour of the lanthanum hydroxide rods obtained in the master thesis work. This spectrum is displayed in Figure 5.5.

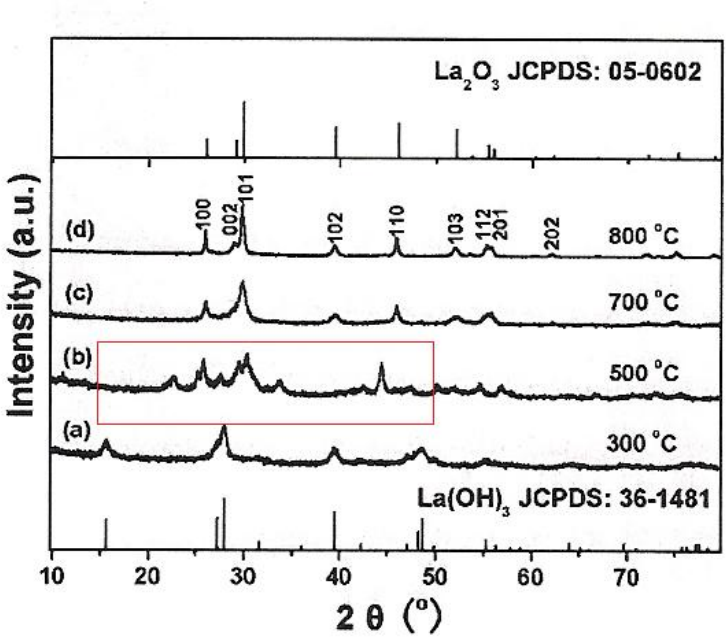

Figure 5.4: XRD spectra of the as-prepared $La(OH)_3$:Ln^{+3} (Ln=Ho/Yb) products calcined at different temperature (a) 300 °C, (b) 500 °C (red box indicates scan in 2θ region 15 ° - 50 °), (c) 700 °C and (d) 800 °C, respectively in the work by Li et al. [19]. The calcination duration was not stated.

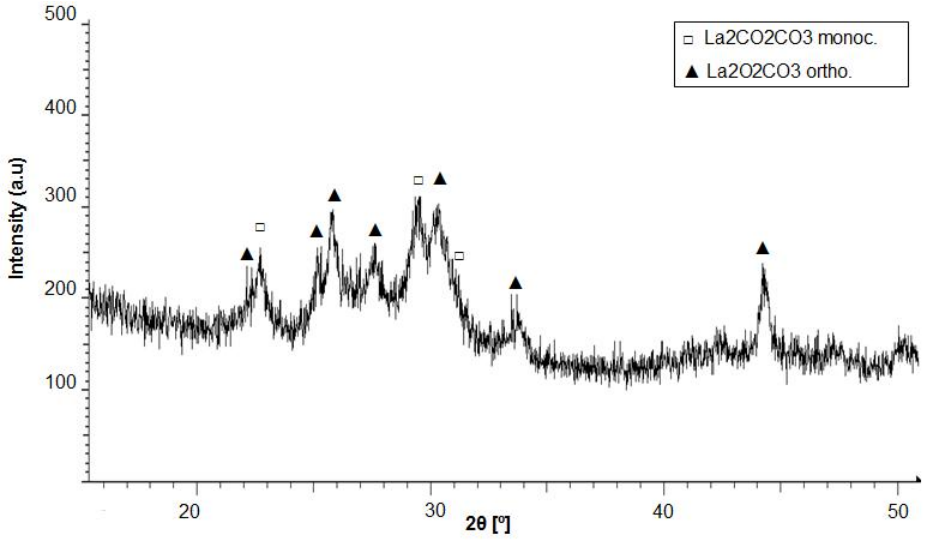

Figure 5.5: XRD spectrum of calcined lanthanum hydroxide nanorods at 500 °C for 1 hour, performed in this master thesis work.

The diffraction scan shown in the red box in Figure 5.4 is the XRD spectrum of doped lanthanum hydroxide calcined at 500 °C in the work of Li et al., in the diffraction angle region 15 ° - 50 °. The XRD scan of lanthanum hydroxide calcined at 500 °C in this master thesis work in Figure 5.5, shows the spectrum in the same 2θ region. Comparing the two scans it can be observed that they have diffraction peaks located at the same positions. The peaks in Figure 5.5 belongs to monoclinic and orthorhombic lanthanum oxide carbonate, located beneath open squares and black triangles respectively. As the two scans have peaks located in the same positions, the product calcined at 500 °C in the work of Li et al. is believed to consists of lanthanum oxide carbonates. The lanthanum oxide carbonates which are indicated present in the spectrum in the red box in Figure 5.4, are no longer present after calcination at 800 °C, shown in the XRD spectrum indicated by the letter (d) in the figure. At this temperature the product consist of lanthanum oxide. The fact that lanthanum oxide carbonates are possibly formed during the calcination of lanthanum hydroxide nanorods in the work by Li et al., indicates that formation of carbonates do not ruin the template effect of lanthanum hydroxide nanorods.

Details concerning the calcination procedure performed by Li et al. are not stated in the article. The heating and cooling rates are not given. However, the conversion to lanthanum oxide is reported to have been performed through a calcination process of gradual elimination of water. If gradual elimination of water involves heating the product in stages, this can have an impact on the rods during heating. If stages are applied and, or other heating rates are used in the work by Li et al., this can be the cause to the different outcomes in the two studies. However, this is a speculation about the cause, since it is not clearly stated in the article that heating stages have been applied in the calcination, or reported which heating rate was used.

5.2.2 Polycrystalline Lanthanum Hydroxide Nanorods

The lanthanum hydroxide obtained in the two-step synthesis is not single crystalline. The presence of several diffraction peaks in the XRD spectrum of this product indicates that the lanthanum hydroxide structure consists of random orientated crystal grains, and is polycrystalline. The XRD spectrum is displayed in Figure 4.9.

One of the consequences of having polycrystalline rods instead of single crystalline rods is that the structure directing template effect is not optimal. However, looking at the diffraction pattern of the lanthanum hydroxide calcined at 300 °C by Li et al. [19], which is indicated by the letter (a)

in Figure 5.4, this spectrum shows diffraction peaks in the same positions as the peaks in the XRD scan of the as-synthesised lanthanum hydroxide obtained in this master thesis work (Figure 4.9). This indicates that the lanthanum hydroxide nanorods obtained by Li et al. also are polycrystalline. The lanthanum hydroxide nanorods used in the topochemical conversion to holmium and ytterbium doped lanthanum oxide worked successfully as a template in the work by Li et al. [19]. This indicates that polycrystalline lanthanum hydroxide nanorods can be utilised as a template for other nanorod structures, where the target structure contains lanthanum.

Another aspect of having polycrystalline rods is that the stability of the structure will be poorer than if the structure was single crystalline. The fact that the rods are polycrystalline is proposed as a possible explanation for why the rod structure is lost during stirring with an ultrasonic finger in the two-step synthesis. The rods are probably not stable and resilient enough to withstand the energy enforced when exposed to ultrasonic stirring.

5.3 Further Work

This section will give suggestions for actions that can be performed in order to improve the syntheses carried out in this work and propose different experiments which could contribute to the understanding of lanthanum ferrite synthesis. It has been divided into two sections, one which address the direct hydrothermal synthesis and one which treats the two-step synthesis.

5.3.1 Direct Hydrothermal Synthesis of LFO

It would be interesting to explore to which temperature the synthesis temperature had to be raised in order to synthesise lanthanum ferrite by direct hydrothermal synthesis. When increasing the synthesis temperature, a temperature will eventually be reached where the driving force for LFO formation is large enough, and lanthanum ferrite will be present in the synthesis product. However, the temperature limit for the autoclaves used in this work is 250 °C, so other autoclaves which can be operated at higher temperatures must be provided in order to explore synthesis temperature exceeding 250 °C. It could also be investigated if a synthesis duration exceeding 100 hours would result in lanthanum ferrite. The kinetics of the system could govern the formation, and if this is slow an increase in the synthesis duration could give a synthesis product containing lanthanum ferrite.

A trend of lowering the transition temperature where lanthanum ferrite becomes stable is seen with increasing amounts of potassium hydroxide in Figure 5.1. It is probable that the difference of free energy between lanthanum ferrite compared to iron oxide and lanthanum hydroxide would increase with increasing concentration of potassium hydroxide. It would be interesting to increase this concentration to explore if lanthanum ferrite could be synthesised at a temperature below or at the temperature limitation of the autoclaves available. However there is a limit of the amount of potassium hydroxide that can be dissolved in water. The saturation limit at room temperature is 21.2 M [20].

Another aspect worth investigating is if lanthanum ferrite powder produced by another technique placed in the autoclave and exposed to the same hydrothermal conditions used in this work would result in disintegration of the lanthanum ferrite, or if the lanthanum ferrite powder is intact after exposure. This experiment would confirm or disprove that lanthanum ferrite is stable under the conditions indicated by the thermodynamic calculations.

The sample chosen for the calcination study of the direct synthesis product was not the ideal synthesis product for this study, as discussed in Section 5.1.2. A calcination study of the product from synthesis number 1 could be performed to investigate if this product would form lanthanum ferrite at a lower temperature, and if the product can be calcined into lanthanum ferrite nanorods.

5.3.2 Two-Step Hydrothermal Synthesis of LFO

The work of Li et al. [19] should be attempted reproduced by increasing the calcination temperature to 800 °C. In this work non-agglomerated lanthanum oxide nanorods were obtained after calcination of lanthanum hydroxide. The heating rate and possible heating stages applied in this work might be the reason why agglomeration is not seen in the product. The lanthanum hydroxide nanorods obtained in this master thesis work should be the subject of a calcination study where heating rates and heating stages are investigated. Elimination of the rod agglomeration could possibly be done by exploring these factors. In this calcination study it might be advantageous to disperse the rods before heating. Dispersing the nanorods would reduce the number of contact points between them, and could restrict the agglomeration. This must be done by another method than stirring with an ultrasonic finger, as the rods disappeared after stirring when this method was applied.

The rods obtained by Li et al. were also of smaller size than the rods obtained in the master thesis work. Exploring the hydrothermal synthesis of lanthanum hydroxide rods to decrease the diameter could be beneficial in the research of obtaining the desired template effect which Li et al. observed in their work. Even though this template effect is obtained, and rod agglomeration is not observed in the work by Li et al., the rods in this work are doped with only a few molar percent of holmium and ytterbium [19]. In order to achieved lanthanum ferrite, 50 molar percent of iron must be introduced into the lanthanum hydroxide rod structure. The demands required of the rods to achieve this will therefore be altered, and experience gained from the work by Li et al. might not be directly applicable in the case of converting lanthanum hydroxide nanorods into lanthanum ferrite nanorods. This should be kept in mind in the process of trying to reproduce the results obtained from converting lanthanum hydroxide to doped lanthanum oxide.

Since the lanthanum hydroxide forms carbonates when heated, it would be of interest to explore if the result of calcination of pure lanthanum hydroxide rods and the product of the two-step synthesis would be altered if the rods were heated in an atmosphere without carbon dioxide, or even heating in vacuum. Lanthanum carbonate species are believed to have formed when lanthanum hydroxide nanorods were calcined in the work of Li et al., and rod shaped lanthanum oxide was still obtained. However, the temperature had to be raised to 800 °C before the desirable lanthanum oxide product was obtained. If the product must be calcined at this temperature in order for the carbonates to be removed, reduced temperatures could be applied if the calcination was performed in an atmosphere where carbonates do not form. This could be beneficial when working with rods which are not stable and lose the rod structure at high temperatures, like the rods obtained in the master thesis work.

The carbonate phase was introduced before calcination of the two-step synthesis products obtained in this master thesis work. Lanthanum hydroxide carbonate was present in both raw products (Figure 4.15 and Figure 4.18). This indicates that in order to avoid carbonates in this system the heating where water is removed have to be performed in an atmosphere without carbon dioxide, or that the process of mixing or covering lanthanum hydroxide with an iron precursor must be done by another manner where elimination of carbon dioxide in the system can be done.

6 Conclusion

Lanthanum ferrite nanorods with high aspect ratio were not obtained in the direct hydrothermal synthesis under the reaction conditions used. All the products of the direct hydrothermal syntheses consisted of iron oxide and lanthanum hydroxide. Since no LFO was obtained, a calculation exploring the temperature where lanthanum ferrite becomes more stable than iron oxide and lanthanum hydroxide was performed. The calculation showed that the transition temperature to the stability region of lanthanum ferrite is close to the synthesis temperature 240 °C. The small driving force for formation of lanthanum ferrite in the temperature region close to the transition temperature is the reason why formation of lanthanum ferrite in the direct synthesis has not been observed.

Lanthanum hydroxide nanorods were covered with an iron precursor and attempted converted into LFO in the two-step synthesis. The results of the calcination study of this product show that the rod structure is lost after calcination at 400 °C, at this temperature LFO has not formed. Lanthanum ferrite appears after calcination at 500 °C. The nanorod structure and the lanthanum ferrite phase is therefore not obtained simultaneously. The loss of nanorod structure is believed to be caused by agglomeration of lanthanum hydroxide rods which begins after heating to 350 °C. The agglomeration starting at this temperature might be correlated with an amorphous phase transition of lanthanum hydroxide.

Since lanthanum ferrite was not obtained in this work, enough experience to reintroduce strontium into the system to synthesise strontium doped LFO have not be gained. Research exploring higher synthesis temperature, longer duration and higher potassium hydroxide concentrations should be performed to investigate if lanthanum ferrite can be synthesised by direct hydrothermal synthesis. In order to convert lanthanum hydroxide nanorods to LFO by topochemical reaction, more knowledge of the lanthanum hydroxide nanorod behaviour during heating must be obtained.

References

[1] A. Reksten. Nanostructuring of oxygen permeable membranes. Project Report, Desember 2010.

[2] H. J. M. Bouwmeester. Dense ceramic membranes for methane conversion. *Catalysis Today*, 82(1-4):141 – 150, 2003.

[3] J. Sunarso, S. Baumann, J.M. Serra, W.A. Meulenberg, S. Liu, Y.S. Lin, and J.C. Diniz da Costa. Mixed ionic-electronic conducting (MIEC) ceramic-based membranes for oxygen separation. *Journal of Membrane Science*, 320(1-2):13 – 41, 2008.

[4] P. V. Hendriksen, P. H. Larsen, M. Mogensen, F. W. Poulsen, and K. Wiik. Prospects and problems of dense oxygen permeable membranes. *Catalysis Today*, 56(1-3):283 – 295, 2000.

[5] B. L. Cushing, V. L. Kolesnichenko, and C. J. O'Connor. Recent advances in the liquid-phase syntheses of inorganic nanoparticles. *Chemical Reviews*, 104(9):3893–3946, 2004.

[6] M. Byrappa, K. Yoshimura. *Handbook of Hydrothermal Technology - A Technology for Crystal Growth and Materials Processing.* William Andrew Publishing/Noyes, 2001.

[7] Parr Instrument Company, www.parrinst.com. *Parr Acid Digestion Vessels, Operating Instruction Manual*, NO. 249M edition, March 2010.

[8] R. I. Walton. Subcritical solvothermal synthesis of condensed inorganic materials. *Chemical Society reviews*, 31:230, 2002.

[9] Phase diagram of water, from Wikipedia. `http://en.wikipedia.org/wiki/File:Phase-diag2.svg`, 13:19pm, 10. June 2011.

[10] S. D. Jackson and J. S. J. Hargreaves, editors. *Metal Oxide Catalysts Volume 1.* Wiley-VCH, 2009.

[11] L. Sun and C. Hu. *Nanotechnology Research: New Nanostructures, Nanotubes and Nanofibers*, chapter 1 Low Dimentional Inorganic Nanomaterials. Nova Publishers, 2008.

[12] W. Hu, Y. Chen, H. Yuan, G. Zhang, G. Li, G. Pang, and S. Feng. Hydrothermal synthesis, characterization and composition-dependent magnetic properties of $LaFe_{1-x}Cr_xO_3$ system ($0 \leq x \leq 1$). *Journal of Solid State Chemistry*, 183(7):1582 – 1587, 2010.

[13] W. Zheng, R. Liu, D. Peng, and G. Meng. Hydrothermal synthesis of $LaFeO_3$ under carbonate-containing medium. *Materials Letters*, 43(1-2):19 – 22, 2000.

[14] X. Wang and Y. Li. Synthesis and characterization of lanthanide hydroxide single-crystal nanowires. *Angewandte Chemie International Edition*, 41(24):4790–4793, 2002.

[15] J. Balej. Water vapour partial pressures and water activities in potassium and sodium hydroxide solutions over wide concentration and temperature ranges. *International Journal of Hydrogen Energy*, 10(4):233 – 243, 1985.

[16] W. D. Jr. Callister. *Materials Science and Engineering*. Wiley, 7th edition, 2007.

[17] K. Byrappa and T. Ohachi. *Crystal Growth Technology*. Springer/William Andrew Publishing, 2003.

[18] M. Ozawa, R. Onoe, and H. Kato. Formation and decomposition of some rare earth (Re = La, Ce, Pr) hydroxides and oxides by homogeneous precipitation. *Journal of Alloys and Compounds*, 408-412:556 – 559, 2006.

[19] G. Li, C. Li, Z. Xu, Z. Cheng, and J. Lin. Facile synthesis, growth mechanism and luminescence properties of uniform $La(OH)_3 : Ho^{3+}/Yb^{3+}$ and $La_2O_3 : Ho^{3+}/Yb^{3+}$ nanorods. *CrystEngComm*, 12:4208–4216, 2010.

[20] G. Aylward and T. Findlay. *SI Chemical Data 5th edition*. Wiley, 2002.

[21] M. W. Chase, C. A. Davies, J. R. Downey, D. J. Frurip, R. A. McDonald, and A. N. Syverud. *JANAF Thermochemical Tables, Third Edition, Part II, Cr-Zr*. American Chemical Society and the American Institue of Physics for the National Bureau of Standards, 1985.

[22] R. D. Chirico and E. F. Westrum. Thermophysics of the lanthanide hydroxides I. Heat capacities of La(OH)3, Gd(OH)3, and Eu(OH)3 from near 5 to 350 K. Lattice and Schottky contributions. *The Journal of Chemical Thermodynamics*, 12:71 – 85, 1980.

[23] S. Stølen, F. Grønvold, H. Brinks, T. Atake, and H. Mori. Heat capacity and thermodynamic properties of $LaFeO_3$and $LaCoO_3$ from T=13 K to T=1000 K. *The Journal of Chemical Thermodynamics*, 30(3):365 – 377, 1998.

[24] L. Merli, B. Lambert, and J. Fuger. Thermochemistry of lanthanum, neodymium, samarium and americium trihydroxides and their relation

to the corresponding hydroxycarbonates. *Journal of Nuclear Materials*, 247:172 – 176, 1997.

[25] E. Povoden-Karadeniz, A. Grundy, M. Chen, T. Ivas, and L. Gauckler. Thermodynamic Assessment of the La-Fe-O System. *Journal of Phase Equilibria and Diffusion*, 30:351–366, 2009.

Appendices

Note that references made in the appendices are listed in References, with the other references referred to in this work.

A Thermodynamic Calculations

A.1 Calculation of Autoclave Pressure

The calculation of the pressure in the autoclave during operation will be presented in this section. Inside the autoclave held at 240°C (513 K), the water will partly exist as liquid water and the rest will have evaporated and be in water vapour state. At this temperature and with the fill factor used in these syntheses, which is 60 %, the point of operation in the phase diagram of water is in the two phase region. After reaching 240 °C and the temperature has become stable, an equilibrium between liquid water and water vapour will be attained. This equilibrium is described by the reaction in Equation A.1.

$$H_2O(liq) \leftrightarrow H_2O(gas) \tag{A.1}$$

The change in Gibbs energy, Δ_rG, for this reaction is given in Equation A.2

$$\Delta_r G = \Delta_r G^\circ + R\,T\,ln(K) \tag{A.2}$$

Δ_rG° is the standard change of Gibbs energy for the reaction given in Equation A.1, R is the gas constant which is 8.314 J/mol K, T is the temperature and K is the equilibrium constant for the reaction. At equilibrium Δ_rG is zero, reducing Equation A.2 to Equation A.3

$$\Delta_r G^\circ = -\,R\,T\,ln(K) \tag{A.3}$$

The equilibrium constant is given by Equation A.4

$$K = \frac{a_{H2O(gas)}}{a_{H2O(liq)}} \tag{A.4}$$

The activity of the water in liquid state, $a_{H2O(liq)}$, assuming that it is pure, is equal to unity. The activity of the water in gaseous state is equal to the pressure of the water, $P_{H2O(gas)}$, divided by the standard pressure, P°. The standard pressure is 1 bar [21].

This reduces the equilibrium constant in Equation A.4 to Equation A.5.

$$K = \frac{P_{H2O(gas)}}{P^\circ} \tag{A.5}$$

Inserting Equation A.5 into Equation A.3, an equation for the pressure as a function of temperature is obtained, which is shown in Equation A.6.

$$P_{H2O(gas)} = P^\circ \, exp\left(\frac{-\Delta_r G^\circ \, (T)}{R\,T}\right) \tag{A.6}$$

Δ_fG° for liquid water and gaseous water are listed in the Thermochemical Table [21] at 500 K (227 °C), and not at 513 K (240 °C). The values at 500 K will be used for the calculation of the change in Gibbs energy going from liquid water to gaseous water. The pressure calculated will therefore deviate a bit from the actual pressure at the synthesis temperature used in the direct hydrothermal syntheses. The change in standard Gibbs energy for the reaction in Equation A.1 is calculated by the use of Equation A.7

$$\Delta_r G^\circ_{500K} = \Delta_f G^\circ_{H2O(gas),\,500K} - \Delta_f G^\circ_{H2O(liq),\,500K} \tag{A.7}$$

$\Delta_f G^\circ_{H2O(liq),\,500K}$ and $\Delta_f G^\circ_{H2O(gas),\,500K}$ have been found in Thermochemical Table to be respectively -206.002 kJ/mol and -219.051 kJ/mol [21]. This gives a value for the change in the standard Gibbs energy at 500 K, $\Delta_r G^\circ_{500K}$, of -13.049 kJ/mol.

Inserting the value of -13.049 kJ/mol, temperature of 513 K and R of 8.314 J/mol K into Equation A.6, a pressure of 21.31 bar is calculated. The pressure in the autoclave at 240 °C is 21 bar. This is approximately what can be found as the pressure at 240 °C with 60 % fill factor in Figure 2.3b in Section 2.2 on page 9.

A.2 Stability of Lanthanum Ferrite

The stability of lanthanum ferrite compared to iron oxide and lanthanum hydroxide has been explored, because lanthanum ferrite did not form in the direct hydrothermal syntheses. The product consisted of iron oxide and lanthanum hydroxide. The thermodynamics of the reaction where iron oxide and lanthanum hydroxide reacts and form lanthanum ferrite has therefore been investigated in order to find the temperature where LFO becomes more stable than iron oxide and lanthanum hydroxide. This reaction is given in Equation A.8.

$$2La(OH)_3 + Fe_2O_3 \rightarrow 2LaFeO_3 + 3H_2O(liq) \tag{A.8}$$

The change in Gibbs energy for this reaction is given by Equation A.9.

$$\Delta_r G(T, a_w) = \Delta_r G^\circ(T) + RT\,ln(a_w^3) = \Delta_r G^\circ(T) + 3\,RT\,ln(a_w) \tag{A.9}$$

Δ_rG(T, a_w) and Δ_rG°(T) are respectively the change of Gibbs energy and the change of the standard Gibbs energy of the reaction described in Equation A.8. R is the gas constant, T is the temperature and a_w is the water activity. The temperature where the Gibbs energy changes from being positive to become negative is the temperature where LFO will be more stable phase than iron oxide and lanthanum hydroxide. This temperature will be referred to as the transition temperature.

The standard Gibbs energy of formation of lanthanum ferrite, Δ_rG°(T), as a function of temperature is given by equation A.10,

$$\Delta_r G^\circ(T) = \Delta_r H^\circ(T) - T\,\Delta_r S^\circ(T) \tag{A.10}$$

The standard enthalpy for the reaction, Δ_rH°(T), as a function of temperature is given in Equation A.11. Equation A.12 describes the standard entropy, Δ_rS°(T), as a function of temperature.

$$\begin{aligned} \Delta_r H^\circ(T) &= \Delta_r H^\circ_{298K} + \int_{298}^{513} \Delta_r C^\circ_{p,298K}\, dT \\ &= \Delta_r H^\circ_{298K} + \Delta_r C^\circ_{p,298K}\ (513 - 298) \end{aligned} \tag{A.11}$$

$$\begin{aligned} \Delta_r S^\circ(T) &= \Delta_r S^\circ_{298K} + \int_{298}^{513} \frac{\Delta_r C^\circ_{p,298K}}{T}\, dT \\ &= \Delta_r S^\circ_{298K} + \Delta_r C^\circ_{p,298K} \ln\left(\frac{513}{298}\right) \end{aligned} \tag{A.12}$$

$\Delta_r C^\circ_{p,298K}$ is the difference in the standard molar heat capacities of products and reactants, and is needed in order to calculate the enthalpy and entropy change in Equation A.11 and Equation A.12. Equation A.13 explains how $\Delta_r C^\circ_{p,298K}$ can be calculated for the reaction in Equation A.9. The values used to perform this computation are listed in Table A.1.

$$\begin{aligned} \Delta_r C^\circ_{p,298K} &= 2\, C_{p,LFO,298K} + 3\, C_{p,H2O,298K} \\ &\quad - 2\, C_{p,La(OH)3,298K} - C_{p,Fe2O3,298K} \end{aligned} \tag{A.13}$$

Table A.1: The molar heat capacities of the species in the reaction where iron oxide and lanthanum hydroxide reacts to lanthanum ferrite and water.

Compound	$\mathbf{C_{p,298K}}$ **[J/mol K]**	**Reference**
$La(OH)_3$	117.38	[22]
Fe_2O_3	103.76	[21]
H_2O (liq)	75.35	[21]
$LaFeO_3$	108.64	[23]

The $\Delta_r C^\circ_{p,298K}$ is calculated to be 104,8 J/mol K by the use of Equation A.13 and the values listed in Table A.1

$\Delta_r H^\circ_{298K}$ and $\Delta_r S^\circ_{298K}$ are respectively the standard change in enthalpy and entropy at 298 K for the reaction in Equation A.9. These values were calculated

by the use of Equation A.14 and Equation A.15. The data used to perform the computations is listed in Table A.2.

$$\begin{aligned}\Delta_r H^\circ_{298} = &\, 2\,\Delta H_{\mathrm{LaFeO_3,\ 298K}} + 3\,\Delta H_{\mathrm{H_2O,\ 298K}} \\ &- 2\,\Delta H_{\mathrm{La(OH)_3,\ 298K}} - \Delta H_{\mathrm{Fe_2O_3,\ 298K}}\end{aligned} \tag{A.14}$$

$$\begin{aligned}\Delta_r S^\circ_{298} = &\, 2\,\Delta S_{\mathrm{LaFeO_3,\ 298K}} + 3\,\Delta S_{\mathrm{H_2O,\ 298K}} \\ &- 2\,\Delta S_{\mathrm{La(OH)_3,\ 298K}} - \Delta S_{\mathrm{Fe_2O_3,\ 298K}}\end{aligned} \tag{A.15}$$

Table A.2: Thermodynamic data used to calculate the change in enthalpy and entropy of the reaction where iron oxide and lanthanum hydroxide reacts to lanthanum iron oxide and water.

Compound	$\Delta_f \mathbf{H^\circ_{298K}}$ **[kJ/mol]**	$\Delta_f\ \mathbf{S^\circ_{298K}}$ **[J/mol K]**	**Reference**
$La(OH)_3$	-1416.70	117.8	[24]
Fe_2O_3	-825.503	87.4	[21]
H_2O (liq)	-285.83	69.95	[21]
$LaFeO_3$	-1368.2	107	[25]

The $\Delta_r H^\circ_{298K}$ and $\Delta_r\ S^\circ_{298K}$ for the reaction in equation A.8 were respectively found to be 65.013 kJ/mol and 100.85 J/mol K.

Equations A.11 and A.12 are inserted into Equation A.10, which is combined with Equation A.9. The resulting equation is given in Equation A.16.

$$\begin{aligned}\Delta_r G(T, a_w) =&\Delta_r H^\circ(T) - T\,\Delta_r S^\circ(T) + 3\,R\,T\,ln(a_w) \\ =&\Delta_r H^\circ_{298K} + \int_{298}^{513} \Delta_r C^\circ_{p,298K}\,dT \\ &- T\left(\Delta_r S^\circ_{298K} + \int_{298}^{513} \frac{\Delta_r C^\circ_{p,298K}}{T}\,dT\right) + 3\,R\,T\,ln(a_w)\end{aligned} \tag{A.16}$$

The water activity, a_w, varies with concentration of potassium hydroxide and temperature. The water activity as a function of potassium hydroxide

concentration and temperature has been found in the work of Balej [15]. The equation found for this relation is demonstrated in Equation A.17.

$$loga_{w(KOH)} = -0.02255m + 0.001434m^2 + \frac{1.38m - 0.9254m^2}{T} \quad \text{(A.17)}$$

The m is the molality [mol/kg H_2O] of potassium hydroxide. If the water density is assumed to be constant and equal to the density at 25 °C molality and molarity is equal. However, the water density is not constant when temperature is increased, and assuming that it is will give an error in the calculated values.

Equation A.17 and the values for $\Delta_r H^\circ_{298K}$, $\Delta_r S^\circ_{298K}$ and $\Delta_r C^\circ_{p,298K}$ are inserted into Equation A.16, and an equation describing the $\Delta G(T,a_w)$ is obtained, and plotted against temperature. The results are presented in Figure A.1. Values of potassium concentration of 9, 13 and 16 M are used in these calculations as these were the concentrations of potassium hydroxide used in the direct hydrothermal syntheses.

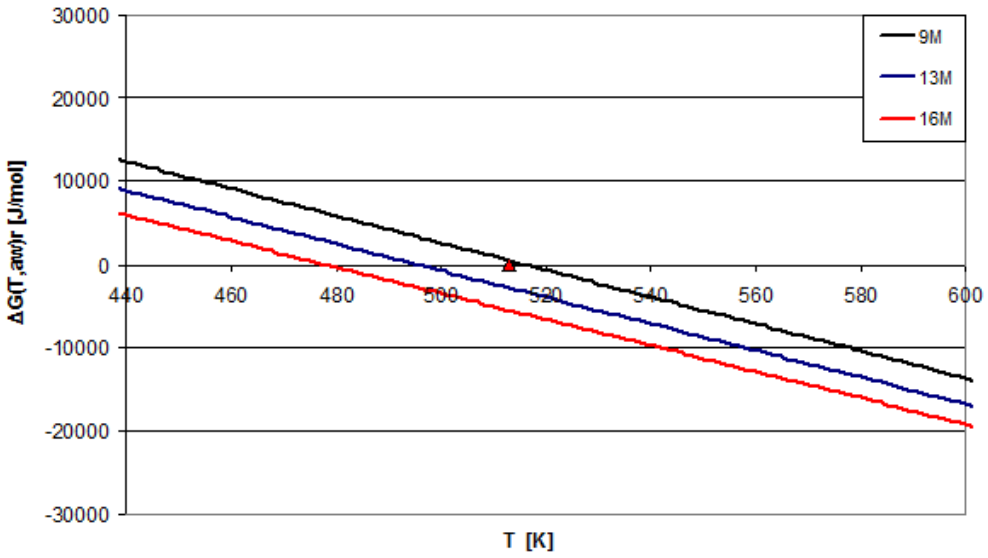

Figure A.1: Gibbs energy as a function of temperature for the reaction where iron oxide and lanthanum hydroxide reacts and form LFO and water from a solution with 9, 13 and 16 potassium hydroxide molality.

As can be observed in Figure A.1, the Gibbs energy, $\Delta_r G(T,a_w)$, is zero at 244 °C (517 K), 224 °C (497 K) and 206 °C (479 K), when concentrations of

potassium hydroxide of respectively 9, 13 and 16 M are used. The synthesis temperature in the direct synthesis was 240 °C (513 K), and is indicated by the red triangle in the figure. Figure A.1 shows that the transition temperature decreases with increasing concentration of potassium hydroxide concentration.

B XRD Spectra

B.1 Direct Hydrothermal Synthesis of LFO

Variation of KOH Concentration

The XRD spectrum of the product obtained after synthesis number 1, where the potassium hydroxide concentration was 9 M, is shown in Figure B.1.

The XRD spectrum of the product obtained from synthesis number 2, where 13 M potassium hydroxide was used, is given in Figure B.2

XRD spectrum of the product from synthesis number 3, where 16 M potassium hydroxide concentration was used, is shown in Figure B.3

Changing the Iron to Lanthanum Ratio

XRD spectrum of the product from synthesis number 4, with molar ratio of iron to lanthanum of 2, is shown in Figure B.4.

XRD spectrum of the product from synthesis number 5, when ratio of iron to lanthanum was 0.5, is given in Figure B.5.

Increasing Synthesis Duration

XRD spectrum of the product from synthesis number 6, when the synthesis duration was increased to 100 hours, is given in Figure B.6.

Calcination of the Direct Hydrothermal Synthesis Product

XRD spectrum of calcined product obtained in synthesis 3, for 2 hours at 600 °C, is shown in Figure B.7.

XRD spectrum of calcined product obtained in synthesis 3, for 2 hours at 700 °C, is shown in Figure B.8.

XRD spectrum of calcined product obtained in synthesis 3, for 2 hours at 800 °C, is shown in Figure B.9.

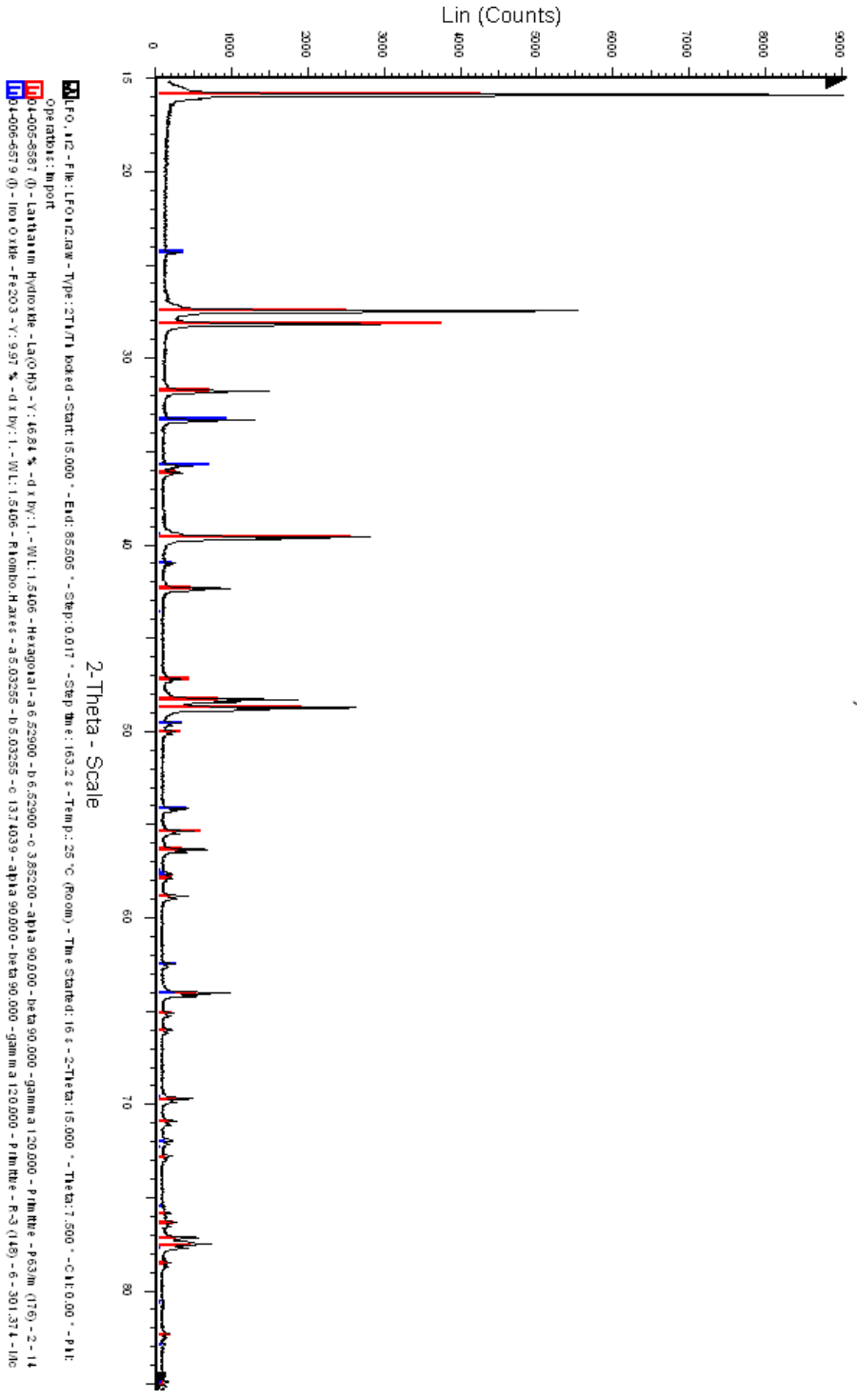

Figure B.1: XRD spectra of product obtained with potassium hydroxide concentration of 9 M, direct synthesis number 1.

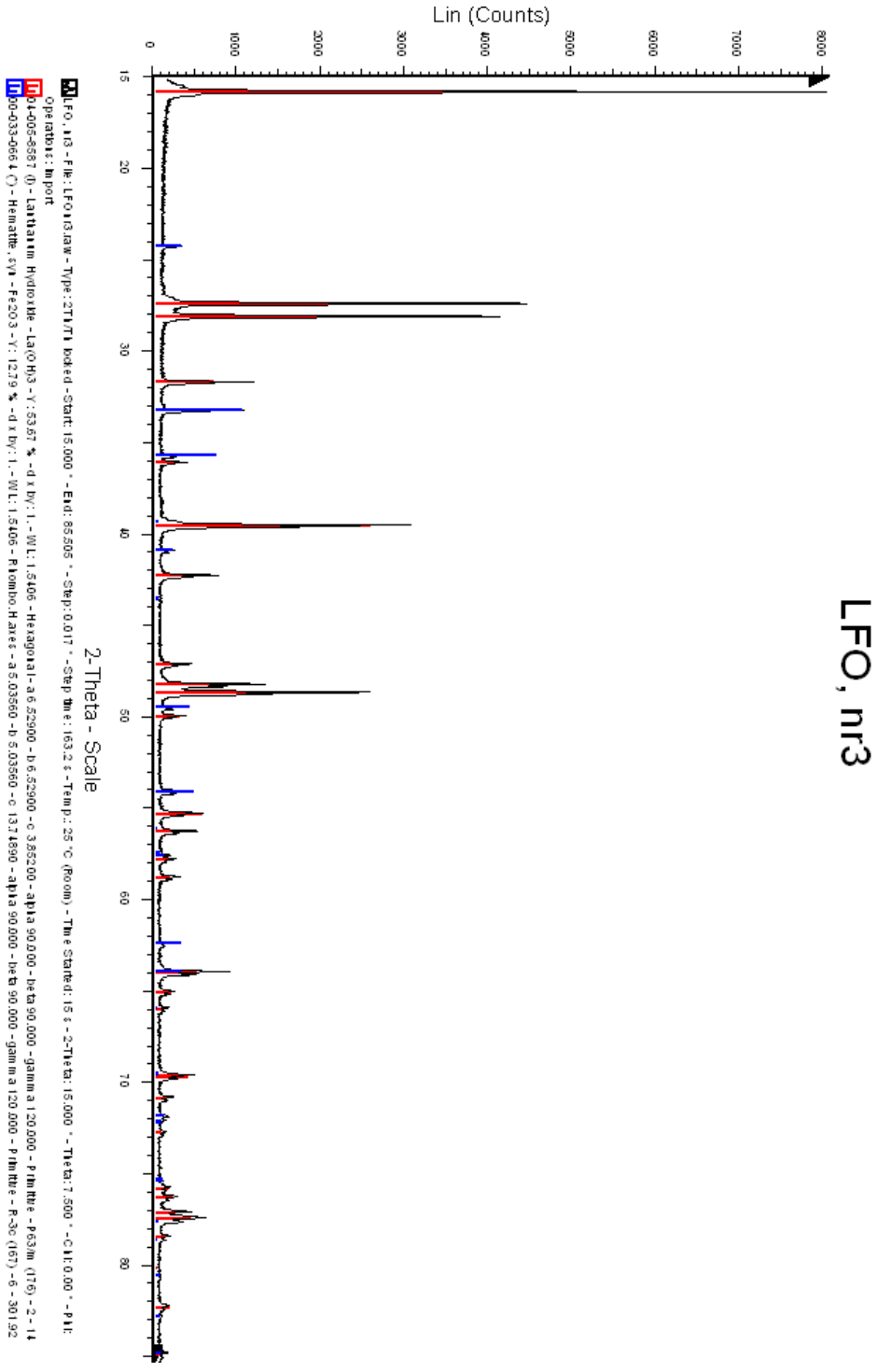

Figure B.2: XRD spectra of product obtained with potassium hydroxide concentration of 13 M, direct synthesis number 2.

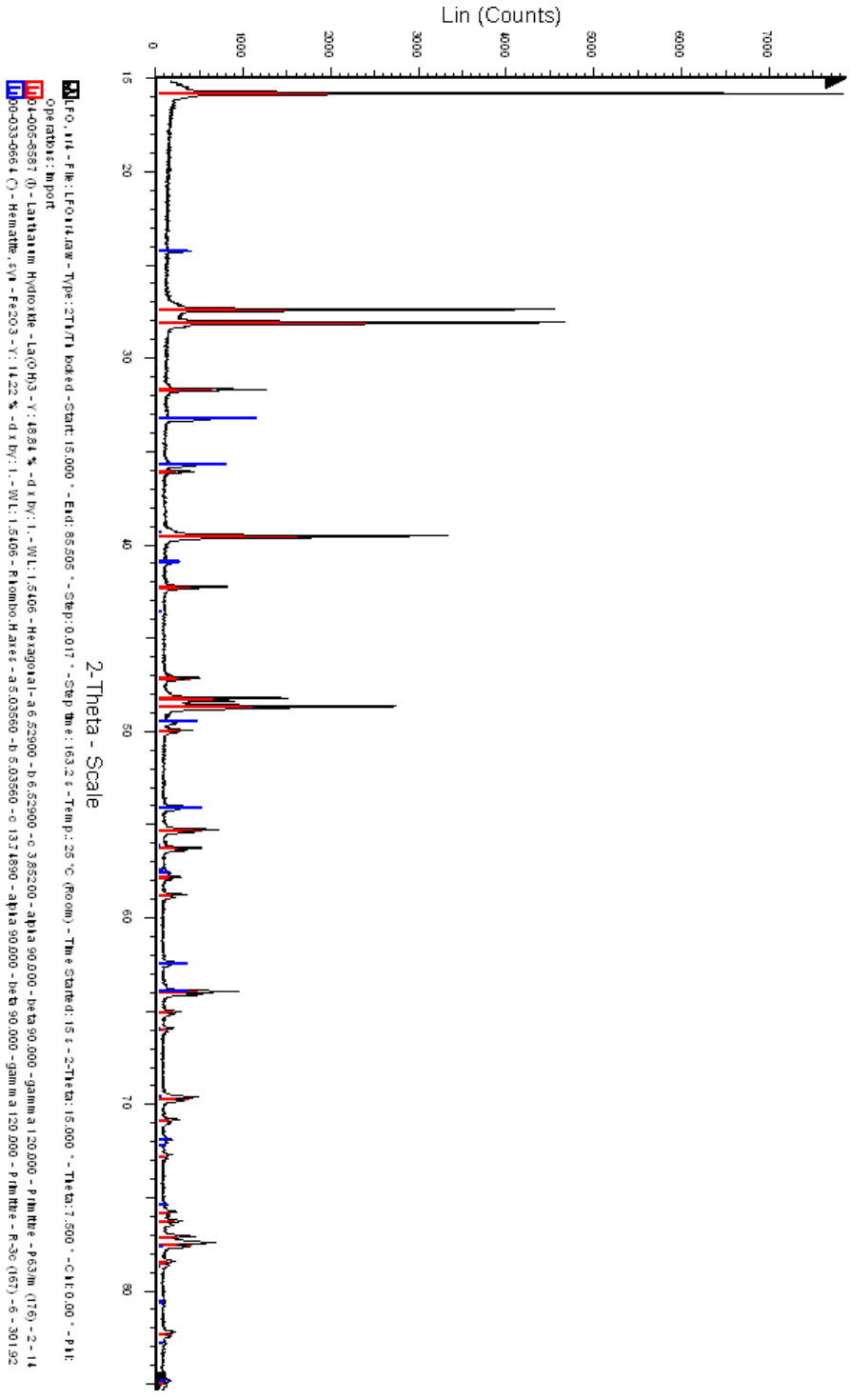

Figure B.3: XRD spectra of product obtained in the synthesis with potassium hydroxide concentration of 16 M, direct synthesis number 3

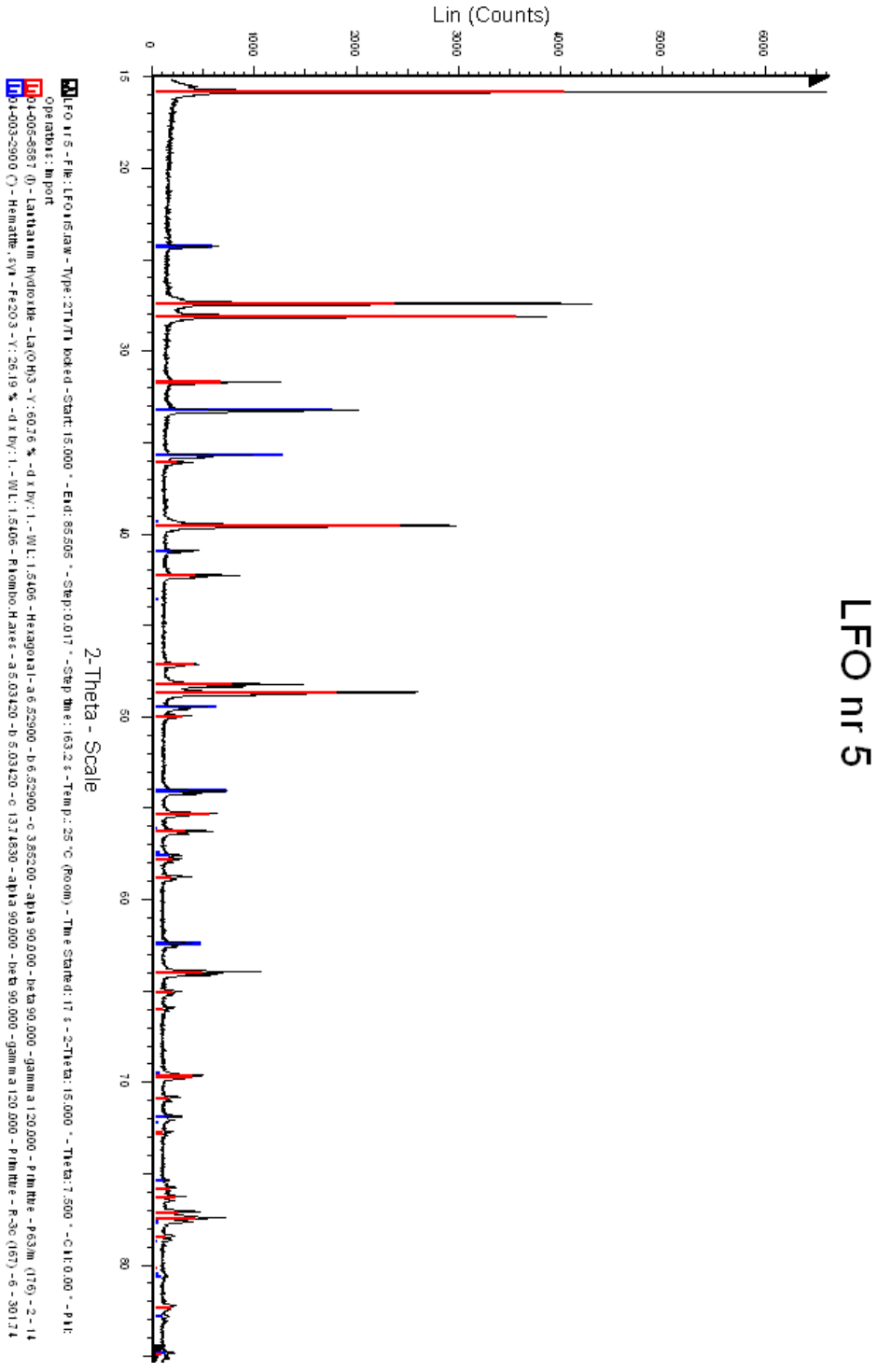

Figure B.4: XRD spectra of product obtained in the synthesis when molar ratio of iron to lanthanum was 2, direct synthesis number 4.

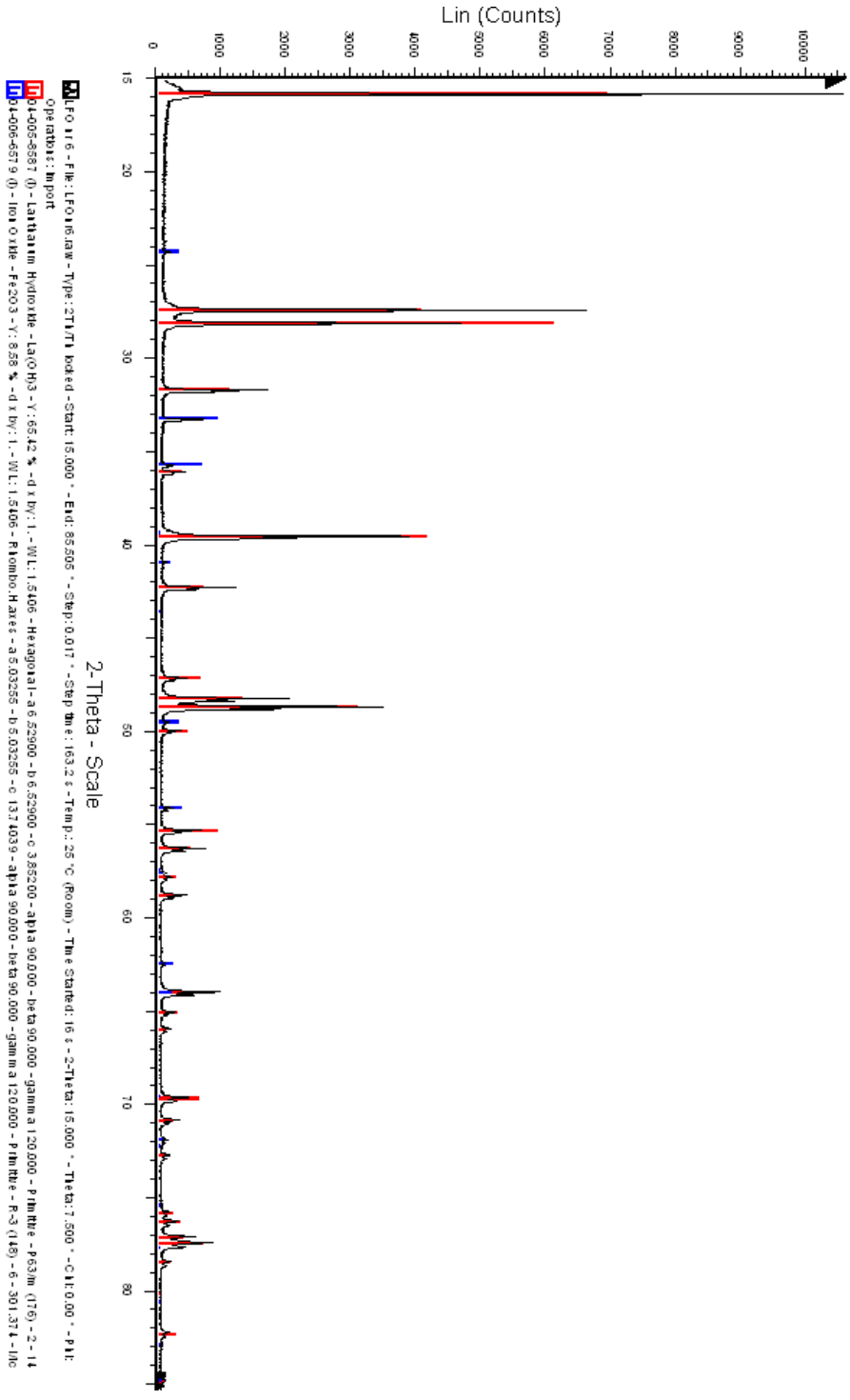

Figure B.5: XRD spectra of product obtained when the molar ratio of iron to lanthanum was 0.5, direct synthesis number 5.

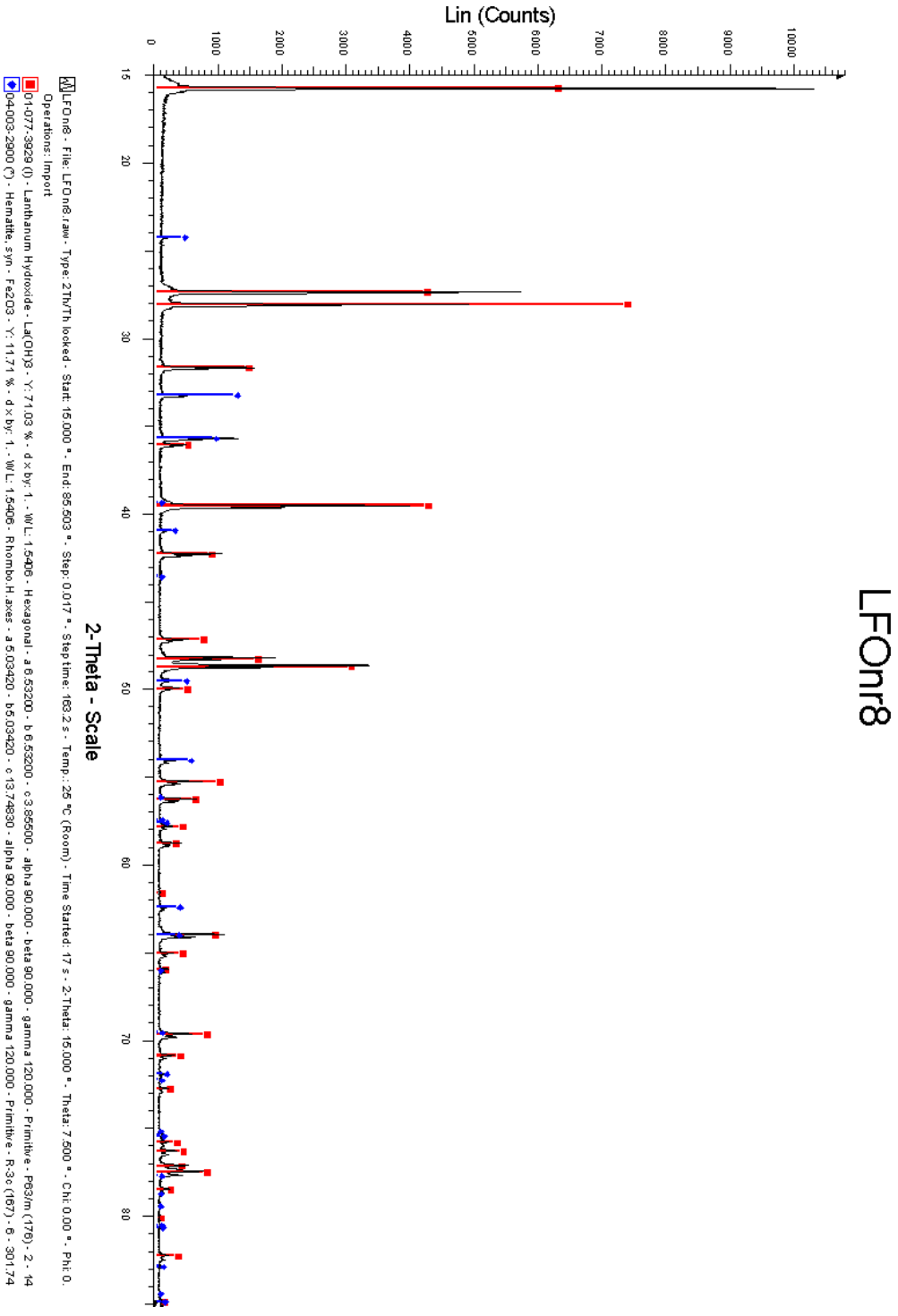

Figure B.6: XRD spectrum of the product obtained from the synthesis when the synthesis duration was increased to 100 hours, direct synthesis number 6.

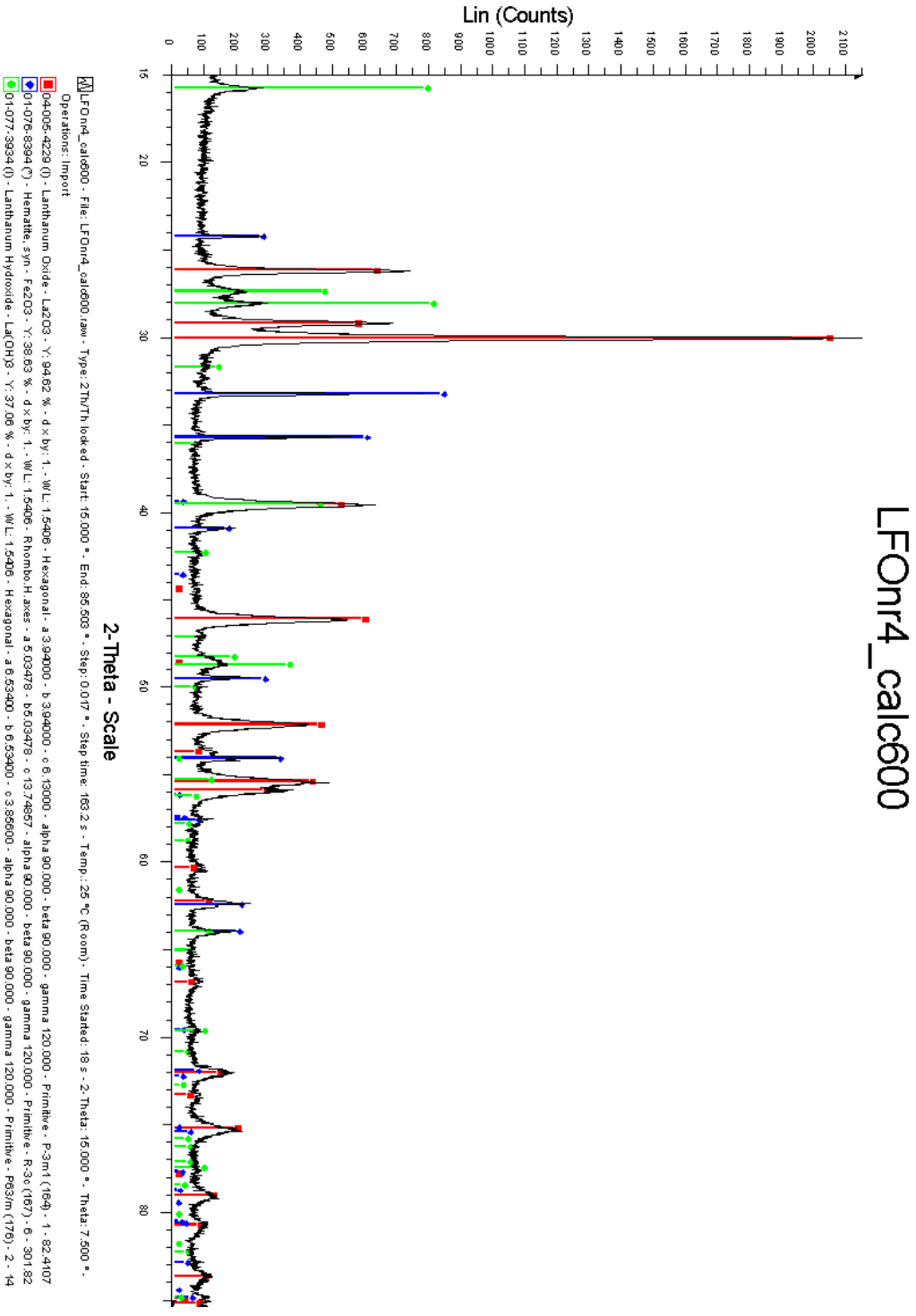

Figure B.7: XRD spectrum of direct synthesis product from synthesis number 3, calcined at 600 °C for 2 hours.

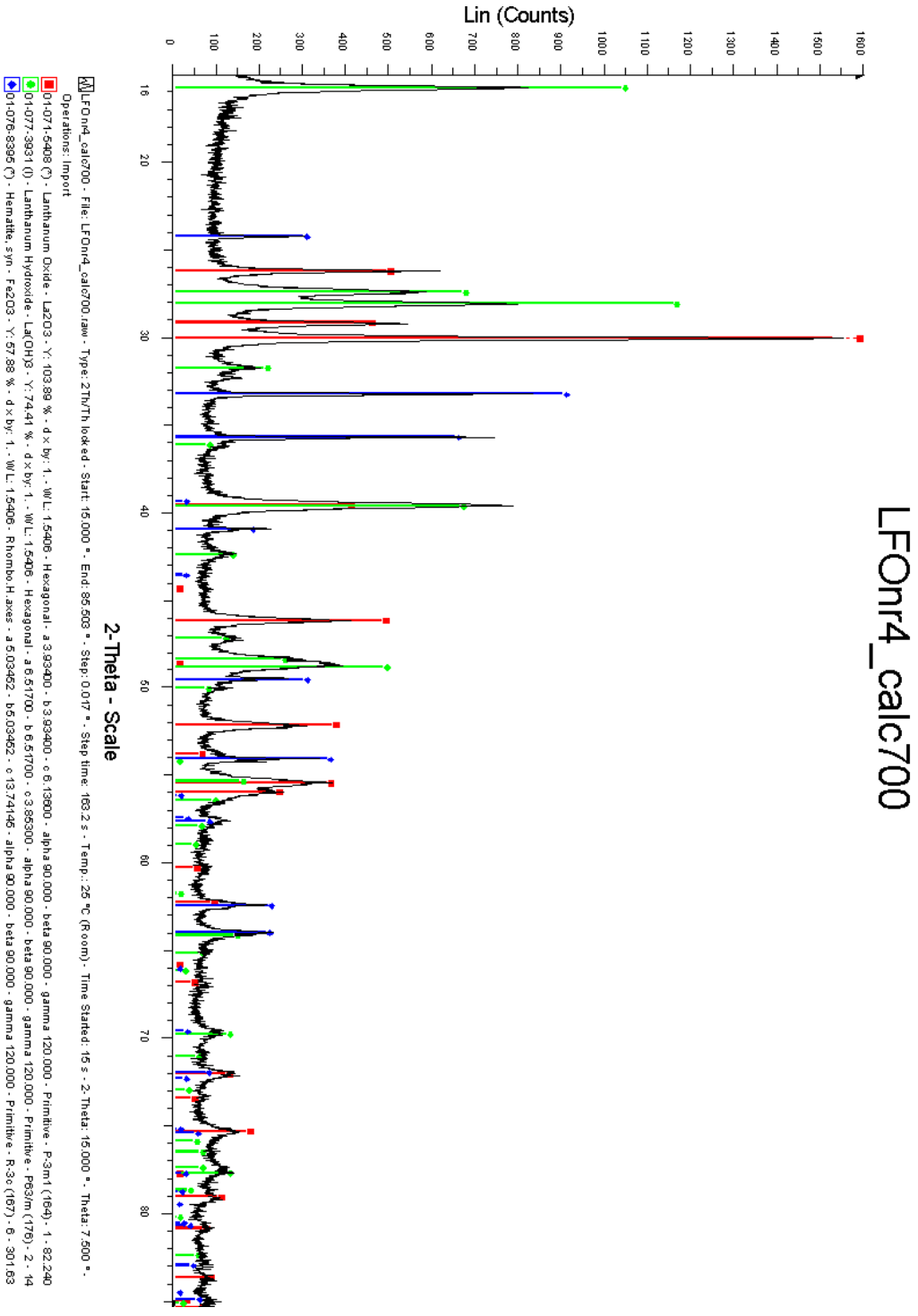

Figure B.8: XRD spectrum of direct synthesis product from synthesis number 3, calcined at 700 °C for 2 hours.

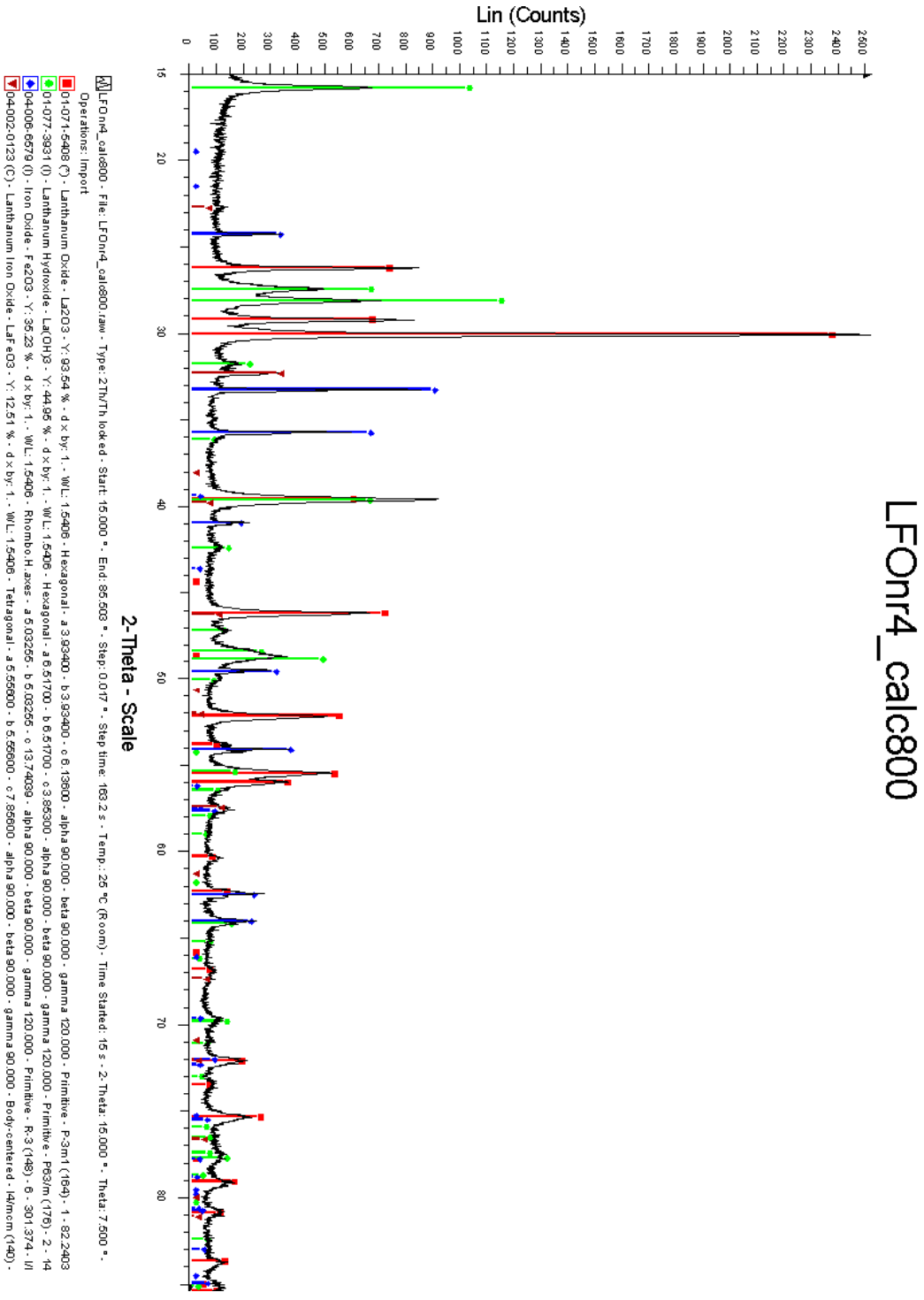

Figure B.9: XRD spectrum of direct synthesis product from synthesis number 3, calcined at 800 °C for 2 hours.

B.2 Two-Step Synthesis of LFO

Synthesis of Lanthanum Hydroxide Nanorods

The XRD spectrum of the lanthanum hydroxide synthesis product is given in Figure B.10.

Calcination of Lanthanum Hydroxide Nanorods

The XRD spectrum of lanthanum hydroxide synthesis product after calcination of 1 hour at 300 °C is given in Figure B.11.

The XRD spectrum of lanthanum hydroxide synthesis product after calcination of 1 hour at 350 °C is given in Figure B.12.

The XRD spectrum of lanthanum hydroxide synthesis product after calcination of 1 hour at 400 °C is given in Figure B.13.

The XRD spectrum of lanthanum hydroxide synthesis product after calcination of 1 hour at 500 °C is given in Figure B.14.

The XRD spectrum of lanthanum hydroxide synthesis product after calcination of 1 hour at 550 °C is given in Figure B.15.

The XRD spectrum of lanthanum hydroxide synthesis product after calcination of 1 hour at 600 °C is given in Figure B.16.

Two-Step Synthesis, Method without Sonication

The XRD spectrum of the raw powder of the two-step hydrothermal synthesis, where sonication was not used, is shown in Figure B.17.

The XRD spectrum of the product of two-step synthesis, where sonication was not used, calcined for 1 hour at 200 °C is given in Figure B.18.

The XRD spectrum of the product of the two-step synthesis without use of sonication after calcination of 1 hour at 400 °C is given in Figure B.19.

The XRD spectrum of calcined product of the two-step synthesis where ultrasonic finger was not used, after calcination of 1 hour at 500 °C is given in Figure B.20.

The XRD spectrum of two-step synthesis product, method without ultrasonic finger, after calcination of 1 hour at 550 °C is given in Figure B.21.

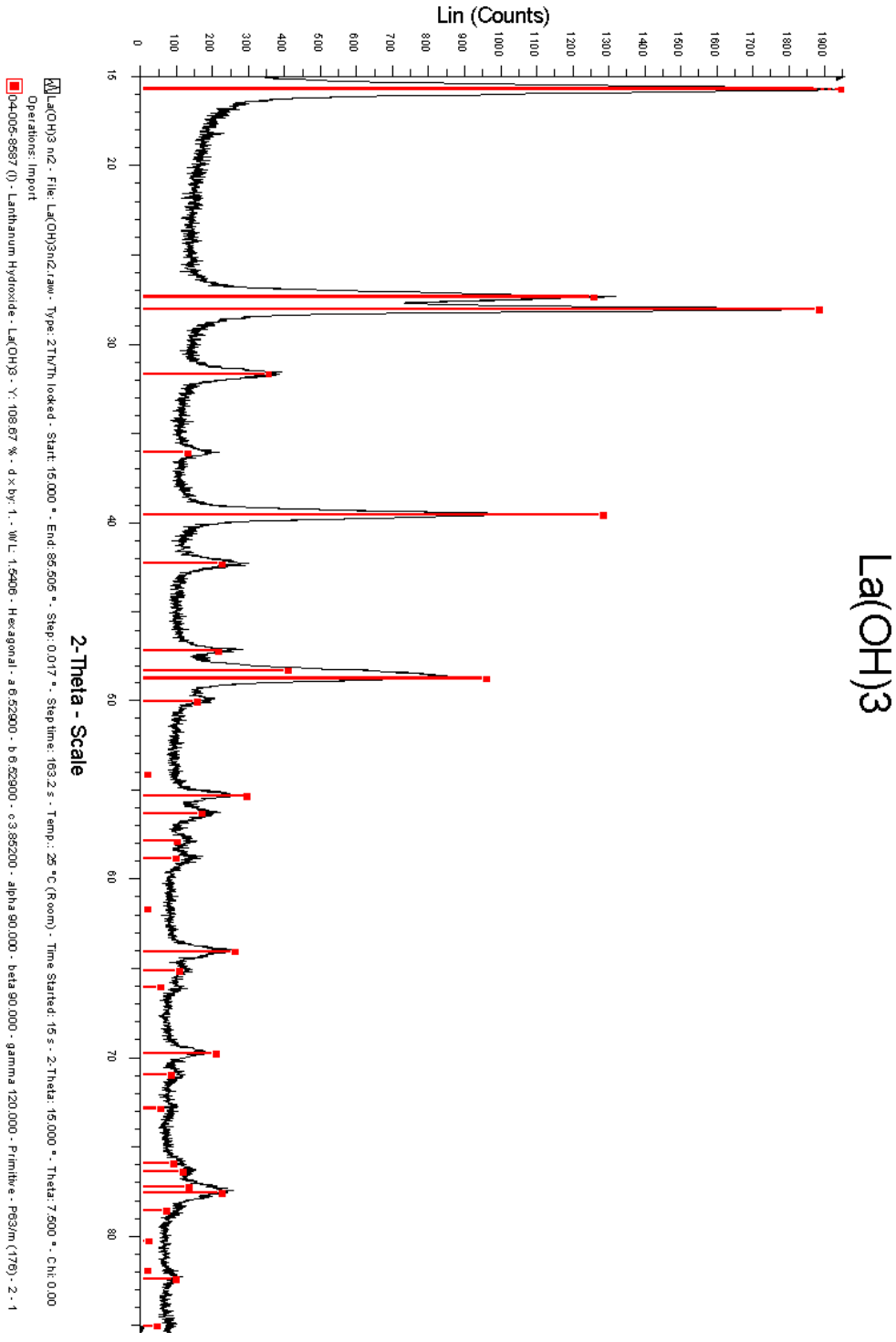

Figure B.10: XRD spectrum of the hydrothermally synthesised, pure lanthanum hydroxide product.

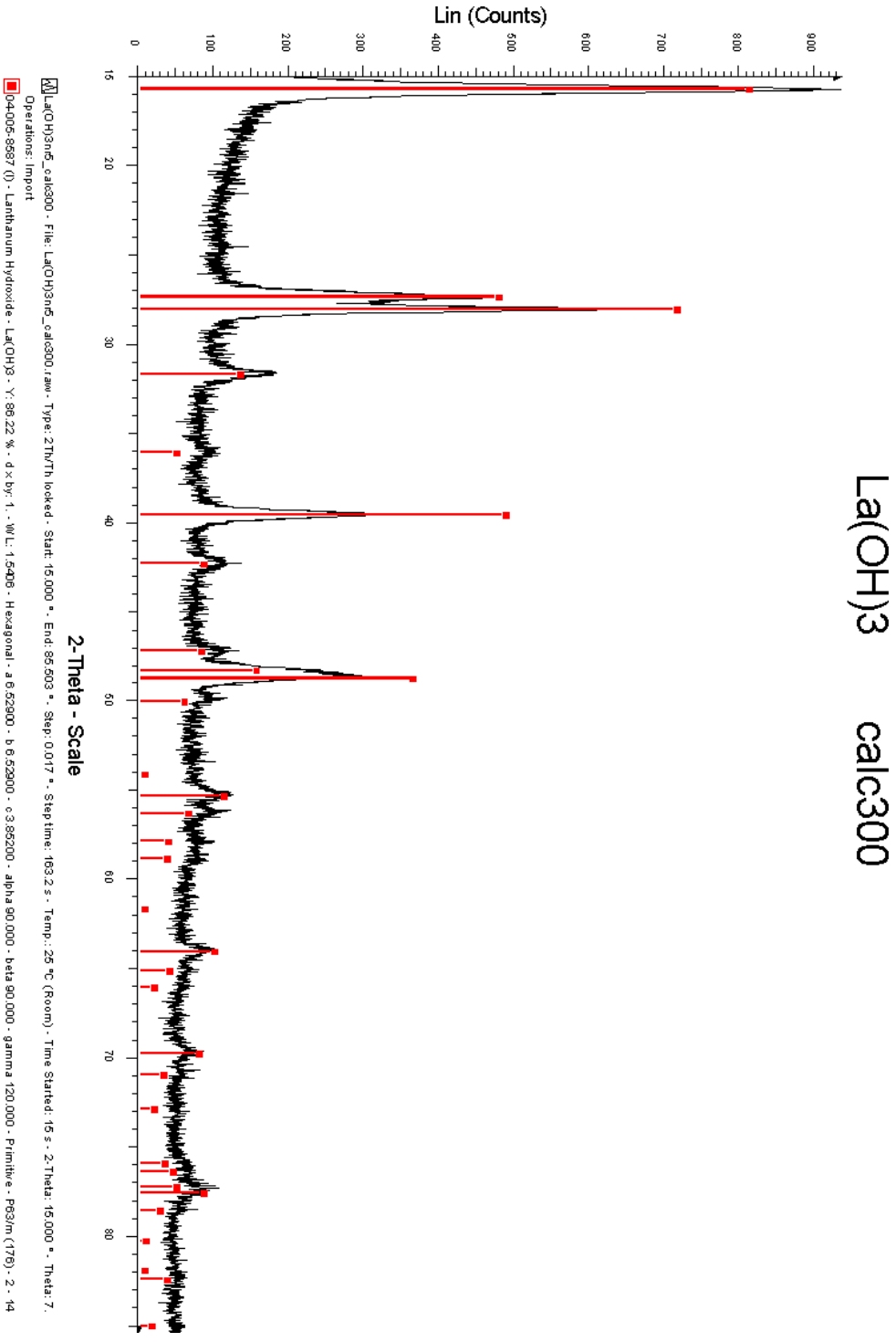

Figure B.11: XRD spectrum of the hydrothermally synthesised lanthanum hydroxide product after calcination for 1 hour at 300 °C.

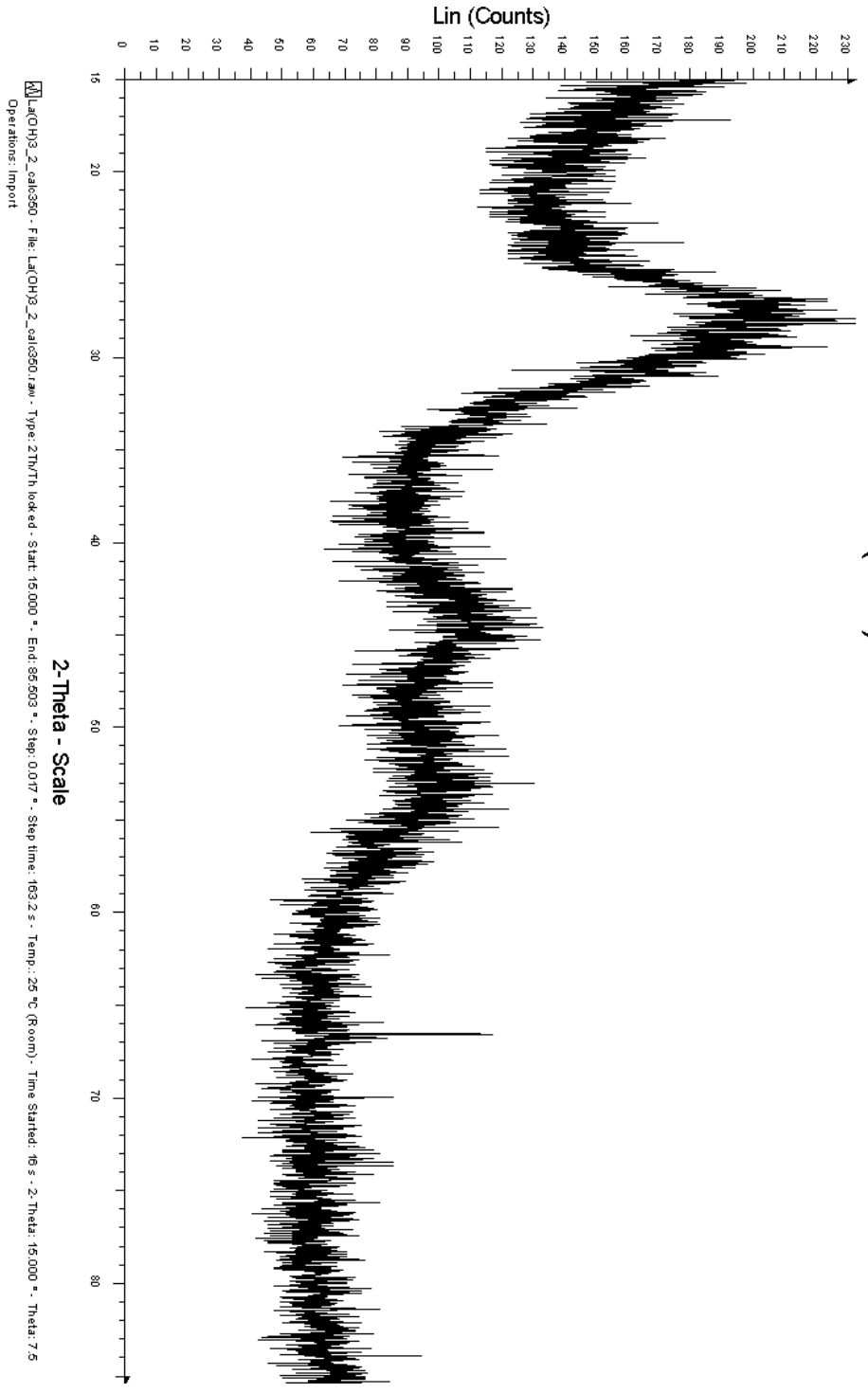

Figure B.12: XRD spectrum of the hydrothermally synthesised lanthanum hydroxide product after calcination for 1 hour at 350 °C.

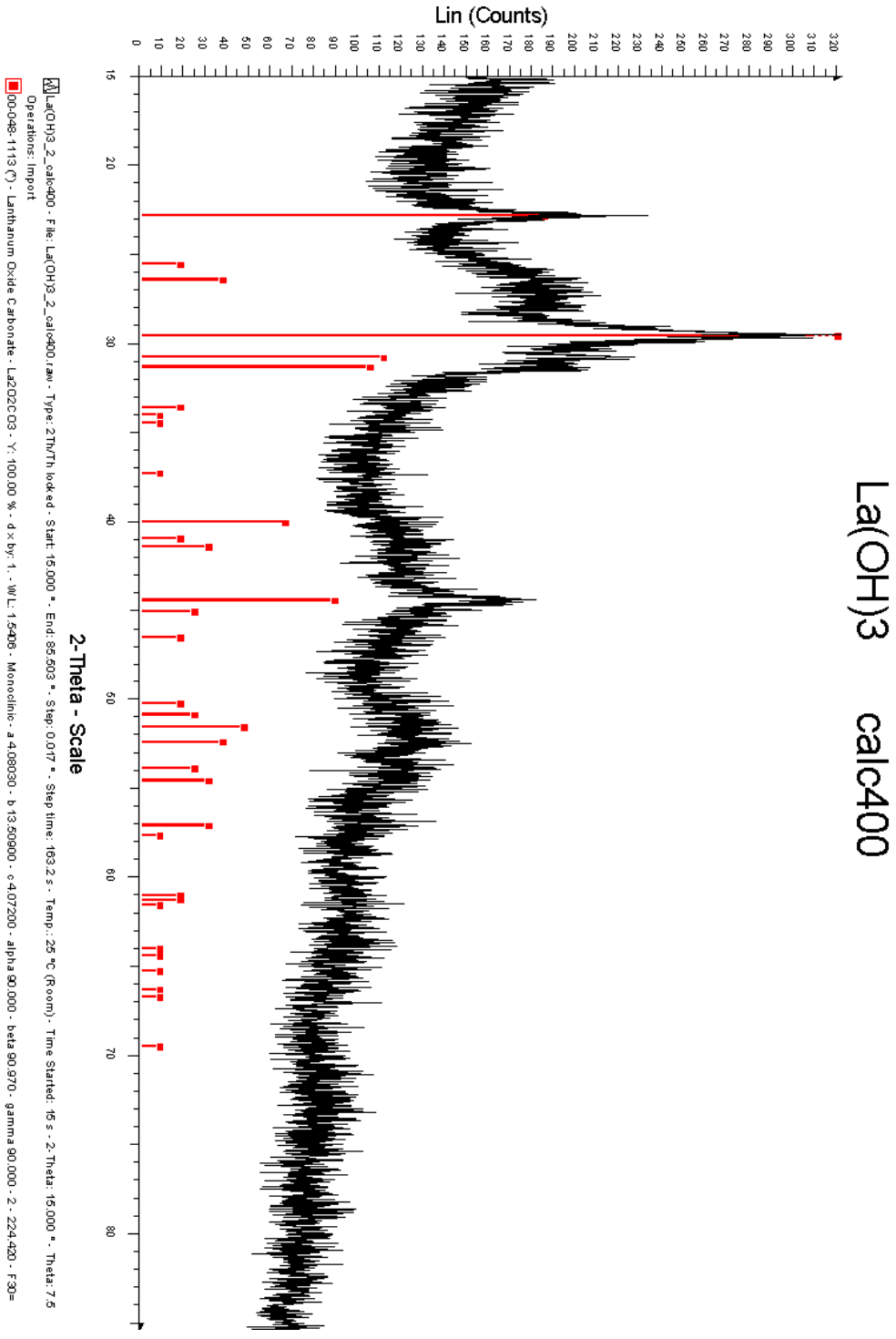

Figure B.13: XRD spectrum of the hydrothermally synthesised lanthanum hydroxide product after calcination for 1 hour at 400 °C.

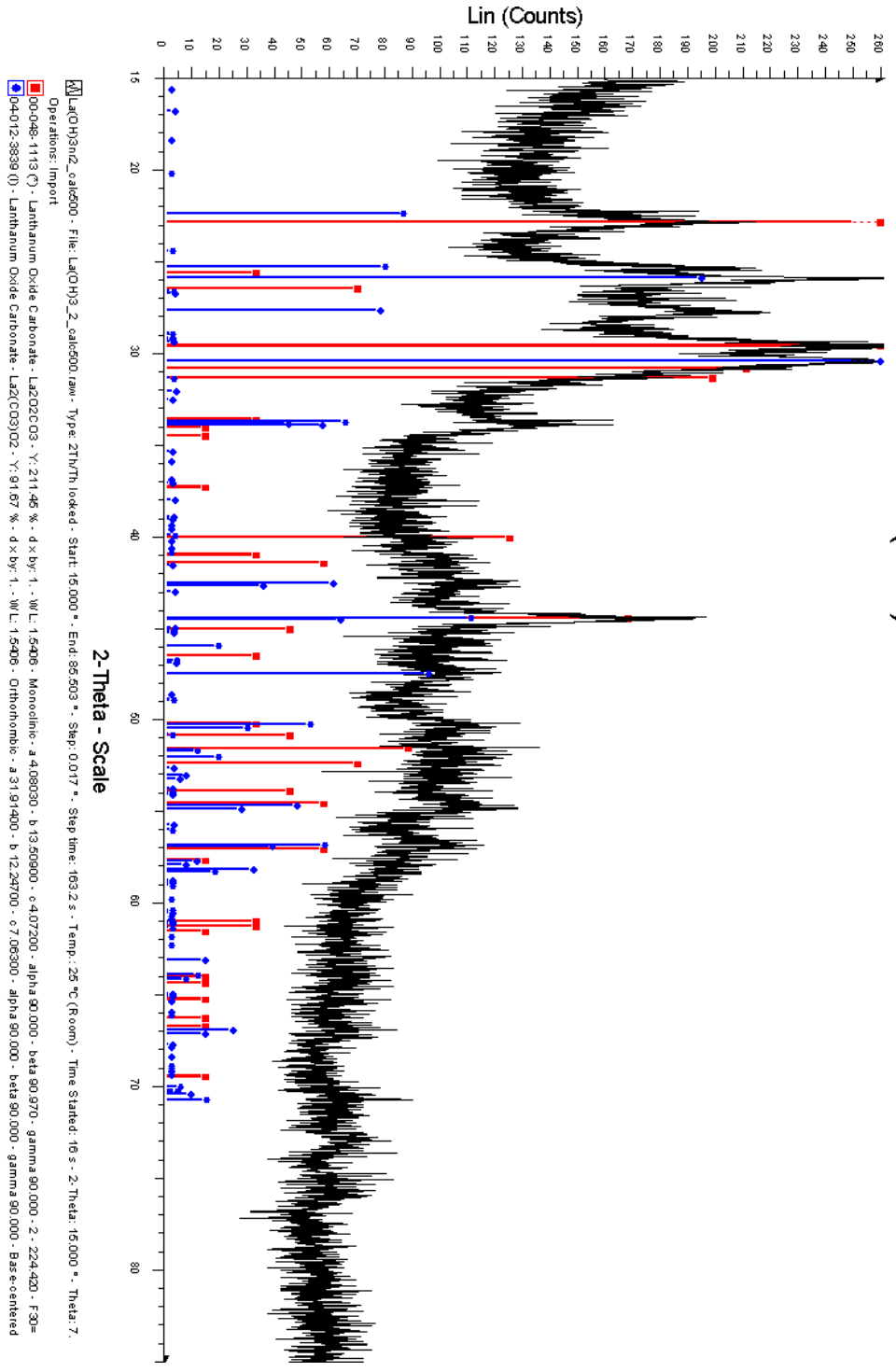

Figure B.14: XRD spectrum of the hydrothermally synthesised lanthanum hydroxide product after calcination for 1 hour at 500 °C.

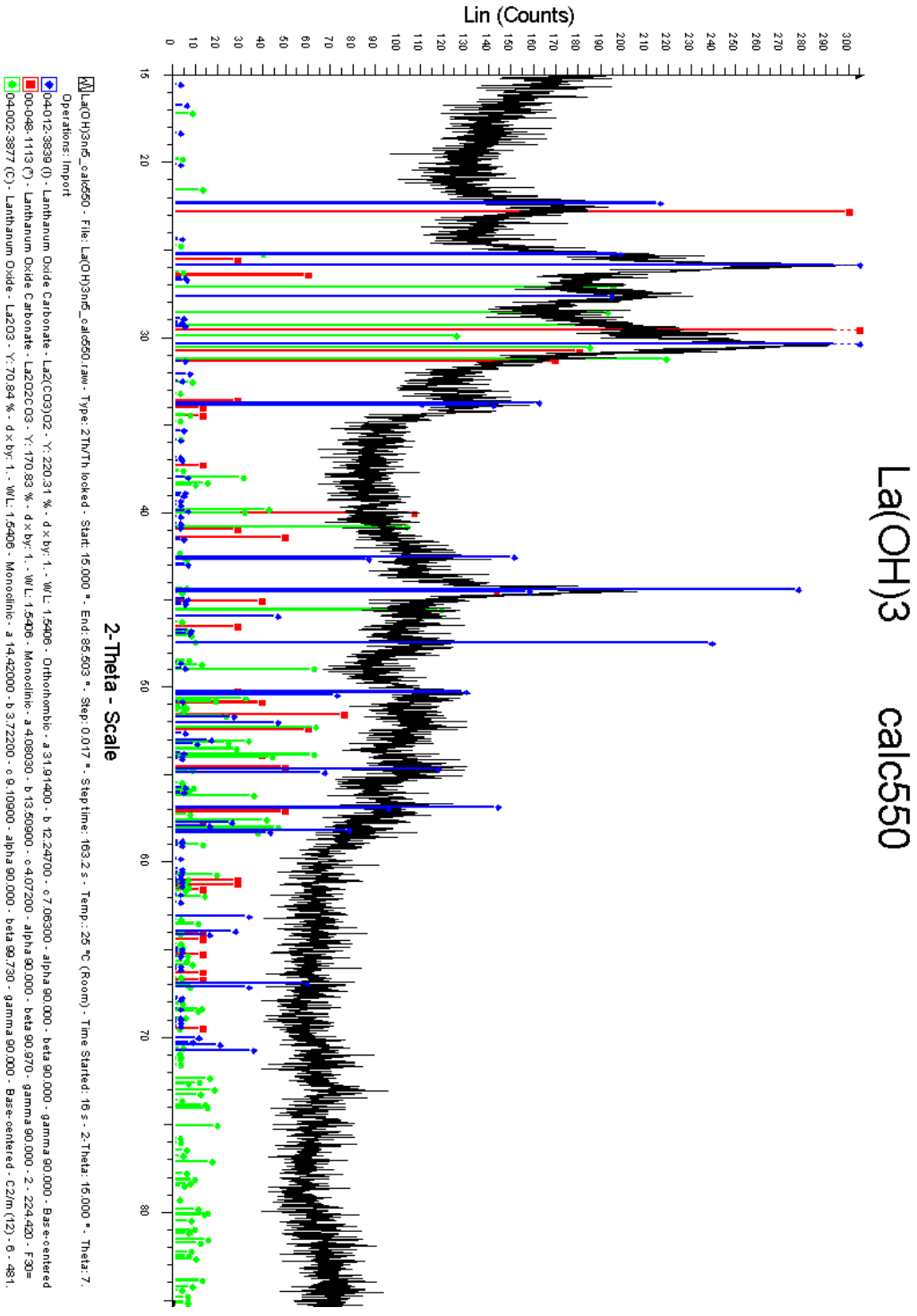

Figure B.15: XRD spectrum of the hydrothermally synthesised lanthanum hydroxide product after calcination for 1 hour at 550 °C.

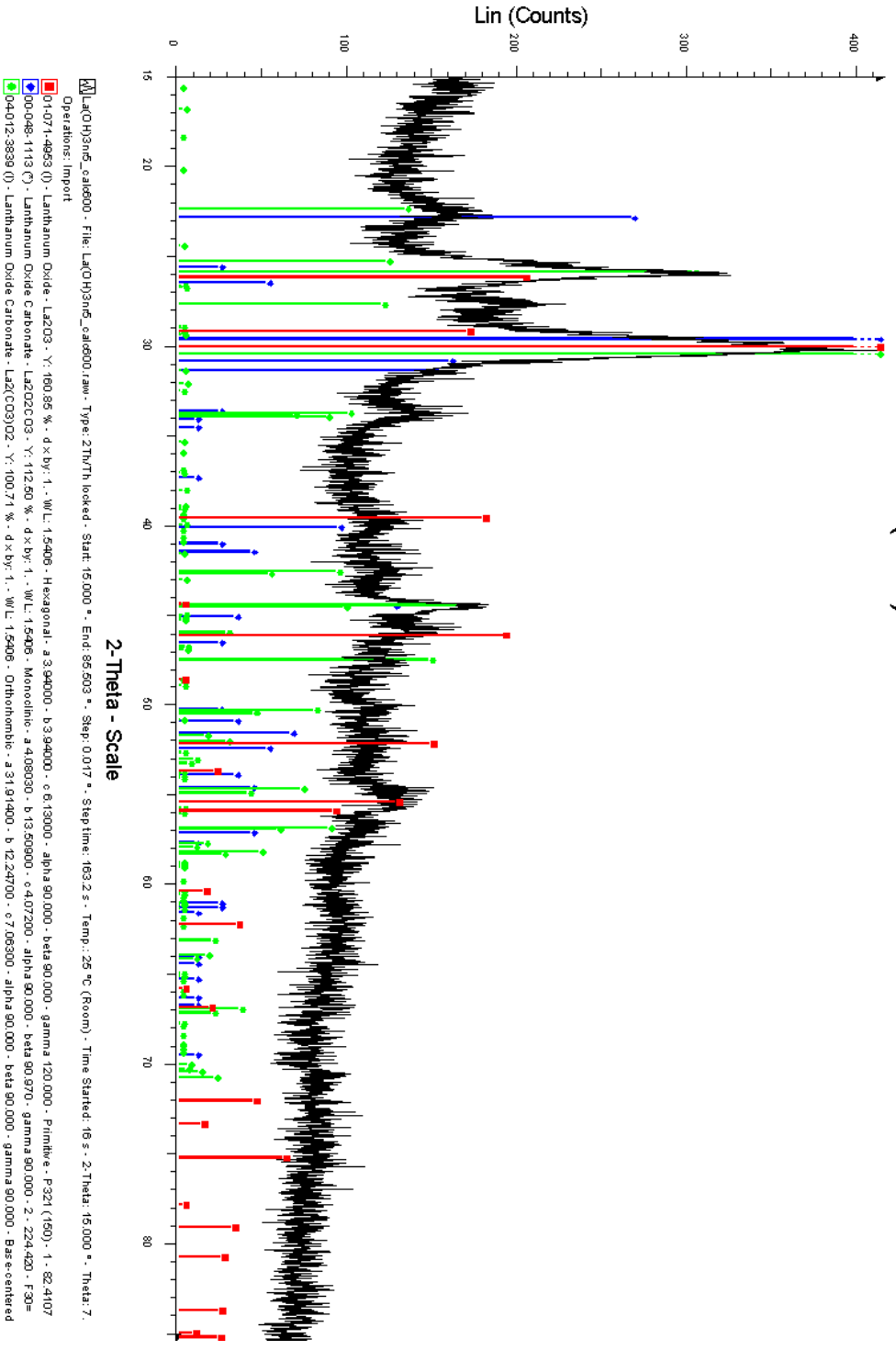

Figure B.16: XRD spectrum of the hydrothermally synthesised lanthanum hydroxide product after calcination for 1 hour at 600 °C.

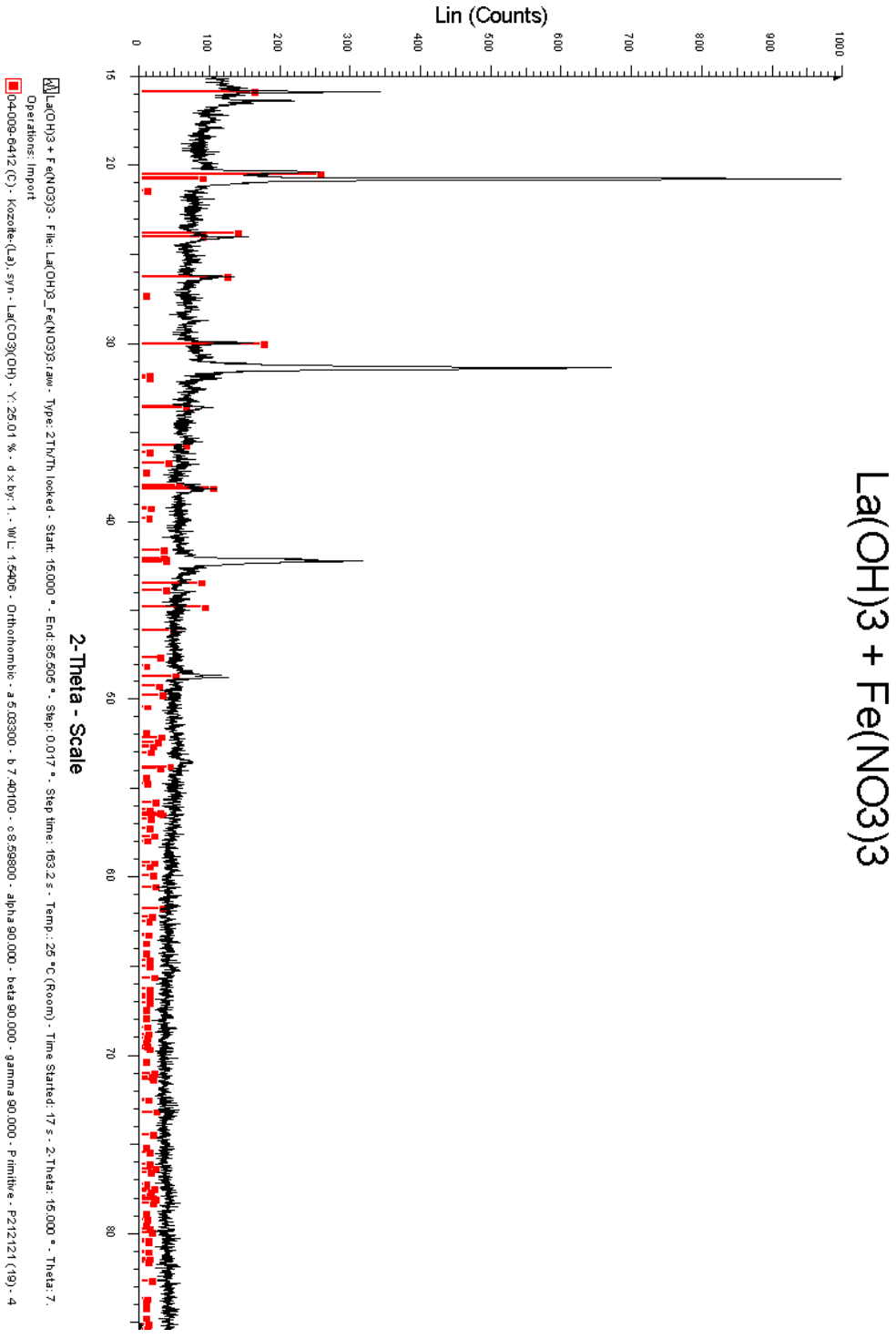

Figure B.17: XRD spectrum of the raw powder of the two-step hydrothermal synthesis, method without the use of ultrasonic finger.

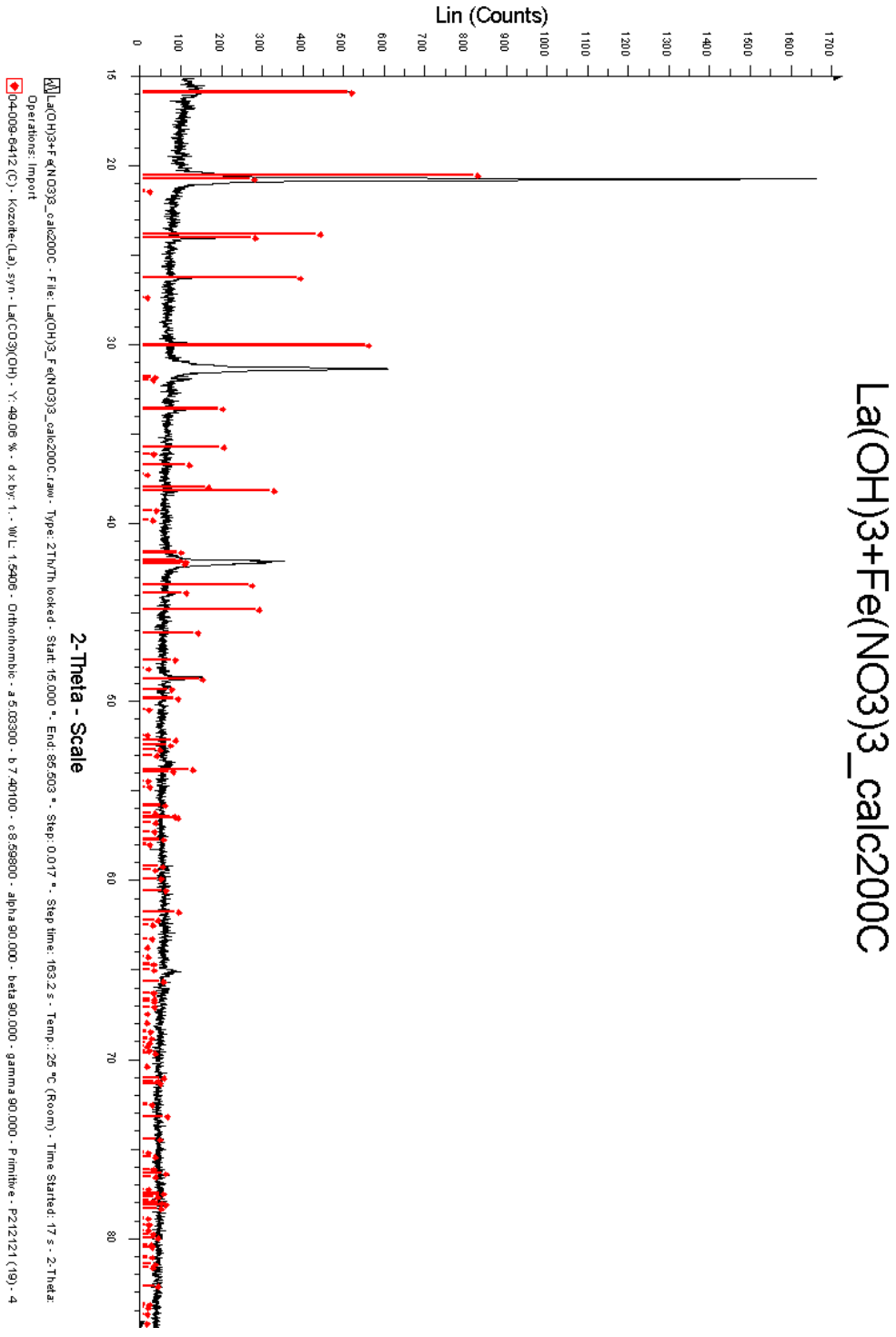

Figure B.18: XRD spectrum of the calcined product, 1 hour at 200 °C, of the two-step hydrothermal synthesis where ultrasonic finger was not used.

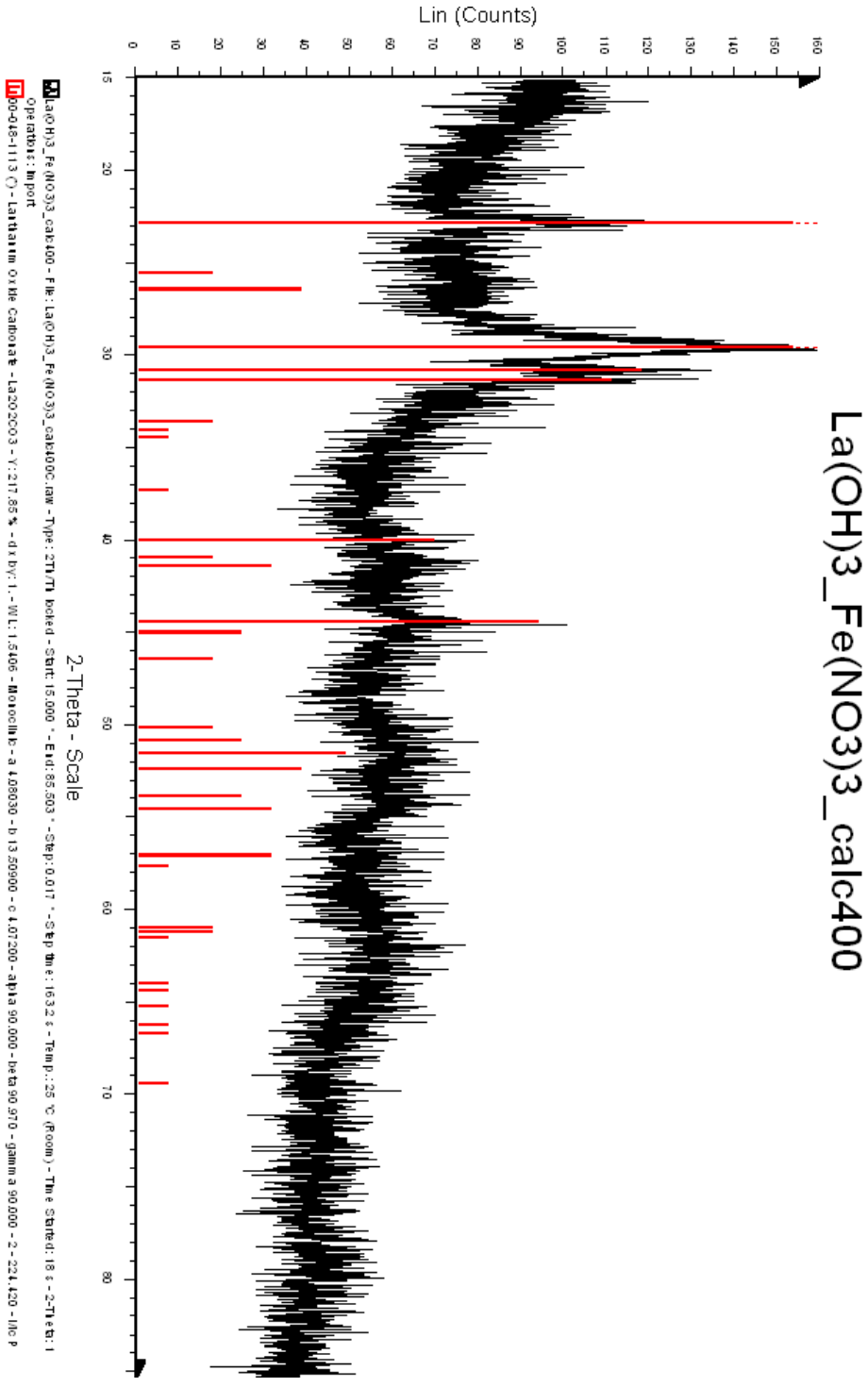

Figure B.19: XRD spectrum of the calcined product, 1 hour at 400 °C, of the two-step hydrothermal synthesis where ultrasonic finger was not used.

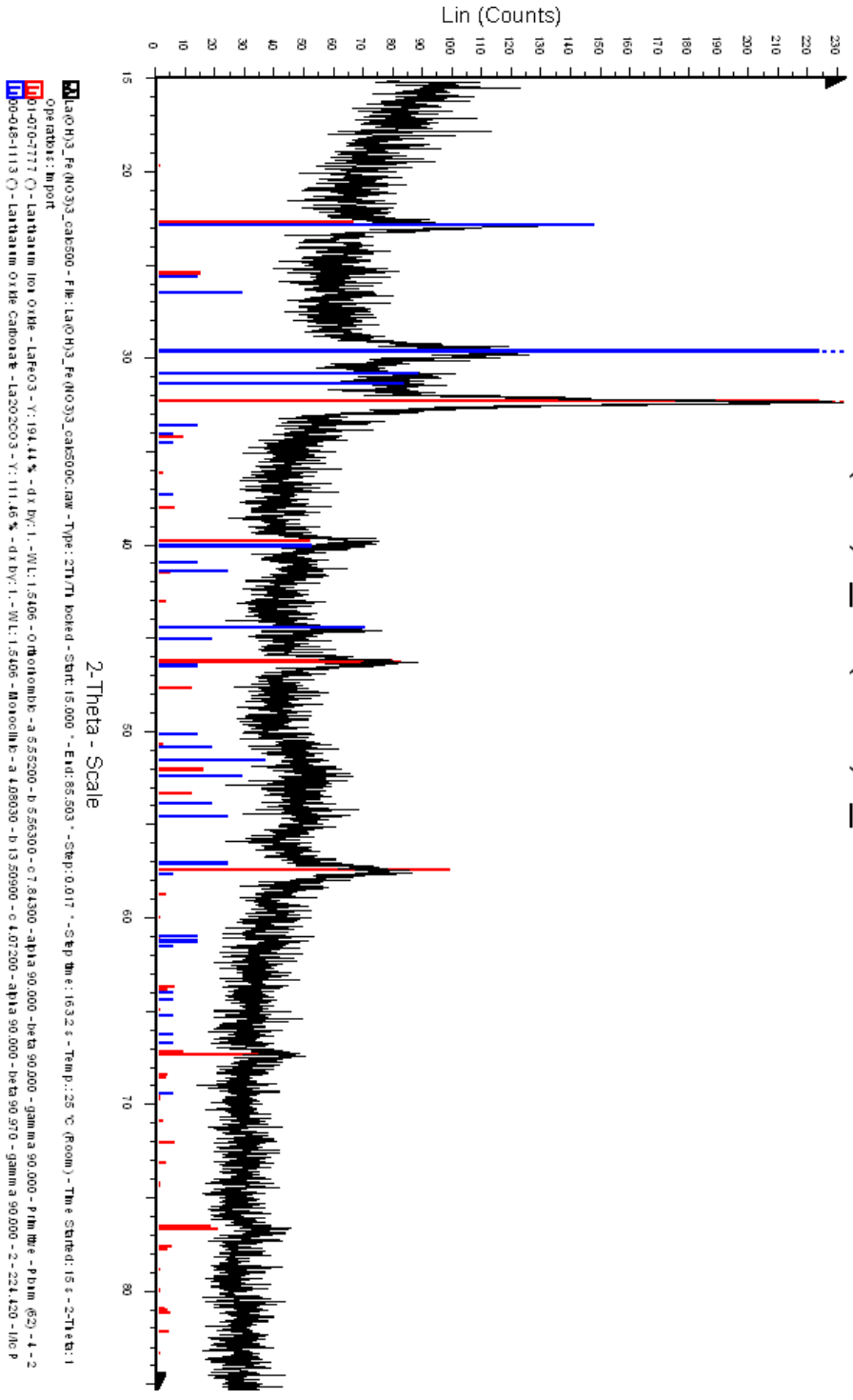

Figure B.20: XRD spectrum of the calcined product, 1 hour at 200 °C, of the two-step hydrothermal synthesis where ultrasonic finger was not used.

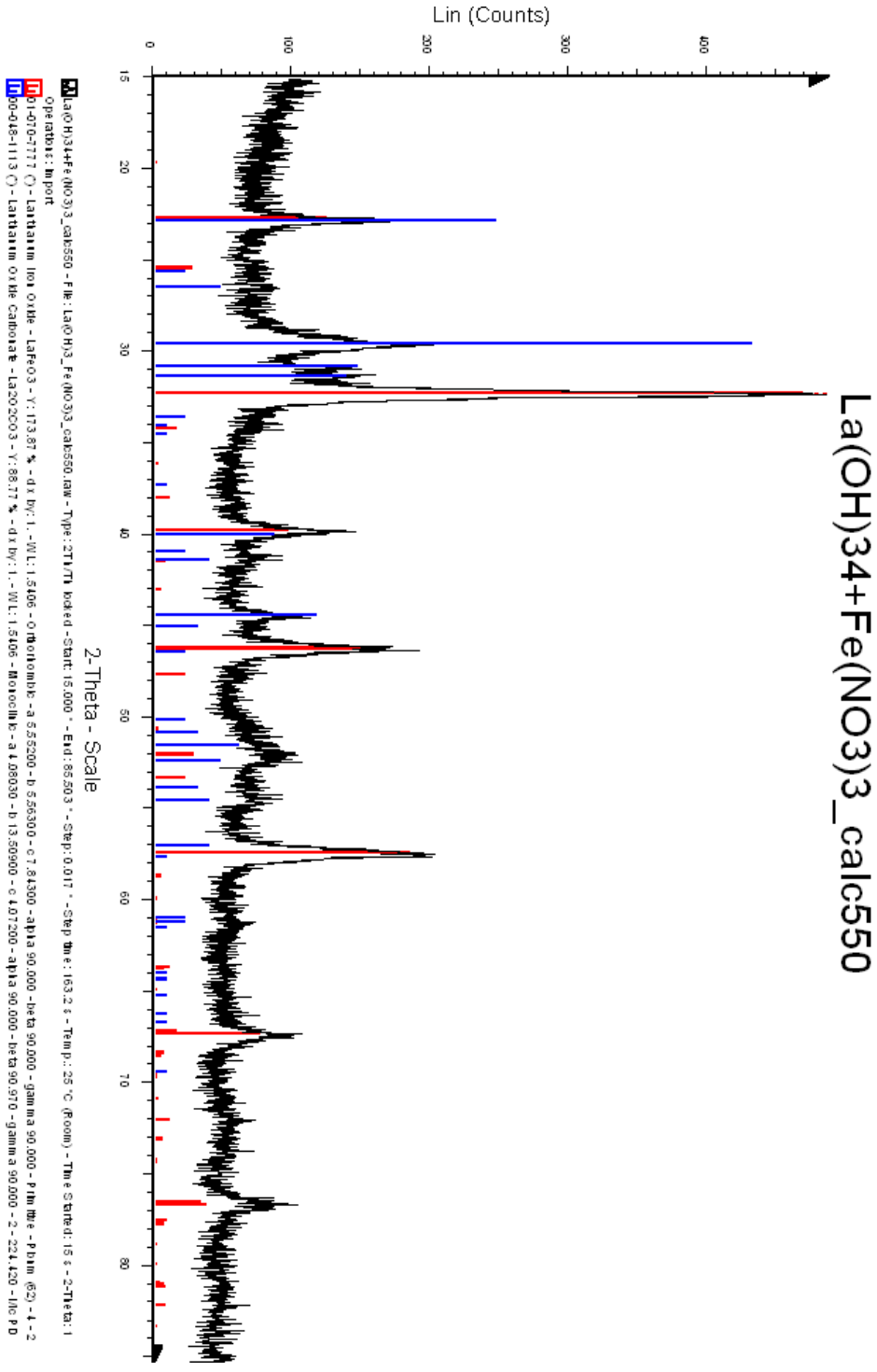

Figure B.21: XRD spectrum of the calcined product, 1 hour at 550 °C, of the two-step hydrothermal synthesis where ultrasonic finger was not used.

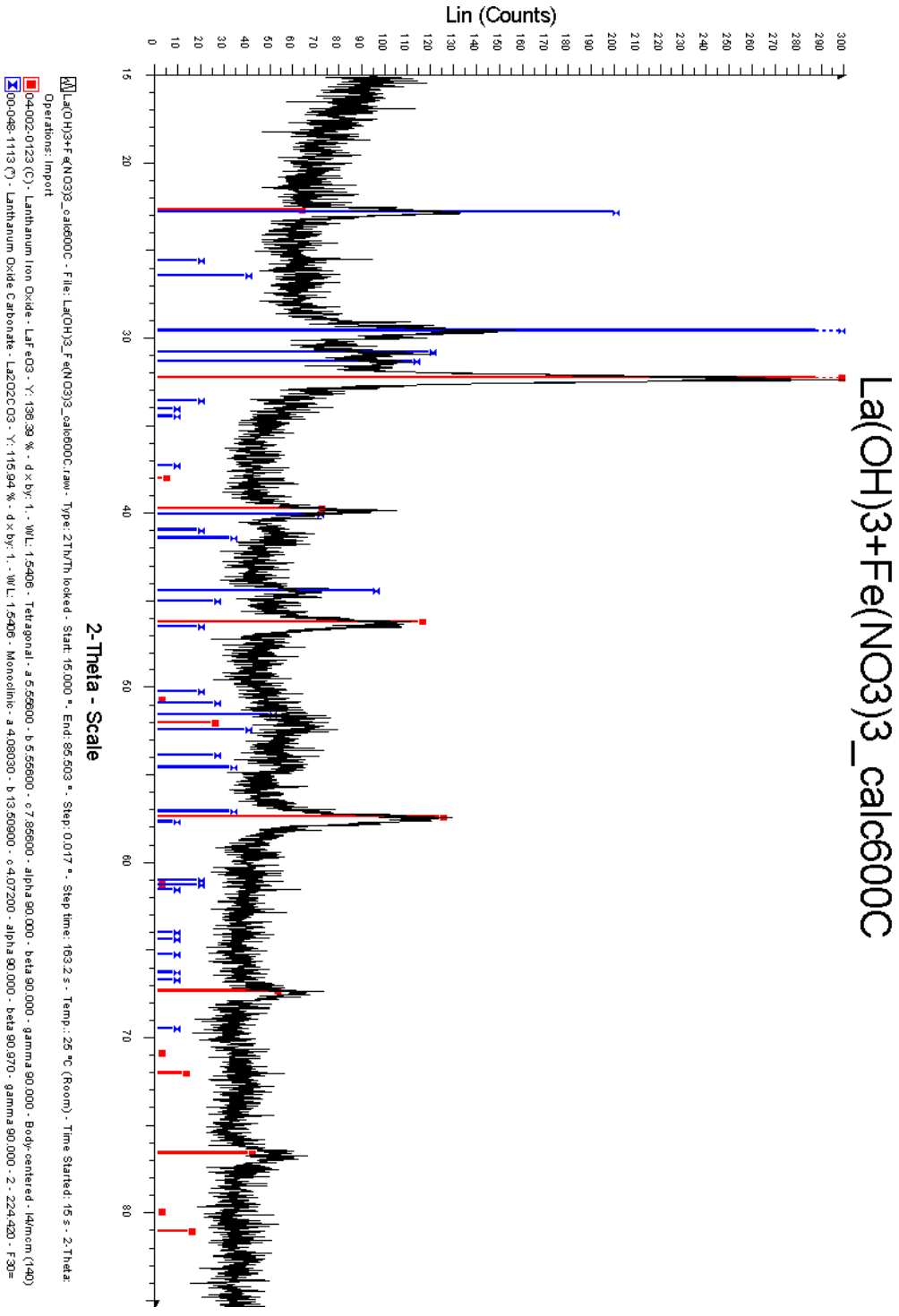

Figure B.22: XRD spectrum of the calcined product, 1 hour at 600 °C, of the two-step hydrothermal synthesis where ultrasonic finger was not used.

The XRD spectrum of the calcined product of the two-step synthesis product, where sonication was not spplied, after 1 hour at 600 °C is given in Figure B.22.

XRD spectrum of the calcined product, 1 hour at 650 °C, of the two-step hydrothermal synthesis where ultrasonic finger was not used is given in Figure B.23.

Two-Step Synthesis, Method with Sonication

The XRD spectrum of the raw powder of the two-step hydrothermal synthesis, method where ultrasonic finger was used, is shown in Figure B.24.

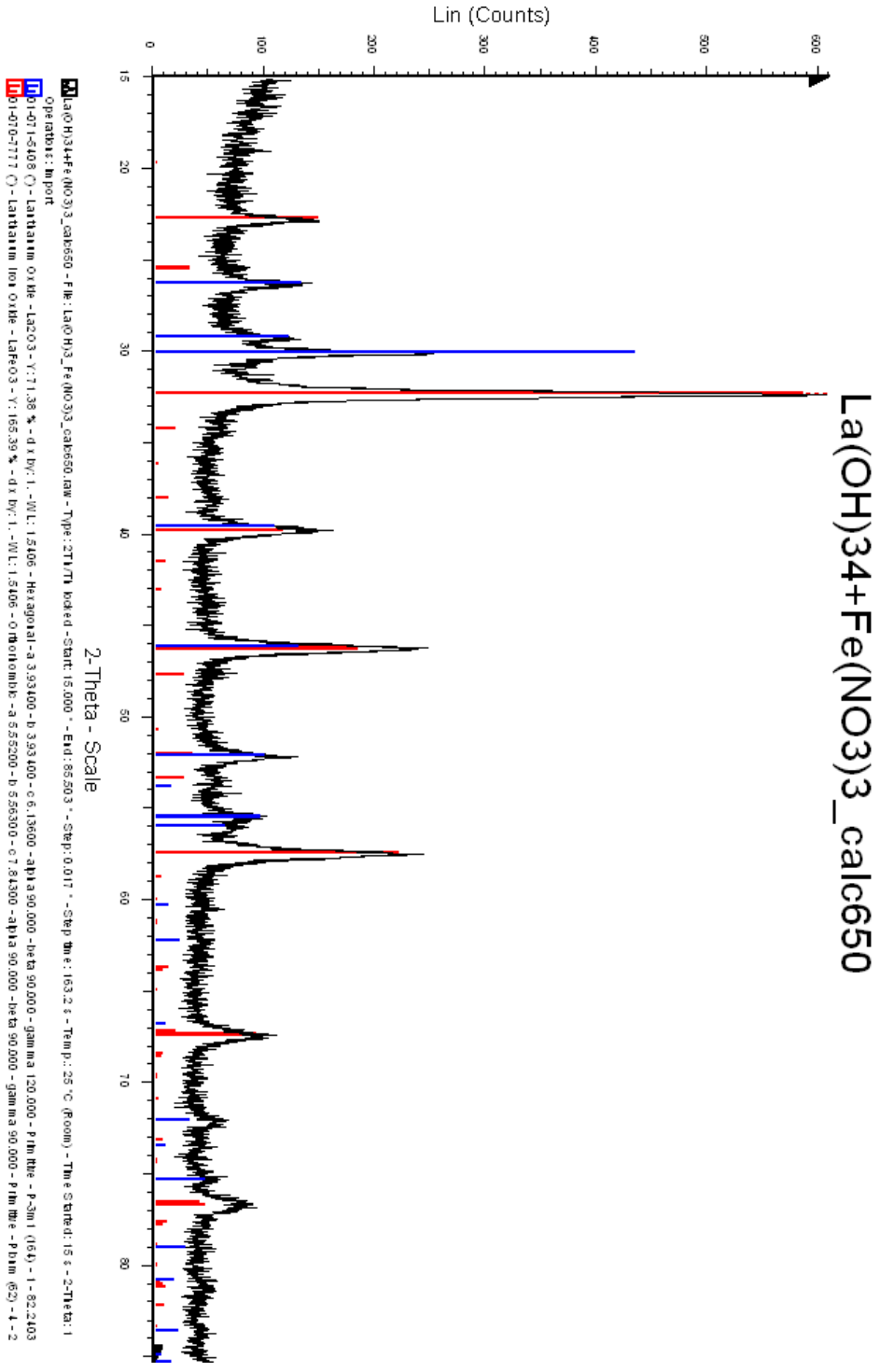

Figure B.23: XRD spectrum of the calcined product, 1 hour at 650 °C, of the two-step hydrothermal synthesis where ultrasonic finger was not used.

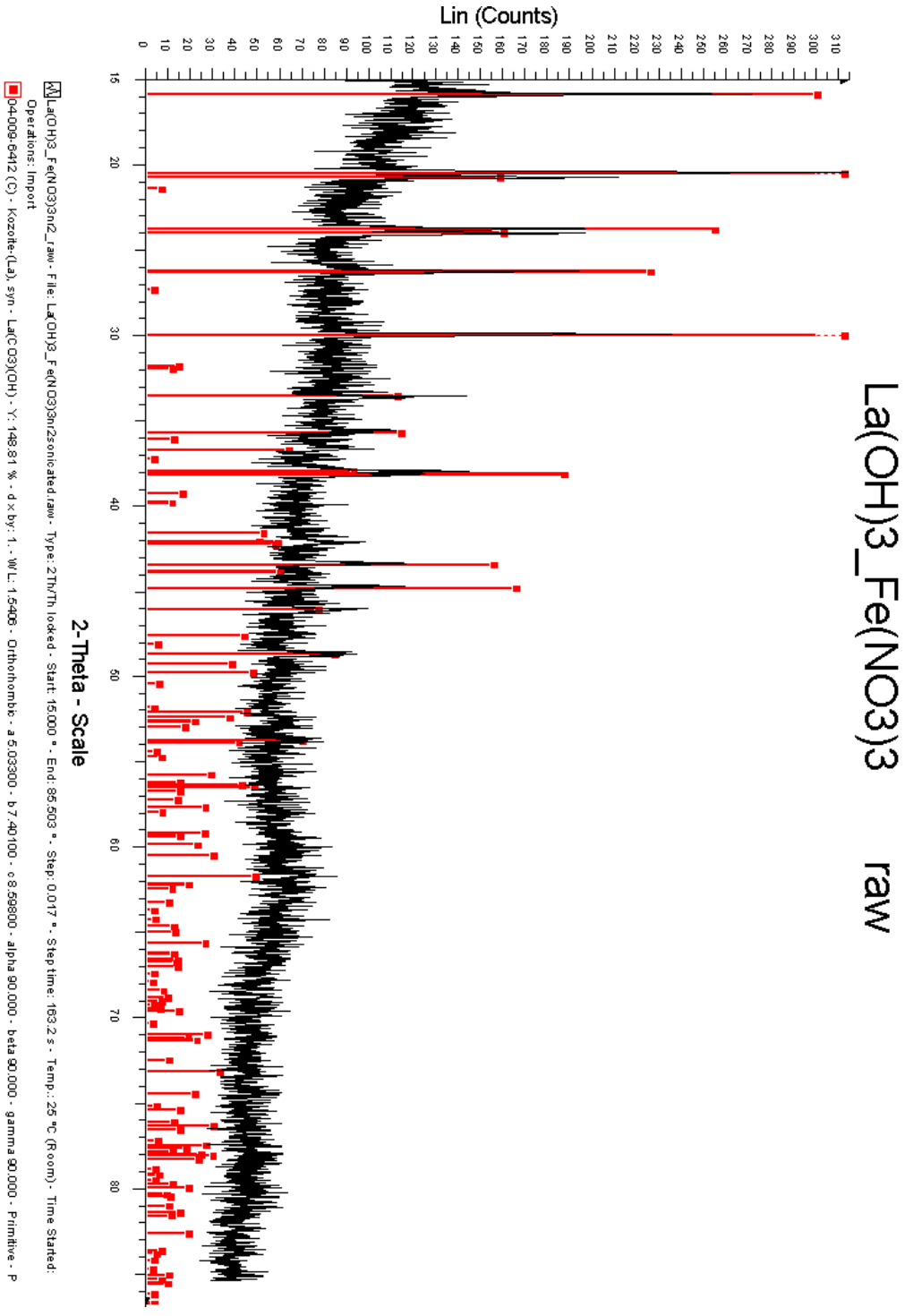

Figure B.24: XRD spectrum of the raw powder of the two-step hydrothermal synthesis, method where ultrasonic finger was used.